FEUP FACULDADE DE ENGENHARIA
UNIVERSIDADE DO PORTO

Encapsulation of Active Compounds: Particle Characterization, Loading Efficiency and Stability

Dissertation presented for obtaining the degree of:
Doctor of Philosophy in Chemical and Biological Engineering
by
University of Porto

by
Ivone Margarida Nunes Ferreira Vieira Peres

Supervisor:
Manuel Álvaro Neto Coelho
Co-Supervisor:
Maria do Carmo da Silva Pereira

Porto, 2011

Resumo

Este trabalho de investigação visou estudar a incorporação/encapsulação de duas moléculas distintas, nomeadamente, a epigalocatequina galato (EGCG) e o colagénio hidrolisado (CH) em partículas compostas por maltodextrina e goma arábica, com o objectivo de preservar as suas propriedades e aumentar a sua estabilidade. EGCG e CH são moléculas distintas, que apresentam diferenças a nível da estrutura química e peso molecular, que corresponde a 458 Da e 3600 Da para a EGCG e o CH, respectivamente.

As moléculas de EGCG e CH foram incorporadas nas partículas de maltodextrina e goma arábica, através de um processo de homogeneização e secagem por atomização, com uma eficiência de encapsulação de 96% para as partículas contendo EGCG. No caso das partículas contendo CH a 5% e 25%, obteve-se uma eficiência de encapsulação de 87% e 85%, respectivamente.

A morfologia e estrutura das partículas contendo EGCG (EGCG/P) foram caracterizadas por microscopia electrónica de varrimento e de transmissão e por microscopia de força atómica. As partículas produzidas são esféricas ou enrugadas, de tamanho polidisperso, com diâmetros inferiores a 20 µm, sendo estas resistentes à aplicação de força mecânica até 8 MPa. A análise do tamanho das EGCG/P em suspensão aquosa foi efectuada aplicando um método de difracção a laser e uma técnica inovadora designada por *nanoparticle tracking analysis*. Os resultados obtidos confirmam um distribuição de tamanho polidispersa, com duas populações predominantes, cujos diâmetros hidrodinâmicos médios correspondem a 40 nm e 400 nm. A aplicação das técnicas de picnometria de hélio e porosimetria de mercúrio, permitiu concluir que as EGCG/P possuem uma estrutura interna porosa. A estrutura dos conjugados de polissacarídeos-EGCG e os mecan-

ismos de imobilização da EGCG na matriz polimérica foram investigados recorrendo à espectroscopia de infravermelho, em particular, à técnica de reflectância total atenuada (RTA), bem como à ressonância magnética nuclear (RMN). Os resultados de RTA sugerem a encapsulação da EGCG na matriz de polissacarídeos, preservando a sua estrutura e propriedades antioxidantes. A medição dos tempos de relaxação nucleares e a aplicação da espectroscopia de RMN ordenada por difusão (DOSY), através do gradiente de campo magnético pulsado sugerem a incorporação da EGCG na matriz de polissacarídeos-maltodextrina/goma arábica e evidenciam o potencial destes sistemas poliméricos na veiculação e libertação controlada de compostos activos como a EGCG. As moléculas de EGCG encapsuladas mantêm a sua actividade biológica, designadamente, anticancerosa, reduzindo a viabilidade celular e induzindo a apoptose das células tumorais da próstata Du145. Ensaios clonogénicos demonstraram que a encapsulação da EGCG resulta num maior efeito inibitório na proliferação das células (10-20%) a concentrações mais baixas (1-2 µm), comparativamente às moléculas de EGCG não encapsuladas. Estas observações destacam o uso destas partículas de polissacarídeos na prevenção do cancro, na medida em que podem ser usadas na veiculação de antioxidantes capazes de inibir etapas do processo de tumorogénese.

A morfologia das partículas contendo CH (CH/P) caracteriza-se essencialmente por uma forma esférica e superfícies lisas. A distribuição de tamanho das CH/P suspensas foi determinada recorrendo à difracção a laser e à semelhança das EGCG/P, a distribuição de tamanho obtida é bimodal, com diâmetros hidrodinâmicos médios de 30 nm e 300 nm. A presença das bandas características de CH no espectro de RTA e dos sinais característicos de ressonância no espectro de ^{1}H RMN das CH/P confirmam a efectiva incorporação do CH na matriz polimérica de maltodextrina e goma arábica. A redução dos coeficientes de difusão do CH incorporado nas partículas de maltodextrina-goma arábica, observada por RMN de difusão, é um forte indício de um processo de associação entre o CH e os polissacarídeos, através de ligações de hidrogénio. Ensaios de libertação *in vitro* demonstram que a difusão do CH da matriz das CH/P diminui em comparação com o CH livre, corroborando os resultados obtidos por RMN e RTA.

O presente estudo demonstra o potencial da matriz de carboidratos na

preservação das propriedades originais das moléculas de EGCG e CH, como prova de conceito a ser utilizada como veículo polimérico para transporte de biomoléculas.

Abstract

In this work, the loadind/entrapment of two distinct molecules, epigallocatechin gallate (EGCG) and collagen hydrolysate (CH), in maltodextrin-gum arabic particles was investigated due to the potential of preserving their properties and increasing their stability. EGCG and CH are distinct molecules with different chemical structure and molecular weight, 458 Da and 3600 Da, for EGCG and CH, respectively.

Maltodextrin-gum arabic particles loaded with EGCG (EGCG/P) and CH (CH/P) were successfully produced by homogenization and spray-drying, with an EGCG loading effciency of 96%. In the case of CH, the loading efficiency was 87% and 85% for CH/P with 5% and 25% of CH, respectively.

The morphology and structure of the EGCG loaded particles were characterized by scanning and transmission electron microscopy and atomic force microscopy. Spray-dried particles are spherical or corrugated, polydisperse with diameters less than 20 µm and are resistant to mechanical strength, up to 8 MPa. Dynamic light scattering and nanoparticle tracking analysis of EGCG/P in aqueous suspension confirm a polydisperse size distribution, comprising two main populations, with mean average diameters of 40 nm and 400 nm. EGCG/P possess a porous internal structure as demonstrated by helium pycnometry and mercury porosimetry. Attenuated total reflection-infrared (ATR) spectroscopy and nuclear magnetic resonance (NMR) spectroscopy experiments, have been performed to determine the structure of the epigallocatechin gallate-polysaccharide conjugates and to clarify the mechanisms of drug immobilization into the polymer matrix. ATR results indicate the entrapment of EGCG into the polysaccharide matrix, preserving its chemical structure and related antioxidant properties. Measurements of the nuclear relaxation times and application of diffusion

ordered spectroscopy (DOSY), obtained through pulsed field gradient (PFG) NMR experiments, suggest the entrapment of EGCG into the polysaccharide matrix of maltodextrin/gum arabic and support the potential of these vehicles for their sustained delivery and release. Encapsulated EGCG retained its chemopreventive biological activity, reducing the cell viability and inducing apoptosis of Du145 prostate cancer cells. Clonogenic assay demonstrated that encapsulation of EGCG enhanced its inhibitory effect on cell proliferation (10-20%) at lower concentrations (1-2 μM), compared with free EGCG. These findings highlight the use of polysaccharide nanoparticles in chemoprevention as they can be used to deliver natural antioxidants capable of inhibiting steps of the tumorigenesis process.

CH/P morphology is mainly characterized by spherical shape with smooth surfaces. Particle size distribution of the suspended CH/P was determined using dynamic light scattering and similarly to EGCG/P, the size distribution is bimodal with average hydrodynamic diameters of 30 nm and 300 nm. The presence of the CH characteristic bands in the ATR spectrum and characteristic resonance signals in ^{1}H NMR spectrum of CH/P defines the successful entrapment of CH within the polymeric matrix of maltodextrin and gum arabic. From the diffusion gradient NMR experiments, the reduction of the diffusion coefficients of CH incorporated in the maltodextrin-gum arabic particles is a strong indication of an association process between CH and polysaccharides, through hydrogen bonds. *In vitro* release experiments show that the diffusion of CH from the CH/P matrix decreases in comparison with free CH, corroborating the results obtained by NMR and ATR measurements.

The present study demonstrates that the carbohydrate matrix is able to preserve EGCG and CH original properties, as proof of concept to be used as polymeric drug carrier.

Acknowledgements

Many people contributed to this dissertation and I am grateful to all of them.

I would like to thank my supervisors Prof. Manuel Coelho e Prof. Maria do Carmo Pereira for their scientific guidance and valuable contributions during the course of this work.

I thank Dr. Galya Ivanova for her training and support in the nuclear magnetic resonance experiments, but also for her helpful suggestions.

I would like to thank Prof. Simone for her help and assistance in the MAE technology.

A special thanks to Sandra Rocha for her helpful comments, knowledge and constructive discussions, that improved the quality of this thesis.

I would especially like to thank Joana Gomes for her support as friend and colleague and Luís Carlos who has been especially helpful.

Thanks to Eng. Pedro Gonçalves for the technical support.

Lastly, I offer my regards to my family and friends who supported me during the completion of this project.

Contents

List of Figures

List of Tables

Preface

The research work presented in this dissertation was developed from 2007 to 2011 at the Faculty of Engineering, University of Porto, resulting in the following publications that are published or submitted for publication:

Ferreira, I., Rocha, S., & Coelho, M. (2007). Encapsulation of antioxidants by spray-drying. Chemical Engineering Transactions, 11, 713-717.

Gomes, J. F. P. S., Rocha, S., Pereira, M. C., Ferreira, I., Moreno, S., Toca-Herrera, J., et al. (2010). Lipid/particle assemblies based on maltodextrin/gum arabic core as bio-carriers. Colloids and Surfaces B: Biointerfaces, 76(2), 449-455.

Peres, I.; Rocha, S.; Pereira, M. d. C.; Coelho, M.; Rangel, M.; Ivanova, G. (2010). NMR structural analysis of epigallocatechin gallate loaded polysaccharide nanoparticles. Carbohydrate Polymers, 82, 86-866.

Rocha, S., Generalov, R., Pereira, M. C., Peres, I., Juzenas, P., & Coelho, M. (2011). Epigallocatechin gallate-loaded polysaccharide nanoparticles for prostate cancer chemoprevention. Nanomedicine, 6(1), 79-87.

Peres, I.; Rocha, S.; Gomes, J.; Morais, S.; Pereira, M. C.; Coelho, M. (2011). Preservation of catechin antioxidant properties loaded in carbohydrate nanoparticles. Carbohydrate Polymers, 86, 147-153.

Peres, I.; Rocha, S.; Pereira, M. d. C.; Ivanova, G.; Coelho, M.; (2011). Carbohydrate particle models as carriers of large proteins: preparation and characterization of collagen hydrolysate loaded particles. *Submitted to* Acta Biomaterialia.

Chapter 1

Introduction

The food & beverage and pharmaceutical industries apply encapsulation process for a variety of reasons: encapsulation can protect the encapsulated compound from degradation by reducing its reactivity to its outside environment (e.g., oxygen, light and water); the material can be modified and made easier to handle, maintaining its original physical properties; the product can be tailor to control the release of the active compound in the desired site of action; the flavor and/ or color of the encapsulated compound can be masked; and it can be employed to separate components within a mixture that would otherwise react with one another. During the recent years, most major food companies around the world developed food and beverage lines incorporating functional ingredients, also called nutraceuticals, which provide health benefits that extend beyond basic nutrition. Often, these functional ingredients may be unstable and sensitive to oxygen, thus producing undesirable oxidation and reducing their shelf life. Encapsulation can provide the necessary protection against oxidation [1], therefore, extend the shelf life, enhance bioavailability and control the release of the bioactive ingredients.

This thesis is focused on the encapsulation of bioactive compounds by natural carbohydrate polymers. Carbohydrate particles were developed to preserve the original properties of the encapsulated compounds, protecting them from degradation, assuring their stability and consequently, allowing their application in the industry. Epigallocatechin gallate (EGCG) and collagen hydrolysate (CH) are the bioactive compounds considered, due to their

wide range of different biological activities.

In this work, EGCG and CH were encapsulated in a polymeric matrix by spray-drying technology. Since spray-drying is an economical, flexible, continuous operation, and produces particles of good quality, it is one of the most widely used encapsulation technique in the industry.

EGCG, the most abundant catechin found in green tea, exhibits strong antioxidant activity in diverse biochemical systems, due to its polyhydroxylated structure. This polyhydroxylated structure allows catechins to act as antioxidants either through the chelation of metals with redox properties or by acting as scavengers of free radicals. Studies have shown that EGCG has a variety of health effects, including antitumour, antioxidative and hypolipidemic activity [2]. EGCG has been demonstrated to inhibit matrix enzymes (proteases), known to play an important role in tumor invasion and metastases [3], inhibiting steps of the tumorigenesis process [4]. Preincubation of collagenase with EGCG reduced the collagenase activity [5]. Collagenase degrades collagen, a protein that plays an important role in the formation of tissues and organs, and is involved in various functional expressions of cells [6]. However, catechin stability is influenced by oxygen concentration and most importantly by pH, increasing the rate of oxidation as the pH value increases [7]. Upon consumption, catechins are exposed to alkaline environment in gastro-intestinal tract, where they degrade. This instability is one of the reasons for catechin poor bioavailability, which is less than 2-5%. Additionally, these catechins possess high systemic clearance [8]. To overcome these drawbacks EGCG was encapsulated in maltodextrin-gum arabic particles produced by homogenization and spray-drying, to preserve its antioxidant properties and improve its bioavailability.

Collagen and collagen hydrolysate are currently used in diverse fields including food, cosmetic and biomedical industries. Collagen is the major structural element of all connective tissues, which major property is to provide tensile strength to tissues such as tendons, ligaments, skin, cartilage, blood vessels, and bone [6]. More than 90% of the extracellular protein in the tendon and bone, and more than 50% in the skin consist of collagen. Collagen macromolecule is characterized by a triple helix configuration of three polypeptide subunits maintained by hydrogen bonding between the $-$NH group of glycine and the carbonyl group C=O of residues from another

polypeptide chain or by hydrogen bonding with water molecules [9]. The hydrolysis of collagen results in gelatin, a high molecular weight polypeptide. Further enzymatic degradation of gelatin derives in collagen hydrolysate, which contains peptides with a mean molecular weight of 3-6 kDa [10]. Due to its biochemical and nutritional properties, it has been proposed that the consumption of collagen hydrolysate might be beneficial for bone health, as a bioavailable source of peptides [11]. Bioactive peptides isolated from CH have shown several bioactivities such as antihypertensive and antioxidative activities [10]. Moreover, in patients with osteoporosis, oral intake of collagen hydrolysate with calcitonin had a stronger inhibitory effect on bone resorption than calcitonin alone. CH represents a key nutrient for bone health and thereby in the prevention of osteoporosis [12].

The most convenient route for the systemic delivery of proteins is oral, although proteins are susceptible to hydrolysis and modification at gastric pH and can be degraded by enzymes in the small intestine [13]. Bioavailability via this route is poor for molecules of molecular mass greater than several hundred daltons. Encapsulation and development of systems for oral protein drug delivery represent a key to solve these limitations, because they ensure physical protection to the encapsulated proteins against inactivation during the gastrointestinal transit, maintain their chemical integrity and assure their convenient delivery. These systems have generally been utilized for prolonging the circulation half-lives of proteins or for delivering targeted payloads of protein pharmaceuticals to specific tissues. Polymeric particles are promising candidates for oral delivery of proteins, such as CH, since they can adhere to the intestinal membrane and can increase residence of included compounds. A stable system of collagen hydrolysate-polysaccharides was developed, applying the same procedure employed in the EGCG/P formulation.

The objective of this research was to develop a system to ensure EGCG and CH stability, allowing their application in the industry. EGCG and CH loaded particles were produced by spray-drying technique, using as encapsulating material a mixture of polysaccharides, such as, maltodextrin and gum arabic. The results obtained demonstrate that the carbohydrate matrix is able to preserve EGCG and CH properties, as proof of concept to be used as polymer drug carrier.

This thesis is organized into six chapters. This chapter, introduction, covers the objectives and scope of this work. Chapter 2, background, presents an overview of the encapsulation concept, techniques and coating materials, including the advantages and disadvantages of their application. Chapter 3, materials and methods, describes the methodology involved in the preparation and characterization of the loaded and unloaded carbohydrate particles. Chapter 4, catechin loaded particles, discusses the observations and results obtained for the EGCG/P. Chapter 5, collagen hydrolysate loaded particles, analyzes the results achieved concerning the formulation and characterization of the CH/P, in comparison to EGCG/P. Chapter 6, concluding remarks, summarizes the main findings of this thesis.

Chapter 2

Background

Contents

2.1 Encapsulation concept

In recent years, a special attention is given to certain bioactive compounds, due to their health benefits. The development of new functional foods and pharmaceuticals requires technologies for incorporating health-promoting compounds, without reducing their bioavailability or functionality. In order to overcome the susceptibility and improve the stability of bioactive compounds during processing and storage, encapsulation technology has been applied in food, nutraceutical and pharmaceutical industries. Encapsulation is a technique, which involves the incorporation of a chemically sensitive

compound in a matrix or sealed capsule, protecting it against adverse reaction, preventing its degradation and increasing its shelf life [14]. Besides protecting it from the harsh processing conditions and adverse storage environment, the encapsulation of bioactive compounds can also achieve targeted delivery and controlled release of entrapped substances to the specific site. In addition, encapsulation may also be useful for taste and odour masking purposes, since some active compounds often have very strong flavours.

There are numerous drug delivery systems, including the polymeric based (polymeric particles) carriers, which are considered to be among the most suitable systems for antioxidant delivery. Particles are solid colloidal structures composed of natural or synthetic polymers. Nanoparticles have a size < 0.2 µm and microparticle's size range from 0.2 to 5000 µm. Depending on the shape of the particle, they can be classified into capsules (reservoir system) and spheres (matrix system). Capsules are vesicular systems with the drug in a core surrounded by a solid shell, whereas spheres are porous matrix systems in which the drug is uniformly dispersed (Figure 2.1).

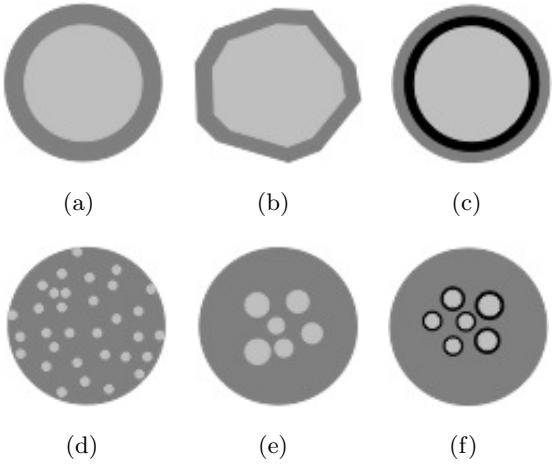

Figure 2.1: Schematic drawing of capsules and spheres: Capsule (a), Irregular capsule (b), Capsule with two layers (walls) (c), Sphere (d), Capsule with several cores (e), Group of capsules (f).

The two principal routes of administration of polymeric particles are the oral and the intravenous routes. Once they have reached the target tissue, drug release depends on the physicochemical characteristics of both carrier and drug: it may occur by desorption from the colloidal surface, by

diffusion through the polymeric wall (capsules) or through the polymeric matrix (spheres), or by particle erosion [15]. In controlled release systems, degradation of the matrix material frequently occurs as a determining factor for the release of the encapsulated compound at desired site, time and at specific rate.

2.2 Encapsulation techniques

The selection of the encapsulation method depends on the physical and chemical properties of the compound to encapsulate and the coating material (or matrix), and the final application. The selection of the encapsulation method and matrix materials is interdependent [14].The current encapsulation methods include coacervation [14], [16], fluidized-bed coating [14], [17], spray-cooling/chilling [18], freeze-drying [19], [20], liposome entrapment, extrusion [21] and spray-drying [22], [23], among others.

2.2.1 Coacervation

Coacervation is defined as the separation of colloidal systems into two liquid phases. The basic mechanism involved in this method is the formation of an emulsion and subsequent precipitation of the continuous phase around the droplets of the discontinuous phase. It employs a three phase system, which includes a manufacturing vehicle (solvent), the material to be encapsulated and the coating material. Coacervation process consists of three steps: (i) formation of the three immiscible phases while mixing under controlled conditions; (ii) deposition of the coating material around the core material; (iii) shrinkage and solidification of the liquid coating to form the solid microcapsules, by thermal, cross-linking or desolventization techniques [14], [16]. Natural extracts, such as Yerba mate extract, has been encapsulated by coacervation in a polysaccharide based system of alginate-chitosan, to promote its protection and controlled release, with a loading efficiency of 50% [24].

Coacervation technique is widely used in the industry, however, the coacervation method possesses some drawbacks. This process is not well suited for producing spheres in the low size range, is very expensive and rather complex.

2.2.2 Fluidized-bed coating

The different fluidized-bed coating methods are: top-spray, bottom-spray, and tangential-spray. In top-spray fluidized bed coating, the coating polymer, usually in the form of an aqueous solution, is continuously sprayed downwards onto the top surface of the fluidized bed. Each particle receives a small amount of coating material each time it passes through the spraying region, which is the bed region in which sprayed droplets and fluidized particles coexist. Repeated movement from and towards the spraying region results in a gradual built-up of a relatively uniform coating layer surrounding each particle [17]. Top-spray method seems more feasible when compared with the other methods, due to its high versatility, relatively high batch size, and relative simplicity [14]. Coating materials, also referred to as wall materials, are a wide variety of natural or synthetic film-forming polymers. This technique is applicable for hot-melt coatings such as hydrogenated vegetable oil, stearines, fatty acids, emulsifiers, and waxes, or solvent-based coatings such as starches, gums, maltodextrins [25]. This technique is used to encapsulate nutritional substances such as vitamin C, B vitamins, ferrous sulfate, ferrous fumarate, sodium ascorbate, potassium chloride, and a variety of vitamin/mineral premixes [14].

The main constraints of fluidized-bed coating as an encapsulation process are the type of core material (i.e. free flowing solid particles with a size varying between 100 µm and several millimeters), and the type of coating material (i.e. mainly water-soluble biopolymers) [26]. In essence, fluidized bed coating is a complex heat and mass transfer process that involves many different microprocesses, such as droplet production, evaporation, heat transfer, droplet impingement, droplet spreading and particle behavior in a fluidized bed. However, little is known about the interactions between these microprocesses and how they relate to process yields, coating uniformity and side effect occurrences [17].

2.2.3 Spray-cooling/chilling

Spray-cooling/chilling is the technology routinely used for the encapsulation of a number of organic and inorganic salts as well as textural ingredients, enzymes, flavors and other functional ingredients to improve heat stability,

delay release in wet environments, and/or convert liquid hydrophilic ingredient into free flowing powders [18]. In spray-cooling and spray-chilling, the core and wall mixtures are atomized into the cooled or chilled air, which causes the wall to solidify around the core. In spray-chilling, the most commonly used coating materials are molten fractionated and hydrogenated vegetable oils with a melting point of 32-42 ℃, vegetable oils or other materials with a melting point of 45-12 ℃ are often used in spray-cooling. However, a wide range of other encapsulating materials may be employed. In spray-chilling, there is no mass transfer (i.e., evaporation from the atomized droplets); therefore these solidify into almost perfect spheres to give free-flowing powders [14].

Microcapsules prepared by spray-cooling and spray-chilling are insoluble in water due to the lipid coating. Consequently, these techniques tend to be utilized for encapsulating water-soluble core materials such as minerals, water-soluble vitamins, enzymes, acidulants, and some flavors. Another disadvantage of spray-cooling and spray-chilling is that special handling and storage conditions can be required.

2.2.4 Freeze-drying

Freeze-drying, also known as lyophilization, is a process used for the dehydration of almost all heat-sensitive substances that are unstable in aqueous solutions. Freeze-drying works by freezing the material and then reducing the surrounding pressure and adding enough heat, to allow the frozen water in the material to sublimate directly from the solid phase to the gas phase [21]. Recently, Laine *et al.* (2008) encapsulated phenolic-rich cloudberry extract by freeze-drying, using maltodextrins DE5-8 and DE18.5 as wall materials. The microencapsulated cloudberry extract offered better protection for phenolics during storage, while the antioxidant activity remained the same or even improved slightly [19].

Nevertheless, there is also some evidence of freeze-drying induced encapsulation being unable to improve stability or bioactivity. In addition, this drying technique is less attractive than others because the costs of freeze-drying are up to 50 times higher than spray-drying [20] and the storage and transport of particles produced is extremely expensive, the commercial applicability is also severely restricted by the long processing time [27].

2.2.5 Liposome entrapment

Liposomes are colloidal particles consisting of a membranous system formed by lipid bilayers encapsulating an aqueous phase [21]. When phospholipids, such as lecithin, are dispersed in an aqueous phase, the liposomes form spontaneously. One can have either aqueous or lipid-soluble material enclosed in the liposome. The underlying mechanism for the formation of liposomes is basically a hydrophilic-hydrophobic interaction between phospholipids and water molecules. A major advantage of their use is the target delivery and the ability to control the release rate of the incorporated materials. Bioactive compounds encapsulated into liposomes can be protected from digestion in the stomach, and show significant levels of absorption in the gastrointestinal tract, leading to the enhancement of bioactivity and bioavailability [21]. Kirby *et al.* have developed a process to stabilize vitamin C in the aqueous inner core of liposomes. Encapsulation of vitamin C gave significant improvements in its shelf life.

The main issues in liposome encapsulation the scaling up of the microencapsulation process at acceptable cost-in-use levels and the delivery form of the liposome-encapsulated compound. Usually, liposome formulations are kept in relatively dilute aqueous suspensions and this might be a very serious drawback for the large-scale production, storage, and shipping of encapsulated compounds [14].

2.2.6 Extrusion

Extrusion is an entrapping method, which involves forcing a core material in a molten carbohydrate mass through a series of dies into a bath of dehydrating liquid. The pressure and temperature employed are typically <100 psi and seldom 115 ℃[14]. In this process, the coating material hardens on contacting the liquids, forming an encapsulating matrix to entrap the core material. Extruded filaments are then separated from the liquid bath, dried to decrease de moisture content and sized. High-dextrose equivalent corn syrup and a combination of sucrose and maltodextrin are often used as the encapsulation matrix [21]. Extrusion has been used to encapsulate different types of flavors and vitamin C [27]. The major advantage of this method is that the material is completely surrounded by the wall material, providing

a good stability against oxidation and therefore prolonging the shelf life.

The limitations of extrusion include its relatively high cost, low flavor loading, low solubility in cold water, and high process temperature. Its processing costs are estimated to be almost double in comparison to spray-drying. The extruded product is not readily soluble in cold water and not stable in beverage application because of its large particle size. Furthermore, the compound to be extruded must be able to tolerate temperatures of 110-120 ℃ for a long period of time.

2.2.7 Spray-drying

Spray-drying is widely used in large-scale production of encapsulated substances, such as antibiotics, medical ingredients, additives, vitamins and polyphenols, among others. The merits of the process have ensured its dominance; these include availability of equipment, low process cost, wide choice of carrier solids, good retention of volatiles, good stability of the finished product and large-scale production in continuous mode.

Spray-drying also offers some advantages to other drying methods; particle size of the powder is controlled in a single step, and the morphology and the density of the particles can be controlled. Size and density are particle properties, which are crucial for several delivery systems (e.g., powders for inhalation and suspensions for dermal delivery). Spray-drying can be used for many heat-labile (low-boiling point) materials because of the lower temperatures that the core material reaches [27]. The process involves the homogenization of the substance to be encapsulated with the carrier material at a different ratio. The mixture is then fed into a spray-dryer and atomized with a nozzle or spinning wheel. Water is evaporated by the hot air contacting the atomized material. The resulting capsules are then transported to a cyclone separator for recovery (2.2).

In order to obtain good encapsulation efficiency and even if the wall material is suitable, optimal spray-drying conditions must be used. The main factors in spray-drying that must be optimized are feed temperature, air inlet and air outlet temperatures [22]. The best spray-drying conditions are a compromise between high air temperature, high solid concentration of the solution, and easy pulverization and drying without expansion and cracks of final particles [23].

Retention of core material during encapsulation by spray-drying is achieved by chemical and physical properties of the wall and core materials [20],[28], solid content of the dryer, processing temperature and also by the nature and the performance of the encapsulating support, i.e. emulsion-stabilizing capabilities, film-forming ability and low viscosity at a high concentration [28],[29]. The functionality profile of wall materials that are optimal for spray-drying includes high solubility in water, low viscosity at high concentration, effective emulsification, film-forming characteristics and efficient drying properties. One limitation of the spray-drying technology is the limited number of shell materials available. Since almost all spray-drying processes in the food industry are carried out from aqueous feed formulations, the shell material must be soluble in water at an acceptable level [14]. Typical shell materials include gum acacia, maltodextrins, hydrophobically modified starch, and mixtures thereof. Other polysaccharides and proteins can be used as wall materials in spray-drying, but their usage becomes very time-consuming and expensive because of their low solubility in water: the amount of water in the feed to be evaporated is much larger due to the lower dry matter content and the amount of active compound in the feed must be reduced accordingly [14]. There is an optimum infeed solid's level for each carrier material, which is the level at which the maximum solubility of the carrier is achieved. This is typically determined experimentally for a given dryer and carrier system [30]. There are various types of spray-dryers used in the industry, differing in size, shape, airflow, type of atomization, etc. In spite of this, they all have the same basic parts in common as shown in 2.2.

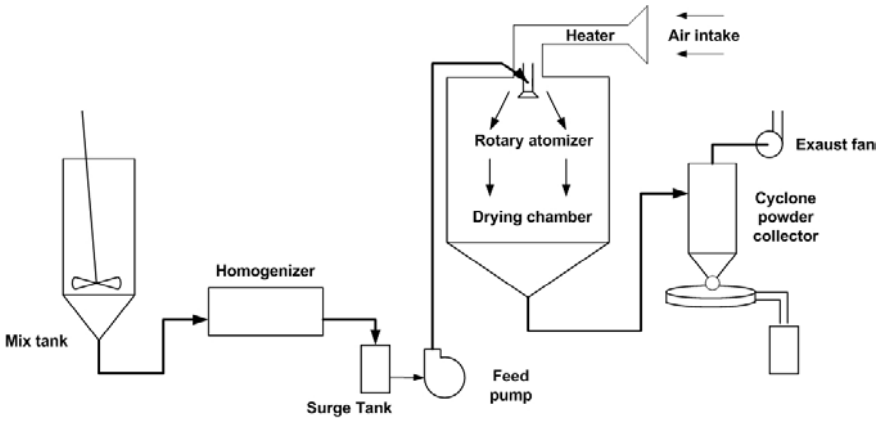

Figure 2.2: Typical spray-drying system with a centrifugal atomizer.

Drying air is most commonly heated by direct firing with natural gas since it is clean burning. The material to be dried (infeed) is prepared separately in a mix tank where materials are dissolved, homogenized and then it is pumped into the atomizer. Atomization is typically accomplished by either a single-fluid high-pressure spray nozzle or centrifugal wheel [30]. The goal of this stage is to create a maximum heat-transferring surface between the dry air and the liquid in order to optimize heat and mass transfers. Spray-dryers working in cocurrent, i.e., product and drying air enter the dryer flowing in the same direction, have lower drying times and do not subject the active substance to as much heat as counter current systems. In cocurrent process the hot air inlet temperature is typically 150-220 ℃, evaporation occurs instantaneously and for which dry powders will be exposed to moderate temperatures (typically 50-80 ℃) which limits thermal degradations. The atomized infeed is cooled by water evaporation and only rises to the dryer exit air temperature when the drying rates low. Drying chamber shape generally is cylindrical with either a conical or flat-bottom. After leaving the drying chamber, the dry product passes through a cyclone collector, sieve, and finally is packaged in a moisture barrier container.

The selection of the wall material is another factor that governs the encapsulation efficiency by spray-drying.

2.3 Systems and Wall materials

The criteria for selecting a coating material are mainly based on the physicochemical properties such as solubility, molecular weight, glass/melting transition, crystallinity, diffusibility, film forming and emulsifying properties. Moreover, the costs should also be considered. Thus, judicious choice of encapsulating material according to the desired application is an important task [23]. The matrix is designed to protect the encapsulated compound from factors that may cause its deterioration, to prevent a premature interaction between the encapsulated material and other substances, to limit volatile losses, and also to allow controlled or sustained release under desired conditions [31]. Depending on the core material and the characteristics desired in the final product, wall materials can be selected from a wide variety of natural and synthetic polymers. Usually, the wall materials employed for encapsulation by spray-drying are milk or whey proteins, gelatin, low molecular weight carbohydrates, hydrocolloids like gum arabic and more recently local materials, such as mesquite gum [23], [32], [33].

Mesquite gum represents an alternative to some commonly used materials, since it has been reported as a good encapsulating agent. It is a neutral salt of a complex acidic branched polysaccharide formed by a core of β-D-galactose residues, comprising a (1-3)-linked backbone with (1-6)-linked branches, bearing L-arabinose, L-rhamnose, β-D-glucuronate and 4-O-methyl-β-D-glucuronate as single sugar or oligosaccharide side chains. It also contains a small amount of protein (up to 6%) [34]. Mesquite gum has been reported as having the ability to encapsulate orange peel oil (80.5% of the starting oil) but to a lesser extent than gum arabic (93.5% of the starting oil) [35]. Cardamom-based oil microcapsules were successfully produced by spray-drying using mesquite gum [33]. The stability against drop coalescence of the emulsions was elevated for all the gum:oil ratios studied. High flavor retention (83.6%) was attained during microencapsulation by spray-drying when a proportion of 4:1 gum:oil was used. This confirmed the interesting emulsifying properties and good flavor-encapsulation ability that qualify mesquite gum as an alternative encapsulating medium. Mesquite gum has a disadvantage in comparison with other gums, in that it has darker color.

The functional properties of proteins allow them to be a good coating material for encapsulation by spray-drying. Furthermore, proteins possess high binding properties for the flavor compounds. The most commonly used proteins for encapsulating food ingredients by spray-drying are milk or whey proteins and gelatin [23]. Because they possess functional properties required for microcapsule forming wall material [36], whey proteins have been successfully used as wall system to encapsulate anhydrous milk fat by spray-drying and an encapsulation yield greater than 90% was obtained [37]. Heat treatments of whey proteins were shown to affect the functional properties of spray-dried powder probably by protein denaturation [38]. During spray-drying the temperature of the drying droplet increases slightly, while its water content decreases at the same time. Protein denaturation, especially globular proteins, can occur only when two parameters are combined: high temperature and high water activity of the drying droplet. As a result, it is very difficult to predict the effect of spray-drying process on the stability of wall proteins [23].

Likewise, gelatin is a water-soluble protein with wall-forming ability in spray-drying [32] and it consists mainly in glycine, proline and 4- hydroxyproline residues [21]. Based on the drying characteristic curves, Imagi *et al.* (1992) showed that, compared to maltodextrin, pullulan, glucose, maltose and mannitol, gelatin had all the properties of an effective entrapping agent: high emulsifying activity, high stabilizing activity and a tendency to form a fine dense network upon drying [39]. The addition of a small amount (1% (w/w)) of gelatin could increase the retention of ethyl butyrate when gum arabic is used as emulsifier. According to Yoshii *et al.* (2001), the early formation of the surface crust due to the presence of gelatin, prevented the loss of ethyl butyrate emerged from the unstable ethyl butyrate emulsion [40]. Pierucci *et al.* (2006) reported that pea protein can be considered as a good coating agent for the microencapsulation of ascorbic acid [41]. In all cases, it should be noticed that there are sometimes certain issues that may limit the use of proteins as encapsulating agents, for example, labelling, allergy and precipitation when protein based microcapsules are added to products having pH near their isoelectric point.

Carbohydrates such as starches, corn syrup solids, chitosan and maltodextrins have been usually used as encapsulating agents. These materials

are considered as good encapsulating agents because they exhibit low viscosities at high solids contents and good solubility, but most of them do not possess the interfacial properties required for high encapsulation efficiency and generally associated with other encapsulating materials such as gums or proteins [23].

Chitosan is a cationic polymer obtained from chitin comprising copolymers of $\beta(1\rightarrow 4)$-glucosamine and N-acetyl-D-glucosamine. Chitin is a natural polysaccharide found particularly in the shell of crustacean, cuticles of insects and cell walls of fungi and is the second most abundant polymerized carbon found in nature [42]. Chitosan is a hydrophilic, biocompatible, and biodegradable polysaccharide of low toxicity. In recent years, it has been used for development of oral controlled drug delivery systems. In previous studies, sustained-release carriers of vitamin C have been prepared by using cross-linked chitosan as a wall material by spray-drying technique [14]. Chitosan has also been used as a wall material in spray-drying of olive leaf extract (OLE) [43]. The loading percent of polyphenolic compounds was 27%, and the OLE loaded microspheres normally had a smooth surface morphology. The FTIR spectroscopy results indicated that the majority of the OLE in the chitosan microsphere was physically encapsulated in the chitosan matrix. Hu *et al.* (2008) also successfully encapsulated tea catechins in chitosan-tripolyphosphate (CS-TPP) nanoparticles by ionotropic gelation method. Under the acidic conditions, the -$NH3^+$ protonized from -NH2 of chitosan can interact with an anion such as tripolyphosphate to form microgel particles [44]. The entrapment efficiency of chitosan particles was low, varying from 20% to 50%, depending mainly on the chitosan molecular weight and the proportion between chitosan and the ionic cross linker (sodium tripolyphosphate). Additionally, chitosan is only soluble in acidic environment, which decreases the availability of catechins in the gastrointestinal tract. Many factors affect the entrapment efficiency of the drugs in chitosan microspheres, e.g. nature of the drug, chitosan concentration, drug polymer ratio, stirring speed, etc. Generally a low concentration of chitosan shows low encapsulation efficiency. However, at higher concentrations, chitosan forms highly viscous solutions, which are difficult to process [45].

Maltodextrins are hydrolyzed starches produced by partially hydrolysis of starch with acid or enzymes, consisting of β-D-glucose units linked mainly by glycosidic bonds (1→4) and are usually classified according to their dextrose equivalency (DE). Hydrolyzed starches have the advantages of being low cost, bland in flavor, and good flavor protection against oxidation. Maltodextrins are reported to improve shelf life of orange oil [46] and carrot carotene. Wagner and Warthesen, also reported that storage stability of core materials increased as hydrolyzed starches DE increased [47]. The DE of a maltodextrin determines its reducing capacity and is inversely related to its average molecular weight [48]. Maltodextrins are widely used for flavors and polyphenol encapsulation. Maltodextrins provide good oxidative stability to encapsulated oil, but exhibit poor emulsifying capacity and emulsion stability and low oil retention. Ethanol extracts of black carrots, which contain a high level of anthocyanins, have been spray-dried using maltodextrins as a carrier and coating agents [49]. High air inlet temperatures (>160-180 ℃) caused greater anthocyanin losses, while the maltodextrin of DE 20-21 gave the highest anthocyanin content powder at the end of the drying process. Maltodextrin can also be mixed with gum arabic as wall material to provide a better protection of the encapsulated compound. A mixture of maltodextrin (60%) and gum arabic (40%) has been used for encapsulation of procyanidins from grape seeds [50].The ratio of core substance to wall material was 30:70 w/w, while the concentration of the slurry was 20% w/v. The encapsulation efficiency was up to 88.8%, and the procyanidin was not changed during drying and the procyanidin microcapsule membrane was uninterrupted and with fairly good integrity. The stability of the products was obviously improved by spray-drying [21]. Maltodextrin chemical structure is illustrated in Figure 2.3.

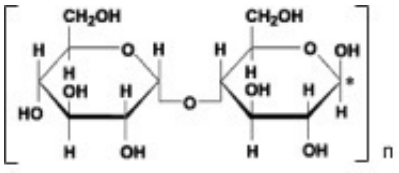

Figure 2.3: Chemical structure of maltodextrin.

Gum arabic, a natural plant exudates polysaccharide of acacia, is a well-known effective wall material for many years and stills a good choice as wall material due to its stable emulsion and good volatile retention [51]. Gum arabic is predominantly a branched chain, complex polysaccharide that is either neutral or slightly acidic, depending on the pH. It is a highly heterogeneous material that possesses both hydrophilic and hydrophobic affinities. This polysaccharide is characterized by a high proportion of carbohydrate, in which D-galactose and L-arabinose are the predominant monosaccharides responsible for the hydrophilic affinity, and a low proportion of protein (approximately 2%), mostly composed of hydroxyproline. The carbohydrate structure consists of a backbone of 1,3-linked β-D-galactopyranosyl units with extensive branching at the C6 position. The branches consist of galactose and arabinose, which terminate with rhamnose and glucuronic acid [52]. The chemical structure of the main components of gum arabic, D-galactose (40%), L-arabinose (24%) and D-glucuronic acid (21%) are illustrated in Figure 2.4.

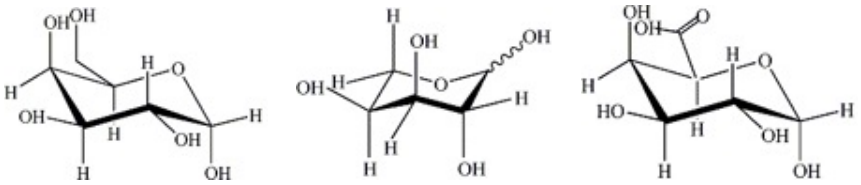

(a) (b) (c)

Figure 2.4: Chemical structure of gum arabic main components: D-galactose (a), L-arabinose (b) and D-glucuronic acid (c).

Gum arabic has been the most widely used encapsulating material in encapsulation by spray-drying, mainly because of its good emulsifying capacity and low viscosity in aqueous solution, which aids the spray-drying process. The emulsification properties of the gum arabic are attributed to the presence of the protein fraction. Kanakdande, Bhosale and Singhal (2007) reported that gum arabic is a better wall material for encapsulation of cumin oleoresin by spray-drying as compared to other wall materials [53]. In addition, it provides good retention of volatile substances and confers effective protection against oxidation [48]. Problems associated with the use of gum arabic in encapsulation are high cost and limited supply.

Chapter 3

Materials and Methods

Contents

3.1 Materials

Gum arabic (250 kDa) and maltodextrin (1000 Da) were purchased from Sigma-Aldrich Co. (USA) and Grain Processing Corporation (USA), respectively. Catechins Sunphenon EGCG (458 Da) and Collagen hydrolysate HM (3600 Da) were purchased from Taiyo Kaguku (Japan) and Copalis (France), respectively. All chemicals were used without further purification. The ultrapure water (resistivity of 18.2 MΩ.cm) was obtained using an EasyPure RF purification system (Nanopure Diamond Water Purification, Barnstead Thermo Scientific, USA).

3.2 Methods

3.2.1 Preparation of carbohydrate particles

Gum arabic was dissolved in ultrapure water at 50 to 60 ℃ adding the maltodextrin, in a proportion of 60 wt.%, under magnetic stirring for 30 min to form an aqueous suspension. The suspension was homogenized at a constant speed (9500 rpm) with a dispersing device IKA DI25 Basic (Staufen, Germany). The resultant suspension was fed to a spray-dryer (designed by Niro A/S) at the following conditions: inlet air temperature between 150-170 ℃, outlet air temperature between 50 and 60 ℃ and a liquid feed flow rate of 10 ml/min. The spray-dried powder was then collected to the spray-dryer's glass collecting vessel. The epigallocatechin gallate (EGCG) and collagen hydrolysate (CH) loaded particles, were prepared following the same procedure but adding EGCG and CH, respectively, to the suspension before homogenization, in the desired proportion (wt.%).

3.2.2 Characterization of carbohydrate particles

3.2.2.1 Electron Microscopy: Scanning and Transmission Electron Microscopy

There are two common types of electron microscopes: scanning and transmission. Scanning electron microscopy (SEM) permits the observation and characterization of heterogeneous organic and inorganic materials on a nanometer (nm) to micrometer (µm) scale. This technique is extensively used due to its capability of obtaining three-dimensional-like surface images of a very wide range of materials. In SEM, the area to be examined is irradiated with a finely focused electron beam, which may be swept in a raster across the surface of the specimen to form images or may be static to obtain an analysis at one position. The types of signals produced from the interaction of the electron beam with the sample, can be used to examine many characteristics of the sample, such as, surface topography, morphology, crystallography and composition [54]. In recent years, cryo-preparation equipment was developed for the conventional scanning electron microscope. This innovation has enabled unique SEM observation of rapidly cooled soft or liquid specimens at low-to-medium magnification (50-50000x) [55].

Transmission electron microscopy (TEM), on the other hand, produces an image that is a projection of the entire object, including the surface and the internal structures. The incoming electron beam interacts with the sample as it passes through the entire thickness of the sample. Therefore, objects with different internal structures can be differentiated because they give different projections. However, the projection is of necessity two-dimensional against the view screen and relations in the z-axis between structures are lost. Besides, the samples need to be thin, or they will absorb too much of the electron beam.

In this study, SEM analysis of the spray-dried particles was performed on a JEOL SEM 6301F microscope (Tokyo, Japan). The samples in solid state were previously fixed on a brass stub using double-sided adhesive tape. Then they were coated with a thin layer of platinum in vacuum to be electrically conductive. Micrographs were taken at an excitation voltage of 7 kV. Cryogenic scanning electron microscopy was used for EGCG/P characterization in aqueous suspension. Samples were fixed on a holder with a layer of carbon-rich conductive glue (conductive to allow discharge of electrons) and rapidly frozen with liquid nitrogen. The holder with frozen material was held in liquid nitrogen to be coupled to a rod and pulled back into a small cylindrical container. This is done to transfer the sample to the high vacuum cryo-unit and prevent too much contamination with gas particles while sliding the sample into the cryo-chamber. The cryo-chamber is equipped with a knife that can be handled from outside by means of a level to fracture the sample for applications in which imaging of the surface of inner structures is aimed. Next, the temperature was raised slightly to sublime any condensed water off the surface of the sample, which was then coated with a thin layer of gold-palladium for good conductance of electrons. Finally the entire or fractioned material was further inserted into the observation chamber with a rod. For TEM analysis, EGCG/P were suspended in PBS (46 mg/ml) and 5 µl were placed on glow discharged formvar-coated Ni grids and stained with 1% filtered uranyl acetate solution. The grids were analyzed in a Zeiss microscope (Germany) operated at 60 kV.

3.2.2.2 Atomic Force Microscopy

Atomic force microscopy (AFM), is powerful tool in imaging that can provide three-dimensional images of surface topography of biological specimens in ambient liquid or gas environments. The high resolution (in the nanometer range) of the atomic force microscope allows topographical imaging of samples [56] and also provides information about the mechanical properties of materials such as stiffness, viscoelasticity, hardness, or adhesion force between the probe and sample can be extracted from the collected force-distance curves by mathematical analysis [57]. An AFM consists of a sharp tip at the end of a flexible cantilever which is moved across a sample surface by piezoelectric actuators. The cantilever deflection may be measured in different ways in order to reproduce the sample topography. Force measurements can be correlated with topography measurements. Operating modes can be classified as contact, non-contact and intermittent. In intermittent mode, the cantilever oscillates near its resonant frequency and lightly taps the surface during scanning. The tip rapidly moves in and out of the sample surface with an amplitude which is sufficiently high to overcome adhesion forces so that it stays in contact only for a short fraction of the oscillation period. Forces that act between the sample and the tip will not only cause a change in the oscillation amplitude, but also change in the resonant frequency and phase of the cantilever. The amplitude can be presented in height (topography) or interaction (amplitude or phase) images.

EGCG/P shape and mechanical strength were studied by AFM, using a JPK NanoWizard II BioAFM microscope (Berlin, Germany) assembled on a Carl ZEISS Axiovert 200 (biomaGUNE, San Sebastian, Spain). Standard glass cover slips of 0.17 mm thickness were washed with acetone and cleaned with tissue paper before being immersed in a 2% Hellmanex solution for 30 min. To decrease the negative charge density of the glass cover slips surface, they were coated with cationic PEI and rinsed with ultrapure water (0.01 M, NaCl 0.5 M). The substrates were then washed with ultrapure water and placed in a UV cleaner apparatus for 30 min. Afterward the substrate was incubated in a particle suspension (0.1 mg/ml) for 20 min and subsequently washed with water. The substrate was mounted into the cover slip holder with 500 µl of buffer solution. AFM imaging was obtained with unmodified

silicon nitride tips (DNP, Veeco Instruments, USA) operating in intermittent contact mode. The nominal radius of curvature of the cantilevers was 20 nm and the spring constant of the cantilever, kc, was calculated by the thermal method and corresponds to 336±18 mN/m.

3.2.2.3 Dynamic Light Scattering and Zeta Potential

Dynamic Light Scattering (DLS) is the technique most used to determine the size of particles and size distribution in dispersion. Shining a monochromatic light beam, such as a laser, onto a solution with particles in Brownian motion, causes a Doppler Shift when the light hits the moving particle, changing the wavelength of the incoming light. This change is related to the particle size. It is possible to determine the particle size distribution and give a description of the particle's motion in the medium, measuring its diffusion coefficient and using the autocorrelation function. The diffusion coefficient, D, which is characteristic of the Brownian motion can be related to k_B, the Boltzmann constant, T, the temperature, η, the viscosity and, d_p, the particle hydrodynamic diameter, using the Stokes-Einstein relation [58]:

$$D = \frac{k_B T}{3\pi\eta d_p} \tag{3.1}$$

The hydrodynamic average intensity radius of the particles, R_H, can be calculated from Eq. 3.1:

$$R_H = \frac{k_B}{6\pi\eta D} \tag{3.2}$$

When a particle suspension is illuminated, the intensity of the light scattered fluctuates with time because of the Brownian movement of the particles. DLS consists of measuring these fluctuations as a function, in order to deduce the diffusion coefficient D and, thus, dp. The time period necessary to detect fluctuations ranges between 10^{-4} and 10^{-3} s, with small particles moving faster than large ones. A photocorrelator determines an autocorrelation function as a function $G(\tau)$ of time. For a monomodal distribution, $G(\tau)$ is proportional to $exp(-2DK^2\tau)$, where K is the scattering

vector, which is a function of n, the refraction index of the medium, λ, the wavelength and θ, the detection angle. For a multi-modal distribution, the interpretation of $G(\tau)$ is more complex because it is a sum of several exponentials, each of which corresponds to one of the particle populations. The major difficulty is in determining the contribution of each population to the overall signal. Moreover, if the intensity due to one of the populations is very low compared to the intensity scattered by the others, this population of particles will be very difficult to detect. This situation arises when one particle population accounts only for an overly small fraction of the total. As we mentioned above, the intensity distribution is an oscillatory function of d_p, so particles of a specified size may correspond to weak detection intensity at a fixed detection angle. This can be overcome in the case of multimodal particle size and particle size distributions, by performing measurements at different detection angles. In this case, the compilation of results collected at each detection angle results in a complex mathematical analysis. In case of a monomodal particle size and particle size distributions, light scattering is a very efficient and fast technique.

The concept of zeta potential is another important parameter to study the particle stability in suspension. The zeta potential is determined by electrophoretic mobility, applying the Henry equation (Eq. 3.3). The electrophoretic mobility is obtained performing an electrophoresis experiment on the sample and measuring the velocity of the particles using Laser Doppler Velocimetry. The magnitude of the zeta potential gives an indication of the potential stability of the colloidal system. One system is colloidal when one of the three states of matter; gas, liquid and solid, is finely dispersed in one of the others. If all the particles in suspension have a large negative or positive zeta potential then they will tend to repel each other and there is no tendency to flocculate or aggregate. However, if the particles have low zeta potential values then there is no force to prevent the particles coming together and flocculating. The general dividing line between stable and unstable suspensions is generally taken at either +30 mV or -30 mV. An important consequence of the existence of electrical charges on the surface of particles is that they will exhibit certain effects under the influence of an applied electric field. When an electric field is applied across an electrolyte, charged particles suspended in the electrolyte are attracted towards

the electrode of opposite charge. This movement is called electrophoresis. Viscous forces acting on the particles tend to oppose this movement. When equilibrium is reached between these two opposing forces, the particles move with constant velocity. The velocity of a particle in an electric field is commonly referred to as its electrophoretic mobility. With this knowledge we can obtain the zeta potential of the particle by application of the Henry equation [59]:

$$U_E = \frac{2ezf\,(ka)}{3\eta} \tag{3.3}$$

where z is the zeta potential, U_E, is the electrophoretic mobility, e, is the dielectric constant, η, is the viscosity and $f\,(ka)$ is the Henry's function. For aqueous medium and moderate electrolyte concentration, $f\,(ka)$ is 1.5. It is the electrophoretic mobility that is directly measured and converted to zeta potential, according to Smoluchowski equation (Eq. 3.5):

$$z = \frac{\eta U_E}{e} \tag{3.4}$$

The essence of a classical micro-electrophoresis system is a cell with electrodes at either end to which a potential is applied. Particles move towards the electrode of opposite charge, their velocity is measured and expressed in unit field strength as their mobility.

Measurements of particle size and zeta potential of the particles were performed by dynamic light scattering and Laser Doppler Velocimetry, respectively, using a Zetasizer Nano ZS (Malvern Ltd, UK). Spray-dried particles were dispersed in ultrapure water and the resulting suspension was evaluated.

3.2.2.4 Particle Tracking Analysis

Nanoparticle Tracking Analysis (NTA) is a unique technique of visualizing and analyzing particles in liquids from 10 to 1000 nm [60]. Based on a laser illuminated microscopic technique, Brownian motion of nanoparticles is analyzed in real-time by a CCD camera, each particle being simultaneously but separately visualized and tracked by a dedicated particle tracking

image analysis program. NTA tracks all random particles movements and calculates the diffusion coefficient. Then using the Stokes-Einstein equation (Eq. 3.1) particle size (hydrodynamic diameter) is estimated. Nanoparticle tracking analysis experiments were performed using a digital microscope LM10 System (NanoSight, Salisbury, UK). A small amount of the diluted sample in ultrapure water was introduced into the chamber by a syringe. EGCG/P were observed using the digital microscope. The video images of the particle movement under Brownian motion were analyzed by the NTA image analysis software (NanoSight, version 2.0). For each sample analysis, 50-70 s video clips were taken.

3.2.3 Particle internal structure

The use of mercury porosimetry to obtain apparent density as well as the use of helium pycnometry to obtain true density, allowed the determination of the total porosity, ε_p, of the spray-dried particles, according to Eq. 3.5:

$$\varepsilon_p = \left(1 - \frac{\rho_{bulk}}{\rho_{true}}\right) \times 100\% \tag{3.5}$$

where ρ_{bulk} is apparent density and ρ_{true} is true density, determined by mercury porosimetry and helium pycnometry, respectively. Porosity describes the fraction of voids in a given volume of a material, i.e., the total porosity is the ratio between the volume of voids and the overall volume of material.

3.2.3.1 Helium Pycnometry

True density is defined as the ratio of the mass to the volume occupied by that mass. Therefore, the contributions to the volume made by pores or internal voids are excluded. True density is also often termed as helium displacement density. Measuring the true density is accomplished by employing Archimedes principle of fluid displacement and Boyle's law to determine the volume. The displaced fluid is a gas, which can penetrate the finest pores and thereby obtain maximum accuracy. Helium (He) is usually used in these experiments as its small dimensions assure penetration into crevices and pores approaching one Angstrom (Å) in dimension. Its behavior as an

ideal gas is also desirable as the instrument uses the ideal gas equation to measure the volume occupied by the sample [61].

True density of the spray-dried particles was determined using a He pycnometer. EGCG/P and CH/P samples were weighted and placed in a cylinder of known volume, which was flushed with He and closed. The pressure inside the cylinder was adjusted to a predetermined value and its exact value was noted. A second, similar cylinder of known volume was filled with He, under a different, known pressure. A valve was then opened between these two cylinders and the new pressure was noted. The ratio between these two pressures is directly related to the volume occupied by the solid material in the sample, providing the density of the particle skeleton. The measurements were repeated at least three times.

3.2.3.2 Mercury Porosimetry

Porosity parameters of spray-dried particles such as pore size distribution, total surface area, average pore diameters and apparent density were evaluated by mercury (Hg) porosimetry. Apparent density is defined as the volume occupied by the solid, including the pores and interparticle voids, divided by the solid mass. It is also known as the bulk density and is less than the true density. Hg porosimetry is based on the concept that the structure of porous solids can be characterized by forcing a non-wetting liquid to penetrate their pores [61]. The mercury porosimeter is a device, which is capable of generating suitably high pressures and measuring simultaneously both the pressure and volume of mercury taken up by a porous material. Mercury does not wet most substances and will only penetrate pores when forced to do so under high pressure. Entry of mercury into pores requires applying pressure in inverse proportion to pore size. In other words, large pores will fill first, with smaller pores filling at increasingly higher pressures. Eq. 3.6, known as the Washburn equation [62], is the basis of the mercury porosimeter method for measuring pore size distribution:

$$D_{pore} = \frac{-4\gamma cos\theta}{P} \tag{3.6}$$

where D_{pore} is the pore diameter, γ is the surface tension, θ is the contact angle and P is the applied pressure. Mercury exhibits a high contact

angle against most solids. Reported contact angles vary, with 130° being the most widely used value. Liquid mercury has a high surface tension, usually its value is taken to be 0.485 N/m at 25 ℃ . High pressure mercury porosimeters can normally attain maximum pressures of 20 000 psi or 60 000 psi (140 kPa-420 MPa). The measurable pore size ranges from a maximum of 500 µm to a minimum of 6 nm (for the 20 000 psi system) or 3 nm (for the 60 000 psi system). In porosimetry, mercury filling apparatus is used to evacuate the sample and then to surround the sample with mercury. Evacuation is achieved by exposing the sample to a vacuum. The sample to be analyzed is contained inside a penetrometer, which is a long glass capillary tube, the sample end being a bulb shape. Using the vacuum control on the filling apparatus, gases and vapors are removed from the sample. The vacuum valve is closed and the penetrometer titled so that the stem end is immersed in mercury. The vent control valve is then slowly opened such that air fills the mercury chamber. Mercury is forced up the capillary stem and into the bulb. The filled penetrometer is then removed and inserted in the high pressure porosimeter for pore analysis. The construction of the glass penetrometer is key to pore measurement. A metal sheath fits over the capillary section. A metal seal is attached to the sample end of the penetrometer as a base electrode. The construction is thus mercury-glass-metal, or conductor-insulator-conductor. In this way a coaxial capacitor is created. The capacitance changes as a result of the change in mercury level within the penetrometer. The mercury level will change as porous samples are filled with mercury under increasingly high pressure [62]. As mentioned above, porosity parameters were determined by means of a high-pressure porosimeter [63], a Quantachrome Poremaster (33/60). Total intruded volume of mercury (V_{tot}), total surface area (S), mean pore diameter (d_{mean}), volume pore size distribution ($D_v(d)$), total porosity and apparent density (ρ_{bulk}) were calculated from the intrusion data with Quantachrome Poremaster software, version 3.0 [64]. Total pore surface area was calculated by Eq. 3.7

$$S = \frac{1}{\gamma \left| cos\theta \right|} \int_0^{V_{tot}} pdV \tag{3.7}$$

where p is the pressure, V is the intruded volume of mercury, γ is the

surface tension, θ is the contact angle of mercury. The mean pore diameter was calculated by Eq. 3.8

$$d_{mean} = 4 \cdot \frac{V_{tot}}{S} \tag{3.8}$$

based on the assumption of cylindrical shape of pores open at the ends. Median pore diameter (d_{mean}) is the pore diameter at which 50% of the total intruded volume of mercury is intruded. $D_v(d)$ is defined as the pore volume per unit interval of pore radius by Eq. 3.9

$$D_v\,(d) = \frac{p}{d} \cdot \frac{dV}{dp} \tag{3.9}$$

Intrusion pressure values were directly converted into the corresponding pore size by using the Washburn equation (Eq. 3.6). The pore size distribution was determined from the volume of mercury intruded at each pressure increment, while the total porosity was based on the total intruded volume.

3.2.4 Determination of the loading efficiency

3.2.4.1 Microwave-assisted extraction

Microwave-assisted extraction (MAE) is a novel process that uses microwave energy to heat the solvents and the sample to increase the mass transfer rate of the solutes from the sample matrix into the solvent [65]. The combination of solvents and heat is expected to increase the extraction yield as compared to other methods. Because of the heat produced, microwave-assisted solvent extraction takes 10-30 min, whereas the other methods can take hours or days to complete. The heat produced by microwaves is due to the interaction of the radiation with the dielectric field associated with polar molecules and ions [66]. The amount of solvent used in microwave extraction is also considerably less than the amount used in the other extraction processes [67]. MAE is a relatively new extraction technique and has been successfully employed to extract tea polyphenols and tea caffeine from green tea leaves [68], piperine from black pepper [66], capsaicinoids from capsicum [69], phenolic compounds from grape seeds [70], puerarin from Radix puerariae [71],

and color pigments from paprika [72]. This technique has a number of advantages over the traditional extraction methods: since it is not extensive and not restricted in solvent selectivity, no concentration/ evaporation step is required, and the possibility of contaminating the sample with solvent impurities is much lower [72].

In this work, MAE was used to determine the active compound loading efficiency. MAE experiments were performed with a MARS-X 1500W Microwave Accelerated Reaction System for extraction and digestion (CEM Corp., Mathews, NC, USA). Samples of 10.0 mg of free EGCG, EGCG/P and control (unloaded) particles were suspended in 15 ml of methanol and transferred to the glass extraction vessels. Samples were extracted at two selected temperatures (90 and 110 ℃), with constant medium stirring, at 100% magnetron power, for 15 min. In the case of the collagen hydrolysate loaded particles (CH/P), samples of 15.0 mg of collagen hydrolysate (CH) alone, and 300 mg of CH/P and control particles were suspended in 15 ml of NaCl 5 mg/ml and transferred to the glass extraction vessels. Samples were extracted at 100 ℃ for 15 min. The maximum vessel pressure cut off was set at 1.38×10^6 Pa. Once the extraction was completed, the samples were cooled for 10 min. The pellet (particles without the active compound) was discarded and the supernatant (extracted EGCG and CH) analyzed by UV-VIS spectroscopy. The loading efficiency was determined according to the EGCG and CH absorbance obtained at 276 nm and in the range of 250-270 nm, respectively. All experiments were performed, at least, in triplicate.

3.2.5 Detection of active compounds

3.2.5.1 Ultraviolet-Visible Spectroscopy

Ultraviolet-visible (UV-Vis) spectroscopy is used to obtain the absorbance spectra of a compound in solution or as a solid. What is actually being observed spectroscopically is the absorbance of light energy or electromagnetic radiation, which excites electrons from the ground state to the first singlet excited state of the compound or material. The UV-Vis region of energy for the electromagnetic spectrum covers 1.5 - 6.2 eV which relates to a wavelength range of 800-200 nm. The Beer-Lambert Law, Eq. 3.10, is the principle behind absorbance spectroscopy. For a single wavelength, A

is absorbance, ε is the molar absorptivity of the compound or molecule in solution ($M^{-1}cm^{-1}$), b is the path length of the cuvette or sample holder (usually 1 cm), and c is the concentration of the solution (M).

$$A = \varepsilon bc \tag{3.10}$$

All UV-visible spectra were obtained using a UV-1700 PharmaSpec Spectrometer, Kyoto, Japan.

3.2.5.2 Attenuated Total Reflection-Infrared Spectroscopy

Attenuated total reflection-Infrared spectroscopy (ATR-IR) is one of the most useful techniques for identifying molecular structures, which is based on the analysis of absorption peaks at certain wave numbers (expressed in cm^{-1}). In the last years, the combination of Fourier transform algorithm with attenuated total reflectance (ATR) techniques has improved the conventional IR spectroscopy with various and important advantages. Thus, ATR-IR spectroscopy is direct and nondestructive, requires only small amounts of dried material (just a few milligrams) and is a quick method. ATR-IR is a well-established analytical tool applicable to full-spectrum characterization of chemical and biological species without particular sample preparation [73]. The basic premise of the technique involves placing the sample in contact with an infrared transmitting crystal with a high refractive index. The infrared beam is directed through the crystal, penetrating the surface of the sample, and obtaining spectral information of that surface. An advantage of this technique is that it requires very little sample preparation; simply place the sample in contact with the crystal [74]. In addition, ATR provides information on the effect of environmental factors on an analyte's vibrational characteristics. Reaction kinetics can be studied by ATR-IR using the Beer-Lambert law (Eq. 3.10). The distance b that the evanescent wave travels through the sample (the path length) is determined by the wavelength of light, the angle of incidence and the indices of refraction for the ATR crystal and the medium being probed [75].

ATR-IR spectra of spray-dried particles were recorded employing a FTLA 2000 Series Laboratory FT-IR Spectrometer (Ettlingen, Germany). The samples were analyzed in solid state and the spectra measured in a frequency range between 4000 and 400 cm^{-1}.

3.2.5.3 Nuclear Magnetic Resonance Spectroscopy

Nuclear magnetic resonance (NMR) spectroscopy is one of the most powerful experimental methods for investigation of the structure and intermolecular interactions of multicomponent systems [76]. NMR is based on the magnetic properties of the atomic nucleus. NMR is a property that magnetic nuclei have in a magnetic field and applied electromagnetic (EM) pulse or pulses, which cause the nuclei to absorb energy from the EM pulse and radiate this energy back out. This is a technique that provides information about the structure and dynamic of a sample subject to a static magnetic field, from the analysis of the interaction between the magnetic moments of the sample nuclei and an applied electromagnetic wave.

The NMR phenomenon is based on the fact that nuclei of atoms have magnetic properties that can be utilized to yield chemical information. Quantum mechanically subatomic particles (protons, neutrons and electrons) have spin. In some atoms (e.g. ^{12}C, ^{16}O, ^{32}) these spins are paired and cancel each other out so that the nucleus of the atom has no overall spin. However, in many atoms (^{1}H and ^{13}C, ^{31}P, ^{15}N, ^{19}F) the nucleus does possess an overall spin (I). All nuclei with non-zero spins have magnetic moments (μ), but the nonspherical nuclei also have an electric quadrupole moment (eQ). In quantum mechanical terms, the nuclear magnetic moment of a nucleus will align with an externally applied magnetic field of strength B_0 in only 2I+1 ways, either with or against the applied field B_0.

The orientations that a nucleus' magnetic moment can take against an external magnetic are not of equal energy. Spin states which are oriented parallel to the external field are lower in energy than in the absence of an external field. In contrast, spin states whose orientations oppose the external field are higher in energy than in the absence of an external field. Where an energy separation exists there is a possibility to induce a transition between the various spin states. By irradiating the nucleus with electromagnetic radiation of the correct energy (as determined by its frequency), a nucleus with a low energy orientation can be induced to "transition" to an orientation with a higher energy. The absorption of energy during this transition forms the basis of the NMR method. In a given sample of a specific NMR-active nucleus, the nuclei will be distributed throughout the various spin

states available. As the energy separation between these states is comparatively small, energy from thermal collisions is sufficient to place many nuclei into higher energy spin states. The number of nuclei in each spin state is described by the Boltzmann distribution:

$$N_{upper}/N_{lower} = e^{-\gamma B_0/kT} \tag{3.11}$$

where the N values are the numbers of nuclei in the respective spin states, γ is the magnetogyric ratio, h is Planck's constant, B_0 is the external magnetic field strength, k is the Boltzmann constant, and T is the temperature. At room temperature, the upper and lower energy spin states are almost equally populated with only a very small excess in the lower energy state that represents spins aligned with the applied field. The amount of signal intensity that can be observed in any spectroscopic method is proportional to the population difference between the two energy levels involved. In NMR, the energy separation of the spin states is comparatively very small, at room temperature, and while NMR is very informative from a chemistry standpoint, quantum mechanically it is considered to be an insensitive technique.

Fourier Transform (FT-NMR) NMR instruments are mainly used at the present time. In FT-NMR, all frequencies in a spectral width are irradiated simultaneously with a radio frequency pulse. Following the pulse, the nuclei magnetic moments find themselves in a non-equilibrium condition. They begin a process called "relaxation", by which they return to thermal equilibrium. A time domain emission signal (called free induction decay (FID)) is recorded by the instrument as the nuclei magnetic moments relax back to equilibrium with the applied magnetic field. A frequency domain spectrum that we are familiar with is then obtained by Fourier transformation of the FID.

The precise resonant frequency of the energy transition is dependent on the effective magnetic field at the nucleus. This field is affected by electron shielding which is in turn dependent on the chemical environment. As a result, information about the nucleus' chemical environment can be derived from its resonant frequency. In general, the more electronegative the nucleus is, the higher the resonant frequency. Other factors such as ring currents (anisotropy) and bond strain affect the frequency shift. The dependence of the transition energy on the position of a particular atom in a molecule

gives NMR spectroscopy it's utility for structural characterization. The resonance frequencies of different nuclei in an atom are described by a relative shift compared to the frequency of a standard. This relative shift is called chemical shift (δ). The effective magnetic field is also affected by the orientation of neighboring nuclei. This effect is known as spin-spin coupling which can cause splitting of the signal for each type of nucleus into two or more lines. The size of the splitting (coupling constant or J) is independent of the magnetic field and is therefore measured as an absolute frequency (usually Hertz). The number of splittings indicates the number of chemically bonded nuclei in the vicinity of the observed nucleus.

In NMR spectroscopy a huge number of pulse sequences and techniques have been created to overcome the low sensitivity of the method and gain more information in the study of the structure and dynamic in both chemical and biological systems. The most common nuclei observed using this technique are ^{1}H and ^{13}C, but also ^{31}P, ^{19}F, ^{29}Si and ^{77}Se. The NMR spectroscopy can be employed for investigations of the molecular structure and stereochemistry, inter- and intra-molecular interactions, intermolecular inclusion complex formation, reaction mechanisms, etc., due to the large number of spectral parameters, such as chemical shifts, spin-spin coupling constants, Nuclear Overhauser Effect (NOE), translation diffusion and relaxation times (T_1, T_2), that can be measured and analyzed. It is a totally non-invasive technique, particularly suited to study molecular dynamics and translational diffusion, and hence structural details in biological and physiological systems [77].

The combined application of diffusion ordered NMR spectroscopy (DOSY) and measurement of the nuclear spin-lattice relaxation times (T_1) offers a chance to gain insight into the structure of intermolecular aggregates in solution [77]. DOSY is nowadays a well-established technique for characterizing the structure and dynamics of complex systems. DOSY provides a means for "virtual separation" of compounds, by providing a 2D map in which one axis is the chemical shift while the other is that of the diffusion coefficient [77]. The method uses a special pulse sequence to obtain a series of NMR spectra using field gradients and is capable of determining diffusion coefficients of molecules without any concentration gradient. The intensity of the detected proton signal belonging to a particular molecular entity at a certain

gradient level is dependent mostly on the rate of diffusion of that molecule as the gradient eliminates more signal intensity of molecules in faster motion. The analysis of attenuation in signal intensity as a function of diffusion time, gradient strength, or gradient time (depending on the experimental setup) provides the related diffusion coefficients [78]. The self-diffusion coefficients and structural properties of the molecules are connected by the dependence of their self-diffusion coefficients on the molecular size, weight, shape, etc [77], [79], [80]. Self-diffusion is the random translational motion of molecules driven by their internal kinetic energy. Translational diffusion and rotational diffusion can be distinguished from each other. Diffusion is related to molecular size, as becomes apparent from the Stokes-Einstein equation:

$$D = \frac{k_b T}{f} \tag{3.12}$$

where D is the diffusion coefficient, k_b is the Boltzmann constant, T is the temperature, and f is the friction coefficient. Therefore, DOSY experimental technique has become a valuable tool for studies of molecular interactions in solution [77].

All NMR experiments have been recorded on a Bruker Avance III 400 spectrometer, operating at 400.15 MHz for protons, equipped with pulse gradient units, capable of producing magnetic field pulsed gradients in the z-direction of 50 G/cm. The spectra have been acquired in D_2O solution at 30 ℃ in 5 mm tubes. Sodium trimethylsilyl-[2,2,3,3-d4]-propionate (TSP) has been used as an internal standard for both the chemical shift and the diffusion measurements. For NMR analysis of EGCG/P the following samples were prepared: unloaded (MD/GA), EGCG loaded particles (EGCG/P), physical mixture of EGCG and unloaded particles (EGCG+MD/GA), and physical mixtures of EGCG, MD and GA (EGCG+MD+GA), mixing the components in the same proportion employed in the preparation of EGCG/P. With the exception of EGCG, in all cases 20 mg of solute, 600 µl D_2O and 20 µl 0.05 mM solution of TSP in D_2O were used. NMR spectra of EGCG were recorded in D_2O at concentration of 10 mg/ml. Two-dimensional $^1H/^1H$ correlation spectra (COSY) and gradient-selected $^1H/^{13}C$ heteronuclear single quantum coherence (HSQC) spectra were recorded using the standard Bruker software. 2D-COSY spectra were acquired with a multiple quantum

filter, gradient pulses for selection, a gradient ratio of 16:12:40 and a relaxation delay of 1.5 s. A total of 2048 data points in F2 and 512 data points in F1 over a spectral width of 6500 Hz were collected. 2D $^{1}H/^{13}C$ HSQC experiments via double inept transfer, using sensitivity improvement and decoupling during the acquisition were carried out with a spectral width of ca. 6000 Hz for ^{1}H and 28000 Hz for ^{13}C, a relaxation delay of 1.5 s, FT size 2 K $\times$ 256 W. The two-dimensional nuclear Overhauser effect spectroscopy (NOESY) experiments were acquired in phase-sensitive mode with gradient pulses in the mixing time, using the standard pulse sequences with optimized mixing time of 400 ms. Generally, 64 scans and 512 F1 slices were obtained and the spectral width in both dimensions was 6500 Hz. The spin-lattice relaxation rates were measured using the inversion-recovery pulse sequence, (180°- τ - 90°). Thirty two τ increments were used for the experiments, with values between 0.01 and 13.0 s and relaxation delay of 13 s. Relaxation times were calculated by exponential regression analysis of recovery curves of longitudinal magnetization components. The DOSY experiments were performed using the bipolar longitudinal eddy current delay (BPPLED - Bipolar Pulsed Field Gradient Longitudinal Eddy Delay) pulse sequence [81].The experimental conditions (amount of the solute and the solvent, temperature, air flow, sample rotation) for all DOSY experiments were kept constant. Before all NMR experiments, the temperature was equilibrated and maintained at 30 ℃, as measured using the spectrometer thermocouple system. The diffusion coefficient of TSP (6.68 $\times$ 10^{-10} m^2s^{-1}, calculated standard deviation of 3.1×10^{-3}) obtained from ^{1}H DOSY experiments was used as an internal reference for the diffusion measurements. The spectra were recorded in 5 mm NMR tubes with an air flow of 535 l/h. Typically, in each experiment a number of 32 spectra of 16K data points and 64 scans were collected, with values for the duration of the magnetic field pulse gradients (δ) of 4 or/and 5 ms, diffusion times (Δ) of 160 - 200 ms and an eddy current delay set to 5 ms. The pulse gradient (g) was incremented from 2 to 95% of the maximum gradient strength in a linear ramp. The spectra were first processed in the F2 dimension by standard Fourier transform and after baseline correction the diffusion dimension was processed with the Bruker Topspin software package (version 2.1). The diffusion coefficients are calculated by exponential fitting of the data belonging to individual columns of

the 2D matrix. The diffusion coefficients (D) were obtained by measuring the signal intensity at more than one place in the spectra. Between five and ten different measurements were done for the determination of each diffusion coefficient. All diffusion coefficients are given as a ratio D/D_{TSP} according procedure published before [82] and average values have been calculated.

Collagen hydrolysate loaded particles were also studied by NMR. Samples of CH/P, MD/GA and CH were prepared by dissolving 20 mg of solute in 600 µl D_2O, containing 20 µl solution of TSP (0.05 mM) in D_2O. The NMR and DOSY analysis of these samples were carried out, applying the procedure described above for EGCG/P.

3.2.6 Antioxidant activity

3.2.6.1 Radical Capacity Scavenging Assay

Several analytical methods are established to evaluate the antioxidant activity of a large variety of compounds both in pure form and in complex mixture, namely, the 2,2-diphenyl-1-picrylhydrazyl (DPPH*) radical scavenging capacity assay (RDSC). The DPPH method is based on the scavenging of the stable DPPH radical by the antioxidant and may be utilized in aqueous and nonpolar organic solvents and also be used to examine both hydrophilic and lipophilic antioxidants. The RDSC uses an area under the curve (AUC) in calculation and reports the RDSC values in trolox equivalents (TE) per mass of testing material, which makes it possible to compare data from different laboratories and different times and which may better meet the needs of antioxidant research. In addition, the high-throughput assay using DPPH* was demonstrated for possible application in establishing the EC_{50} values for selected antioxidant samples [83].

Antioxidant activity of free EGCG, EGCG/P and unloaded particles (MD/GA) was determined according to the RDSC [83] in a 96-well plate, using a SynergyTM 2 Multi-Detection Microplate Reader (BioTek Instruments, Vermont, USA). Five different EGCG concentrations, between 5.00 and 30.00 µM, were used for free EGCG and EGCG/P analysis. A sample of unloaded particles was also analyzed. The assay was performed as follows: 100 µl of DPPH* methanol solution (0.208 mM) was added to 100 µl of sample into each well, using an eight channel micropipette followed by

gentle shaking. The absorption was measured at 515 nm immediately after shaking and read once per minute for 90 min. A blank with the mixture of 100 µl water and 100 µl methanol, and a control with the mixture of 100 µl methanol and 100 µl DPPH* (0.208 mM) were also measured. The percentage of radical remaining at 40 min (%DPPH* remaining) was determined according to the following equation:

$$\%DPPH^*_{remaining} = \frac{A_{sample} - A_{blank}}{A_{control} - A_{blank}} \times 100 \tag{3.13}$$

where A_{sample}, A_{blank} and $A_{control}$ stand for the absorbance of sample, blank and control reactions at 40 min. EC_{50} values for the selected antioxidant samples were calculated. EC_{50} represents the required concentration of a selected antioxidant to reduce the DPPH* concentration to 50% of its original in the reaction mixture. The EC_{50} parameter is also commonly used to evaluate and compare the antioxidant activity and was determined by plotting the %DPPH* remaining at 40 min against the EGCG concentrations. To estimate the total DPPH* scavenging capacity of each sample, the percentage of DPPH* quenched (%DPPH* quenched) was determined according to the following equation:

$$\%DPPH^*_{quenched} = \left(1 - \frac{A_{sample} - A_{blank}}{A_{control} - A_{blank}}\right) \times 100 \tag{3.14}$$

where A_{sample}, A_{blank} and $A_{control}$ stand for the absorbance of the certain concentration of a selected sample, blank and the control at 515 nm measured at the reaction time t. The values of %DPPH* quenched obtained from equation 3.14 were plotted against the reaction time and the value of the area under the curve (AUC) was determined. Trolox demonstrated a linear relation between AUC and concentration changes with a correlation coefficient (r^2) of 0.9982. The RDSC values were determined, according to equation 3.15:

$$RDSC = \frac{AUC_{sample}}{AUC_{trolox}} \times \frac{molarity_{trolox}}{molarity_{sample}} \tag{3.15}$$

The RDSC value was determined using a standard curve prepared with trolox at five concentrations within the linear range of 16-75 µM. Triplicate reactions were carried out for each concentration of antioxidant sample.

3.2.7 Release studies

3.2.7.1 Dialysis

Membrane diffusion techniques permit the determination of the release of a variety of drugs from the carrier. The carrier is suspended in a small volume of the continuous phase, and separated from a large bulk of sink phase by a dialysis membrane permeable to the drug. The drug diffuses out of the sample and through the membrane to the sink, wherein it is periodically assayed [84]. This technique is widely used for studying drug release kinetics of nanoparticulate carrier systems [85], [86].

EGCG *in vitro* release studies from EGCG/P were performed using dialysis membranes of regenerated cellulose (Spectra/Por, Netherlands). EGCG/P suspensions (3 ml) were placed into the regenerated cellulose dialysis membrane (molecular weight cut-off (MWCO) 1 kDa) and dialyzed against 80 ml ultrapure water. The dialysis was performed at room temperature under magnetic stirring. Free EGCG molecules, which diffuse to the membrane exterior, were monitored by UV-Vis spectroscopy at 276 nm (SynergyTM 2 Multi-Detection Microplate Reader, BioTek Instruments, USA). The concentration of EGCG released was calculated from the standard calibration curve of EGCG solution. Antioxidant activity of released EGCG was studied by High-Throughput Relative DPPH* Radical Scavenging Capacity Assay, as described above. These studies were performed in triplicates in identical manner. The *in vitro* release profile of CH from CH/P was also investigated by dialysis, applying the procedure reported previously. CH (25%) loaded particles were suspended in ultrapure water (60 mg/ml), with constant magnetic stirring in regenerated cellulose dialysis membrane with a 10 kDa MWCO. CH concentration outside the membrane was monitored over time by UV-Vis spectroscopy (at 270 nm) and the concentration of CH released was calculated from the standard calibration curve of CH solution. These experiments were repeated two times.

3.2.8 *In vitro* cell culture studies

3.2.8.1 Cell line culture

Human prostate carcinoma Du145 cells were grown in surface-treated Nunclon culture dishes (Nunc AS, Roskilde, Denmark) using a standard RPMI-1640 medium supplemented with 10% (v/v) fetal bovine serum, 1% (w/v) penicillin and streptomycin, and 1% l-glutamine. All cell culture dishes were maintained at 37 ℃ in 95% humidified atmosphere and 5% CO_2. For subculturing, approximately 5×10^5 cells were seeded per 25 cm^2 culture flask and split twice a week. Viable cells were counted using an automated Coulter counter (Vi-Cell XR, Beckman-Coulter Inc., Miami, FL, USA). For cytotoxicity experiments, the cells were harvested from the splitting culture and seeded in six-well plates (clonogenic assay) or in 25 cm^2 flasks (viability and apoptotic assays) at a density of 200 cells/well and 0.15×10^6 cells/flask, respectively. Nanoparticles (NPs) were incubated with cells at a concentration of 0.9 mg/ml (for EGCG/P the mass corresponds to 100 µM EGCG), for 64 h at 37 ℃ for viability and apoptotic assays, and at concentrations from 0.009 to 0.9 mg/ml (1-100 µM EGCG) for 9 days at 37 ℃ for clonogenic assay. The medium was not changed or replenished during the incubation time. After that, the cells were washed with RPMI medium and the assays were carried out. Only the overall end point effects (cell viability and clonogenic potential) of both EGCG/P and free EGCG were studied to compare their activity.

3.2.8.2 Cell viability assay

Cell viability was determined by the MTT (3-[4,5-dimethylthiazol-2-yl]-2,5-diphenyltetrazolium bromide) reduction assay, which relies on the reduction of MTT by mitochondrial dehydrogenases. MTT reagent (50 µl/ml of 2 mg/ml MTT) was added to each flask, which was incubated at 37 ℃ for 4 h. The cells were then washed twice with ice-cold PBS solution. The crystallized formazan was subsequently dissolved in DMSO. The absorbance of the samples was measured at 570 nm using a plate reader (Multiscan EX, type 355, Labsystems, Helsinki, Finland). Background absorbance values, as assessed from cell-free wells, were subtracted from the absorption values of each test sample. Percentage of MTT reduction was calculated by dividing

absorbance of the sample by the absorbance of a control (cells treated in an identical manner but without EGCG or particles). Averages from three replicates were used for each sample and control.

3.2.8.3 Caspase-3 activation assay

Du145 cells were grown as previously described. EGCG/P were dissolved in PBS buffer and incubated with cells at an EGCG final concentration of 100 µM for 64 h. Toxicity of the samples was evaluated by activation of caspase-3, measured using the CASP3C colorimetric 96-well plate assay kit (Sigma, MO, USA), following the manufacture's instructions. Caspase-3 is activated in response to different inducers of apoptosis. Upon activation through proteolytic processing, caspase triggers substrate proteolysis and other changes that result in chromatin condensation, DNA fragmentation, and ultimately the apoptotic phenotype. The detection of activated caspase-3 could therefore be a valuable and specific tool for identifying apoptotic cells in tissue sections, even before all the morphological features of apoptosis occur [87]. Briefly, confluent cells were incubated with EGCG (either free or loaded) and unloaded particles for 64 h. Subsequently, cells were trypsinized, concentrated by centrifugation and the cell pellet was lysed in 100 µl hypotonic lysis buffer (Promega); 40 µl of each cell lysate were used in duplicate to determine caspase-3 activation. The remaining cell lysate was used to measure total cellular protein concentration with the Fluka protein reagent absorbing at 595 nm, using bovine serum albumin as standard. Values shown are the mean of three independent assays.

3.2.8.4 Clonogenic assay

EGCG, free or loaded in carbohydrate particles, was dissolved in PBS buffer and added to the cells at different concentrations (1, 2, 5, 10, 25, 75 and 100 µM in EGCG content). After the incubation period (9 days), survival and proliferation of the cells were determined by methylene blue staining. The medium was discarded and cells were washed with 0.9% NaCl and fixed with 70% ethanol. The cells were then stained with methylene blue solution (10% in 0.01% w/v NaOH). The number of colonies with 50 or more cells/colony was determined. The surviving fraction was calculated by the

number of colonies counted divided by the number of colonies plated with a correction for the plating efficiency (PE), defined as the number of colonies observed/the number of cells plated of a control sample:

$$Surviving\ fraction = Number\ of\ colonies/\ Number\ of\ cells\ seeded \times PE$$

3.2.8.5 Statistical analysis for *in vitro* studies

Values are reported as mean ±STD. Student's t-test statistical analysis was used to determine statistical significance between cells exposed to assay media and cells exposed to EGCG and EGCG/P.

Chapter 4

EGCG loaded particles

Contents

4.1 Introduction

Epigallocatechin gallate (EGCG) belongs to the group of the polyphenolic compounds. EGCG chemical structure is illustrated in Figure 4.1.

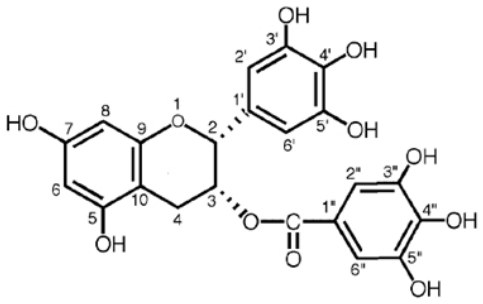

Figure 4.1: Chemical structure of EGCG.

Free radicals and oxidative stress (OS) are related to certain degenerative diseases including cancer, cardiovascular disease, diabetes, autoimmune disorders and neurological disorders [88]. OS can cause cellular damage and subsequent cell death, because the reactive oxygen species (ROS) oxidize vital cellular components such as lipids, proteins, and DNA [89]. ROS are produced in cells, due to a partial reduction of the oxygen molecule during the cellular metabolism. Free radicals, also classified as ROS, are highly reactive molecules containing unpaired electrons that cause oxidative stress [90]. The intermediate steps of oxygen reduction are the formation of the superoxide anion radical (O_2^-), hydrogen peroxide (H_2O_2) and hydroxyl radical ($OH^{\cdot}$), corresponding to the steps of reduction by one, two and three electrons, respectively. Further ground-state molecular oxygen (triplet), as a diradical, can be electronically excited to singlet molecular oxygen [91]. Peroxynitrate (O_2NOO^-) is a nonradical reactive specie formed from the nitric oxide and superoxide anion radicals. Singlet oxygen is now recognized as the main intermediate in photosensitized cell killing [92]. Photosensitized oxidation induces pathological effects such as cell damage, mutations, cell death and photooxidation of cell constituents, such as proteins and DNA [93]. Singlet oxygen can also be generated by aminoacids and proteins absorbing ultraviolet [94] or directly by infrared radiation [95], [96]. Singlet oxygen besides acts as an intermediate for activation or impairment of cell signaling pathways by producing oxidation products, which are either positive or negative regulators [97]. The half-lives of the major reactive oxygen species are vastly different, underscoring the necessity for different types of defense

mechanisms [98]. Cells possess mechanisms that help maintaining their normal redox balance, ensuring that ROS generation is transitory [89]. What is the main protective mechanism? Human antioxidant defense is equipped with enzymatic, hydrophilic scavengers (e.g. flavonoids) and lipophilic scavengers (e.g. tocopherols and carotenoids). Cells synthesize some of these compounds, but the main part is obtained from dietary sources. The cell's ability to produce adequate amounts of antioxidants is determined by age, inheritance, nutrition and stress [99]. Antioxidant defense mechanisms include: removal of O_2, scavenging reactive oxygen/nitrogen species or their precursors, inhibition of ROS formation, binding of metal ions needed for the catalysis of ROS generation and up-regulation of endogenous antioxidant defenses. The protective efficacy of antioxidants depends on the type of ROS that are generated, the place of generation (body barriers such as the blood brain barrier reduce the permeability of most antioxidants) and the severity of the damage [100]. Epidemiological studies have shown that a diet enriched in antioxidants is associated with reduced risk of such disorders [90]. Polyphenols from green tea including flavonoids, such as, catechins, are effective antioxidants because they act as free radical scavengers, and chelators of metal ions [101], thus protecting DNA damage and organelles from damage. They may protect tissues against free oxygen radicals and lipid peroxidation. Their biological activities include antithrombotic, vasodilatory and anticarcinogenic effects, as well as anti-inflammatory, antiallergic, antiulcer, antibacterial and antiviral properties [102].

Biological properties of polyphenols depend on their bioavailability, which includes: availability for absorption, absorption, tissue distribution and bioactivity [103]. Oral administration is the most efficient delivery system of antioxidants, but serious pre-systemic eliminations of green tea catechins had been reported after oral administration. Oral bioavailability (fraction that enters the bloodstream) of tea catechins is very low, less than 2-5% [104], [105], and their systemic clearance is also high [104], [106]. Catechins bioavailability is affected by several factors, such as their chemical properties, conjugation form in the intestine, intestinal absorption and available enzymes catalyzing the metabolism. New delivery systems need to be developed in order to improve catechin solubility, stability, permeability and bioavailability. Utilization of nanoscale vehicles loaded with antioxidants

instead of free compounds can improve bioavailability and half-life of the compound *in vivo* and *in vitro*, optimize routes of their administration, and achieve site specific or targeted drug delivery combined with controlled release profile [107]. Antioxidants should be able to reach the site of action, for example cross the blood brain barrier to treat neurodegenerative disorders and target the tumors in treatment of cancer. Encapsulation of polyphenols in micelles, carbohydrate nanoparticles, liposomes or other pre-formed materials, represents a solution to increase their efficacy of therapy. Encapsulation of EGCG by homogenization and spray-drying can be employed to improve EGCG stabilization, ensure its bioavailability and for industrial purposes.

In this work, unloaded particles (MD/GA) and EGCG loaded (in a proportion of 5 wt.%) particles (EGCG/P) with a polymeric shell matrix, based on polysaccharides, were produced by homogenization and spray-drying.

4.2 Morphology and Structure of EGCG loaded particles

SEM micrographs of spray-dried particles show size polydispersity and diameters less than 20 µm (Figure 4.2). The results depict structural differences between the particles. A population of disk-like and corrugated particles with highly dented surfaces is observed. Previous works demonstrated that spray-dried particles with wall materials consisting of polysaccharides exhibit notable surface indentation [108]. On the other hand, Figure 4.2 also reveals a particle population with spherical shape and smooth surface free of visible cracks and pores. Two intentionally crushed particles, shown in Figure 4.2 (E and F), clearly demonstrate that the particles are hollow and have a dense shell. The evaporation rate during spray-drying is determined by the solute/solvent properties and processing parameters, predominantly air flow rate and temperature. The solidification mechanism, which depends on the nature of the component, is initiated once a critical concentration is reached at the surface [109]. The resulting particles will have different morphologies, depending on their size and the properties of their shells in the final stages of the drying process. Hollow spheres with smooth surface are formed, if the shell becomes rigid rapidly and does not buckle or fold [109].

The hollow particle may finally collapse or wrinkle (corrugate structure), depending on the thickness and mechanical properties of the shell. Also if the time to reach the critical concentration for shell formation at the surface decreases, i.e. shell formation occurs earlier in the evaporation process on a larger droplet, particles with wrinkled surfaces are formed. It has been demonstrated that thermal expansion of air or water vapors inside the drying particles ("ballooning", associated with high drying rates) can smooth out dents (to a varying extent). The effectiveness of dent smoothing is dependent on the drying rate and on viscoelastic properties of the wall matrix [110]. Expansion and smoothing out of dents can occur only prior to solidification of the matrix when the wall matrix is elastic enough to enable such structural changes [110]. There are numerous examples in the literature reporting hollow and wrinkled or dimpled morphologies for spray-dried polymer particles [111], [112], [113], [114], [115], [116]. In addition, corrugated particles are typically produced by homogenization and spray-drying when using gum arabic as encapsulating agent [110], [117].

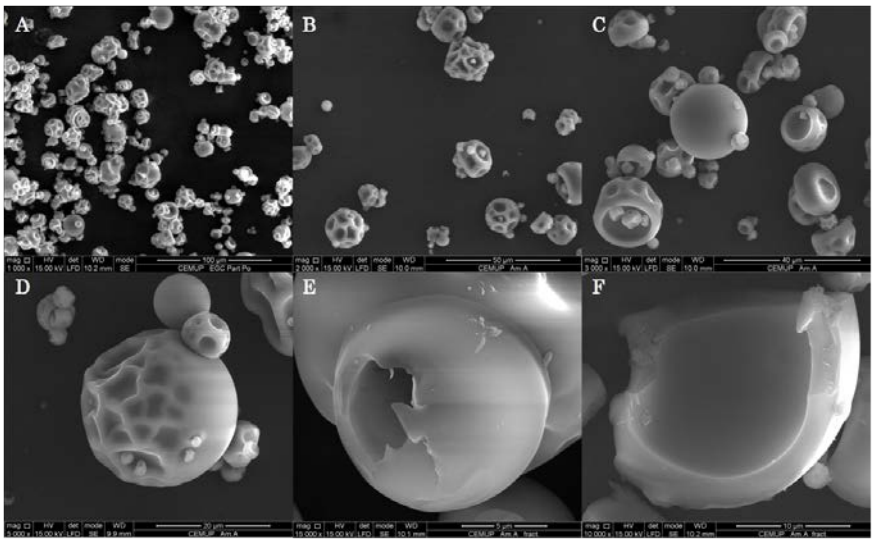

Figure 4.2: Morphology of spray-dried EGCG/P. The particles on the bottom-right were intentionally crushed to show their internal structure. Scale bars represent 100 µm (A), 50 µm (B), 40 µm (C), 20 µm (D), 10 µm (E) and 5 µm (F).

Cryo-SEM analysis of the spray-dried EGCG/P dispersed in ultrapure water showed that corrugated particles disappeared and bridging of the particles occurred (Figure 4.3).

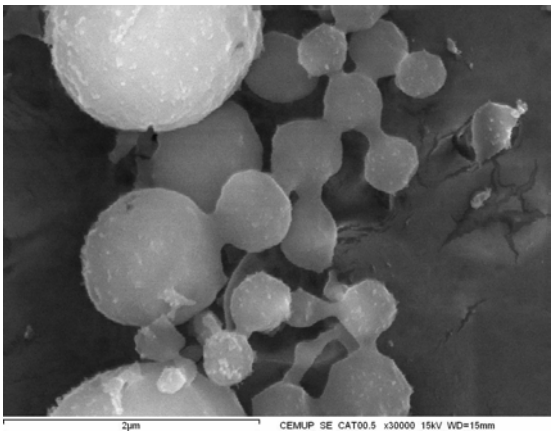

Figure 4.3: Cryo-SEM micrograph of EGCG/P after re-suspension in ultrapure water. Scale bar represents 2 µm.

TEM analysis (Figure 4.4) was used to visualize EGCG/P size in suspension.

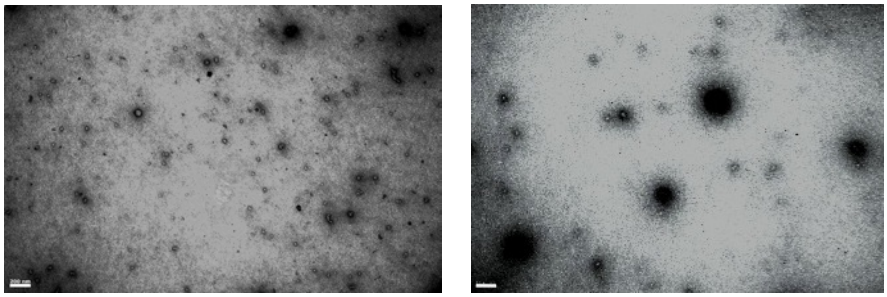

Figure 4.4: Transmission electron microscopy images of EGCG loaded nanoparticles. The scale bar is 200 nm.

Figure 4.4 discloses particles with sperical shape and polydisperse size, ranging from 40 to 400 nm.

AFM measurements (Figure 4.5) confirm that EGCG/P have a spherical shape and are resistant to mechanical strength, up to 8 MPa. AFM studies concerning lipid coated carbohydrate particles demonstrated that polysaccharide core provides high resistance and mechanical strength [118].

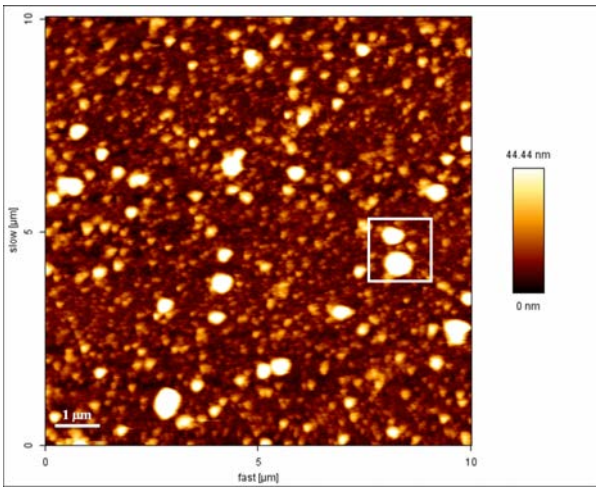

(a)

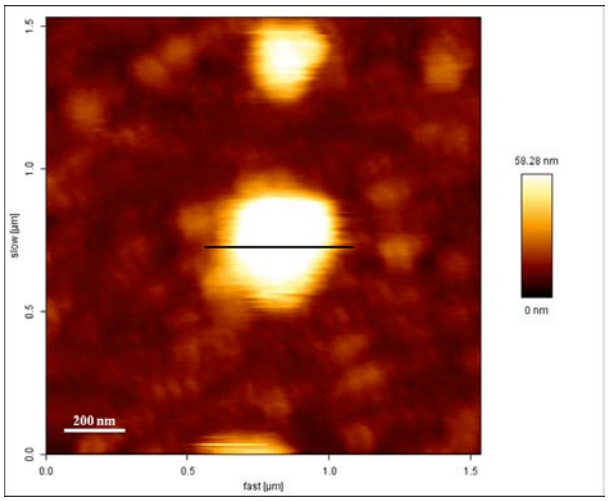

(b)

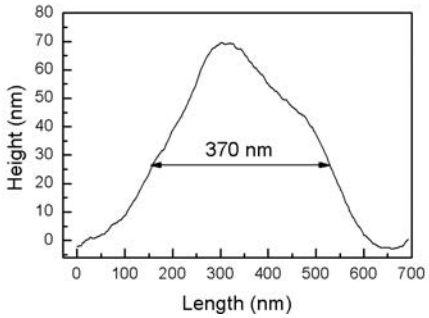

(c)

Figure 4.5: AFM height images of EGCG/P. The signed area in image (a) was zoomed (b) to evidence the spherical shape of the particles. Scale bars represent 1 µm (a) and 200 nm (b). The profile analysis of one particle is shown in image (c).

AFM force-distance curves (Figure 4.6) are also useful to determine the elastic properties of the nanoparticles.

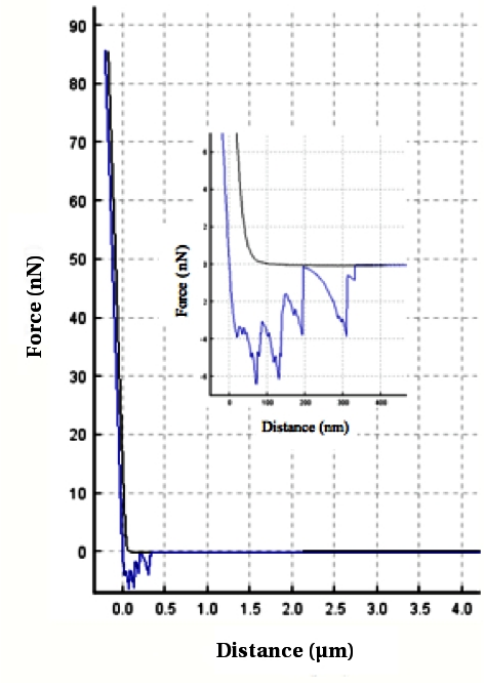

Figure 4.6: AFM force-distance curves of EGCG/P.

Considering the force-distance curves depicted in Figure 4.6, it can be noted that the approach and the withdrawal lines overlap each other. This is due to the absence of plastic deformations. Indeed, during the withdrawal of the tip, the nanoparticles (NPs) regains its original shape. The non-overlapping behavior of the approach and withdrawal contact lines is called hysteresis of the force-displacement curves. In this case no hysteresis is clearly observed, thus the NPs exhibit an elastic behavior. The energy that has been transferred by the tip to the NPs during the approach contact phase is completely transferred back to the tip during the withdrawal contact phase. This elastic behavior is explained by the mechanical and shape stability of the carbohydrate matrix of the nanoparticles.

4.3 Hydrodynamic Diameter and Zeta Potential of EGCG loaded particles

The size distribution of EGCG/P was investigated by DLS (Figure 4.7) and NTA (Figures 4.9 and 4.10). DLS measurements of EGCG/P and MD/GA in suspension revealed a bimodal size distribution, as depicted in Figure 4.7. EGCG/P size distribution by intensity shows particles with mean diameters of 40 and 400 nm, as obtained by TEM and AFM and, a polydispersity index of 0.58±0.06. Identically, the average hydrodynamic diameters of MD/GA are 60 and 400 nm. The formation of small sized particle populations can be explained by the ion-dipole and hydrogen bond interactions between gum arabic and maltodextrin during homogenization.

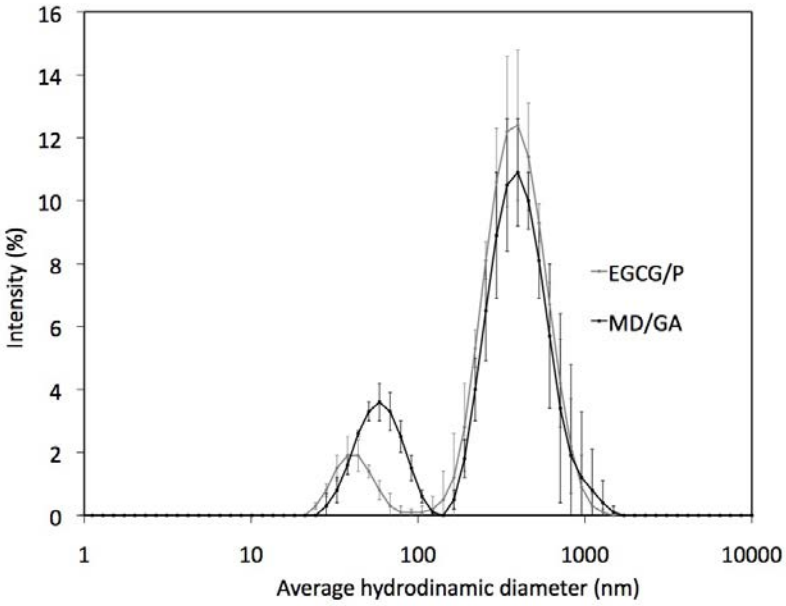

Figure 4.7: Average hydrodynamic diameter distribution of EGCG/P and MD/GA. Average value ± standard deviation, number of experiments = 3.

The mean zeta potential of EGCG/P was -36±6 mV, favoring the stability of the particle suspension (Figure 4.8).

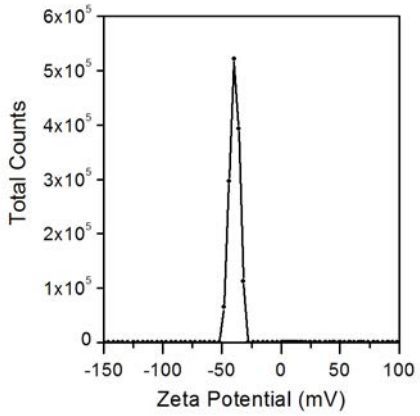

Figure 4.8: Zeta Potential of EGCG/P.

NTA is based on a laser illuminate microscopic techinque, as EGCG/P are very weak scatterers, therefore to be able to observe the smallest particles, it was necessary to use blue laser and a more sensitive camera (andor). As a consequence of using an andor camera, it wasn't possible to use Extended Dynamic Range to track and size accurately all particles in one analysis (Figure 4.9). For this reason the sample was analysed in parts, according to their size range in different dilutions (Figure 4.10).

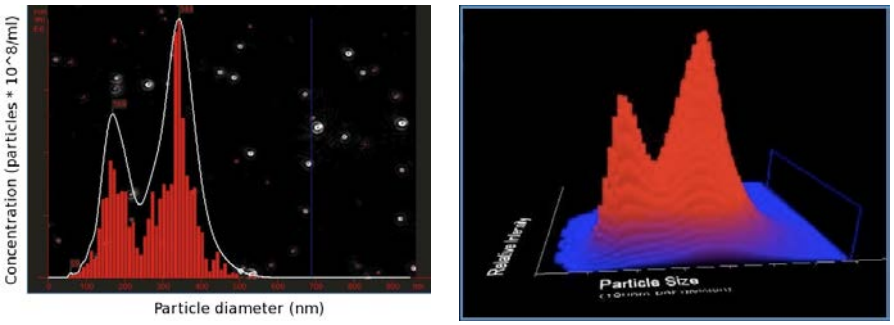

(a) (b)

Figure 4.9: Nanoparticle tracking analysis of EGCG/P: (a) Concentration (particles $\times 10^8$/ml) vs particle diameter (nm). (b) 3D plot of particle diameter, x (nm) vs concentration, y (particles $\times 10^8$/ml) and relative scatter intensity, z (log scale).

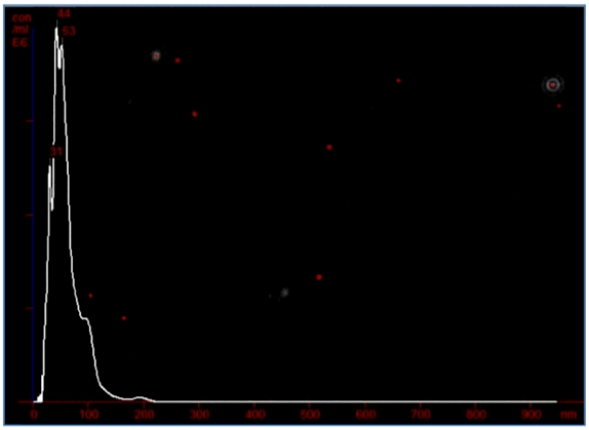

(a)

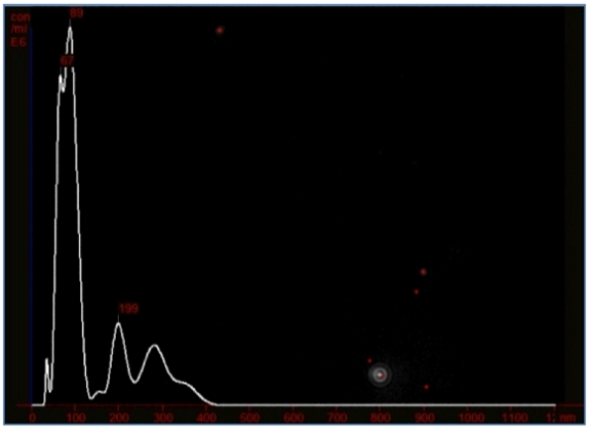

(b)

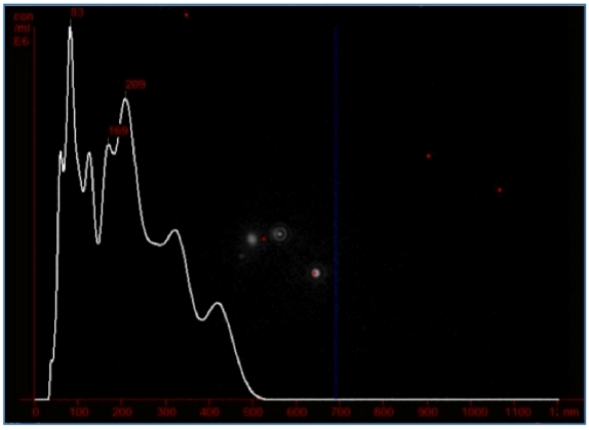

(c)

Figure 4.10: NTA of EGCG/P: (a) Concentration (1.82×10^8 particles/ml) vs particle diameter (nm) of the smallest particles. (b) Concentration (0.87×10^8 particles/ml) vs particle diameter (nm) of the middle range particles. (c) Concentration (1.26×10^8 particles/ml) vs particle diameter (nm) of the biggest particles.

NTA measurements revealed a polydisperse size distribution of EGCG/P that can be divided in three size ranges. The smallest particles (Figure 4.10a) are sized between 25 and 60 nm, with a bigger fraction around 45 nm. In the middle range, particles with diameters from 90 to 250 nm are observed (Figure 4.10b). The diameters of the biggest particles are approximately between 350 and 480 nm (Figure 4.10c). NTA measurements confirm the results obtained by DLS.

4.4 Particle internal structure

EGCG/P internal structure and density were studied by Hg porosimetry and He pycnometry. Figure 4.11 shows usual patterns of the Hg porosimetry of EGCG/P. The dependence measured in Hg porosimetry is the pressure/volume relationship (Figure 4.11a). Intrusion pressure values are directly converted into the corresponding pore size using the Washburn equation [62]. When mercury enters the pores of the sample, as in the usual case, the pressure/volume relationship can be interpreted as distribution of pores. The pore size distribution is reported in Figure 4.11b. The pore diameters range from 10 to 100 nm, with an average diameter of 24 nm. It is assumed that in high pressure porosimetry measurements - 20-60 000 psi (140 kPa-420 MPa), Hg fills all the cavities with a pore size between 3.5 nm and 900 µm, i.e. mesopores and macropores, whereas in He measurements, pores in diameter range of 0.1-300 nm [119] are determined. The intraparticle porosity obtained from Hg porosimetry for EGCG/P was 0.2. Chemical composition of the particle surface such as an accumulation of polymeric material can change the permeability of the surface and hence the apparent particle density becomes less than the true density [120], [121]. Apparent density is the mass of a particle divided by its volume excluding open pores but including closed pores (that have not been penetrated by mercury at a pressure of 1 bar) [120], [122]. The apparent density determined from these data was 0.76 g/cm^3. Helium displacement density of EGCG/P was determined by He pycnometry - 1.36 g/cm^3. Unloaded particles revealed similar values of porosity and density. According to previous studies the apparent particle densities of the spray-dried carbohydrates as determined by nitrogen pycnometry were negatively correlated to the concentration of the feed

solution during spray drying: 1.54 g/cm^3, 1.45 g/cm^3 for lactose 5% and lactose 20% w/w, respectively; and 1.52 g/cm^3, 1.33 g/cm^3 for sucrose/dextran 20% w/w and sucrose/dextran 50% w/w, respectively. The apparent particle density of mannitol 15% w/w was 1.47 g/cm^3 [119]. Apparent particle densities close to the true density of the materials are correlated to either a network-like structure (porous solid) or completely gas permeable particles [121]. In contrast, lower apparent densities seem to be related to hollow particle appearance, which is corroborated by our results (Figure 4.2). Particle structure and density have been related to the crystallization propensity of carbohydrates. Hollow particles were shown to be formed by amorphous carbohydrates (e.g. lactose), whereas particles with network-like structure (porous solid) were more likely to be obtained from crystalline carbohydrates (e.g. mannitol) [109], [120]. Both gum arabic and maltodextrin are amorphous materials and film forming excipients [123] thus prone to form hollow particles.

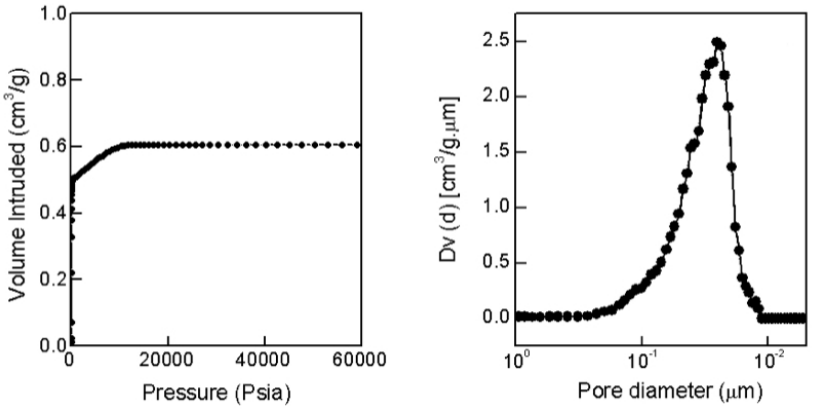

(a) (b)

Figure 4.11: Curves for EGCG/P obtained from Hg porosimetry: pressure/volume dependence (a) and pore size distribution (b).

4.5 Loading Efficiency and Antioxidant Activity

The loading efficiency was determined after MAE by measuring the total amount of EGCG in 10.0 mg sample of EGCG/P suspended in methanol, in which maltodextrin and gum arabic are insoluble. Methanol has a high dielectric constant, dipole moment and dissipation factor (the ability of a solvent to absorb microwave energy and pass it on in the form of heat to other molecules) [124] allowing appreciably superior recoveries than those obtained with other solvents [125], [126]. The EGCG quantification by UV-Vis spectroscopy revealed a loading efficiency of 92±1% and 96±3% at 90 ℃ and 110 ℃, respectively. Accordingly with previous studies, higher recoveries of catechins using methanol as pressurized liquid solvent were attained at 110 ℃ [124], [125], [126]. Similarly to our results, EGCG encapsulation rate was nearly 100% in liposomes incorporated with ethanol [8]. The main issues of using liposomes are related to the scaling up of the encapsulation process and to the delivery form of the liposome-encapsulated compounds. Usually, liposome formulations are kept in relatively dilute aqueous suspensions and this might be a very serious drawback for the large-scale production, storage, and shipping of encapsulated active compounds [14]. The entrapment efficiency of chitosan particles can vary from about 20% to 40-50%, depending mainly on the chitosan molecular weight and the proportion between chitosan and the ionic cross linker (sodium tripolyphosphate) [44], [127]. Chitosan is only soluble in acidic environment, which decreases the availability of catechins in the gastrointestinal tract.

Fluorometric detection of encapsulated EGCG was performed using a Confocal Laser Scanning Microscope (CLSM) TCS Leica. The maximum excitation wavelength of the fluorophore generated in the reaction with EGCG and boric acid was 458 nm and the maximum emission wavelength was 550 nm. The confocal micrograph of EGCG/P in fluorescence mode (Figure 4.12) shows that EGCG is concentrated in the core of the particles, proving the successful encapsulation of EGCG.

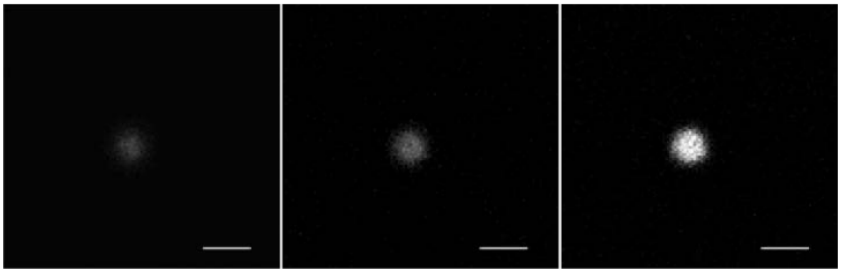

Figure 4.12: Confocal slicing of encapsulated EGCG. The scale bar is 1 µm.

ATR-IR spectrum of EGCG/P (Figure 4.13) shows two absorption bands at 1560 cm^{-1} and 1475 cm^{-1}, not present in the spectrum of unloaded particles, which are attributed to C=C stretching of aromatic rings [128]. The results confirm that EGCG molecules are incorporated in the carbohydrate matrix by intermolecular dipole-dipole interactions, since no chemical interaction was detected. In addition, this also indicates that EGCG chemical integrity was maintained after the spray-drying process.

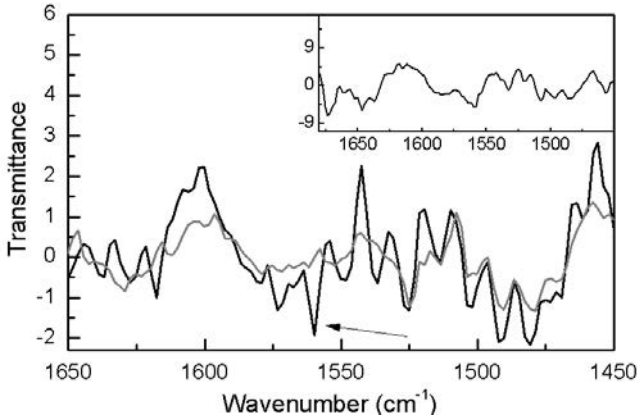

Figure 4.13: ATR-IR spectra of EGCG/P (black line) and unloaded particles (gray line). The inset shows the spectrum of free EGCG.

Figure 4.14 represents the values of DPPH* quenched at different EGCG concentrations for both free EGCG and EGCG/P samples.

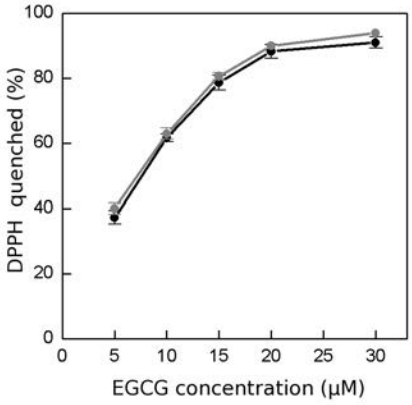

Figure 4.14: Concentration effects of antioxidant-DPPH radical reactions for free EGCG (gray line) and EGCG/P (black line). Average value ± standard deviation, number of experiments = 3.

EGCG and EGCG/P exhibit similar antioxidant activity for all concentrations tested, whereas the control particles, at the same mass concentration of EGCG/P, do not possess antioxidant activity (Figure 4.15). In fact, the exhibited antioxidant activity is only due to the antioxidant properties of EGCG.

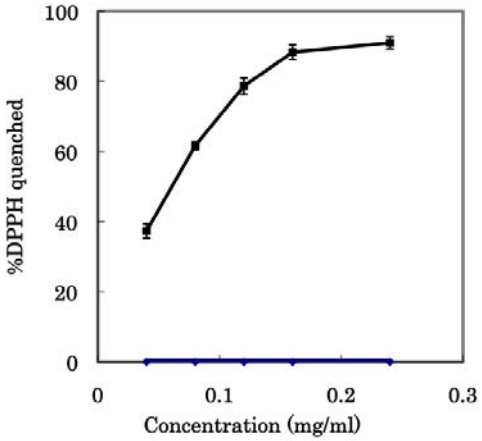

Figure 4.15: Concentration effects of antioxidant-DPPH radical reactions for EGCG/P (black line) and MD/GA (blue line).

The EC_{50} average values attained for free EGCG and EGCG/P were 7.3±0.5 and 7.6±0.3 µM, respectively. RDSC values of free EGCG and EGCG/P at several concentrations are presented in Table 4.1.

Table 4.1: Relative DPPH* Scavenging Capacity (RDSC) of free EGCG and EGCG/P at different concentrations.

Standard concentration (µM)	RDSC value (µM TE/µM) [1]	
	Free EGCG	EGCG/P
5.00	8.02±0.37	7.48±0.51
10.00	6.03±0.10	6.12±0.29
15.00	5.25±0.06	5.37±0.14
20.00	4.57±0.08	4.62±0.16
30.00	3.42±0.01	3.34±0.05

[1]Data correspond to the mean ± standard deviation of triplicate measurements.

RDSC is expressed in terms of trolox equivalents (TE) per unit of EGCG in order to compare the free radical scavenging capacities of antioxidants. Trolox can be applied to report the relative radical scavenging capacities of both hydrophilic and lipophilic antioxidants, which allow to compare directly the DPPH* scavenging capacities of these antioxidants [83]. The study confirmed that EC_{50} values and RDSC determined at different concentrations are similar for both EGCG free and EGCG/P, which demonstrates that the loading method preserved the original antioxidant properties of the EGCG. The main objective of this study was to provide information about the antioxidant and radical scavenging potential of EGCG before and after incorporation in the carbohydrate matrix. The results obtained from these experiments demonstrated that free EGCG and EGCG/P manifested strong antioxidant and radical scavenging activities.

4.6 Intermolecular interactions of EGCG with particle wall materials

The behaviour and intermolecular interactions of EGCG with the polysaccharides were studied by NMR spectroscopy, measuring and analyzing (OR monitoring) a number of NMR parameters, such as chemical shifts, spectroscopic line shape, spin-lattice relaxation (T_1) and translational diffusion. For comparison, NMR spectroscopic investigations of EGCG (chemical structure depicted in Figure 4.1), MD/GA, physical mixtures of EGCG+MD/GA and EGCG+MD+GA were also performed. Additionally, the hydrodynamic diameters of MD/GA and EGCG/P were correlated to the self-diffusion coefficients of the corresponding species.

4.6.1 Structure and NMR spectral characterization

Typical 400 MHz ^{1}H NMR spectrum of EGCG/P is presented in Figure 4.16. The spectra obtained for EGCG, MD/GA and their physical mixtures (EGCG+MD/GA and EGCG+MD+GA) are included for comparison. The assignment of the proton resonances of the samples was based on the analysis of the one- (1D) and two-dimensional (2D: ^{1}H/^{1}H COSY, and ^{1}H/^{13}C HSQC) NMR spectroscopic data and is consistent with the data published before [129], [130], [131], [132], [133], [134]. The assignments of the resonance signals in the spectra of EGCG and polysaccharides are shown in Figure 4.16.

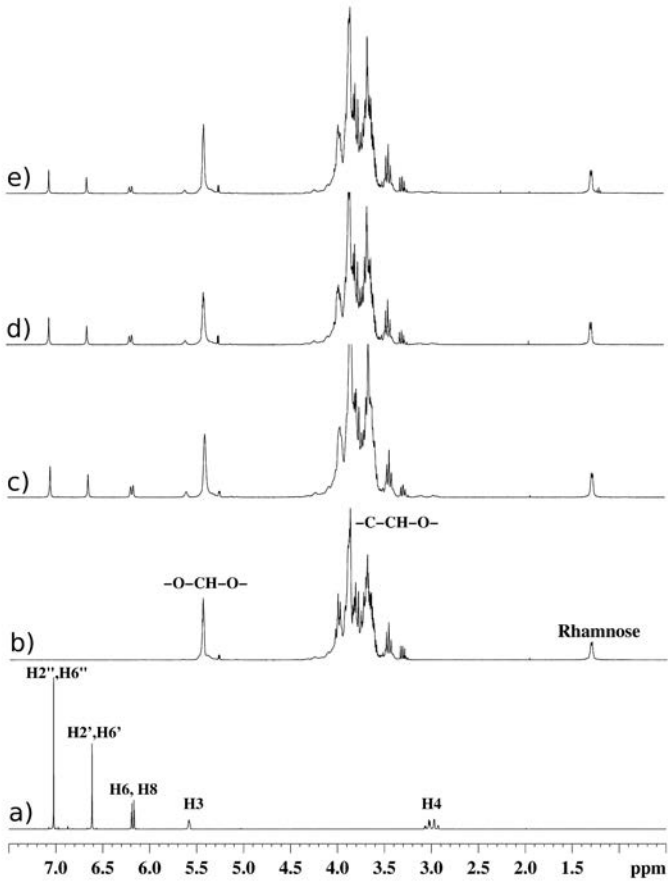

Figure 4.16: 400.15 MHz ^{1}H NMR spectra of EGCG (a), MD/GA (b), EGCG+MD/GA (c), EGCG+MD+GA (d) and EGCG/P (e). The assignment of ^{1}H resonances of EGCG and MD/GA is included.

The ^{1}H NMR spectra of EGCG/P, EGCG+MD/GA and EGCG+MD+GA, are dominated by the intense, broad and overlapped resonance signals characteristic for the polysaccharide structures of maltodextrin (MD) and gum arabic (GA). MD is a polysaccharide consisting mainly of $\alpha(1\rightarrow4)$ and $\alpha(1\rightarrow6)$ D-glucose units connected in chains of variable length (from three to nineteen glucose units) [129], [132], [134]. However, GA is a complex multifraction material consisting mainly of highly branched polysaccharides

and small fractions of high molecular weight protein-polysaccharide complex and glycoproteins. The GA polysaccharides consist of β-(1→3) galactose backbone with linked branches of arabinose and rhamnose, which terminate in glucuronic acid as it was confirmed by NMR spectroscopy and chromatography [133]. Recently, X-ray and neutron scattering investigation of the overall structure and inner heterogeneity of GA in aqueous solution have been reported [131]. Resonance signals of the anomeric and hydroxymethine protons of saccharide residues of the polysaccharide structures of MD and GA in the ^{1}H NMR spectra of EGCG/P, EGCG+MD/GA and EGCG+MD+GA were observed at 5.40-5.20 and 4.5-3.2 ppm. The broad signal at 5.40 ppm was attributed to the anomeric protons of α(1→4) and α(1→6)-linked glucose units of MD. The corresponding resonance signals of the glucose methine protons appeared in the spectral area 4.15 - 3.5 ppm. The resonances at 5.23, 5.04, 4.70 and 4.50 ppm were assigned to the anomeric protons of arabinose, α-glucoronic acid, rhamnose and β-glucoronic acid, respectively, in agreement with the data published before [133]. The analysis of 2D COSY and TOCSY spectra and the distinct resonance signal at 1.27 ppm of C6 methyl protons (doublet, J=5.7 Hz) also confirmed the presence of rhamnose moieties. The observed broadening of the resonance lines suggests involvement of the saccharide residues into high molecular polysaccharide structures with low mobility and variation in the spin-spin relaxation time (T_2). In the ^{1}H NMR spectra of EGCG/P, EGCG+MD/GA and EGCG+MD+GA, an appearance of signals belonging to the protons of EGCG were clearly observed (Figure 4.16). A down field chemical shift of 0.03-0.04 ppm was detected for H3, H4, H2', H6', H2"and H6"protons of EGCG in the spectra of EGCG/P and EGCG+MD+GA but smaller in EGCG+MD/GA (Table 4.2). The stronger downfield chemical shift of these protons in EGCG/P and EGCG+MD+GA was attributed to more effective H-bonding of EGCG included into the polysaccharide matrix. A possible explanation for the smaller chemical shifts in EGCG+MD/GA is the fact that the EGCG molecules are located on the surface of the MD/GA nanoparticles and thus have less effective H-bonding.

Table 4.2: Selected ^{1}H chemical shifts (in ppm) and chemical shift differences with respect to pure EGCG (in italics) of EGCG, EGCG+MD/GA, EGCG+MD+GA and EGCG/P.

Proton	EGCG	EGCG+MD/GA	EGCG+MD+GA	EGCG/P
H2", H6"	7.018	7.046	7.047	7.048
		0.028	*0.029*	*0.030*
H2', H6'	6.604	6.637	6.643	6.645
		0.033	*0.039*	*0.041*
H6, H8	6.17	6.184	6.177	6.175
		0.014	*0.007*	*0.005*
H3	5.567	5.581	5.597	5.598
		0.014	*0.030*	*0.031*
H4	2.984	3.017	3.033	3.033
		0.033	*0.049*	*0.049*

Despite the ^{1}H/^{1}H NOESY spectra of EGCG/P (Figure 4.17) being dominated by nuclear Overhauser effects (NOE) between the protons belonging to the polysaccharide chains, weak signals were detected due to intermolecular dipole-dipole interactions between H2", H6" protons of EGCG (7.05 ppm) and glucose methine protons of MD/GA in the spectral area 4.15-3.5 ppm. The dipole-dipole interactions between EGCG and MD/GA protons confirm the entrapment of EGCG into the polysaccharide matrix of maltodextrin-gum arabic of EGCG/P.

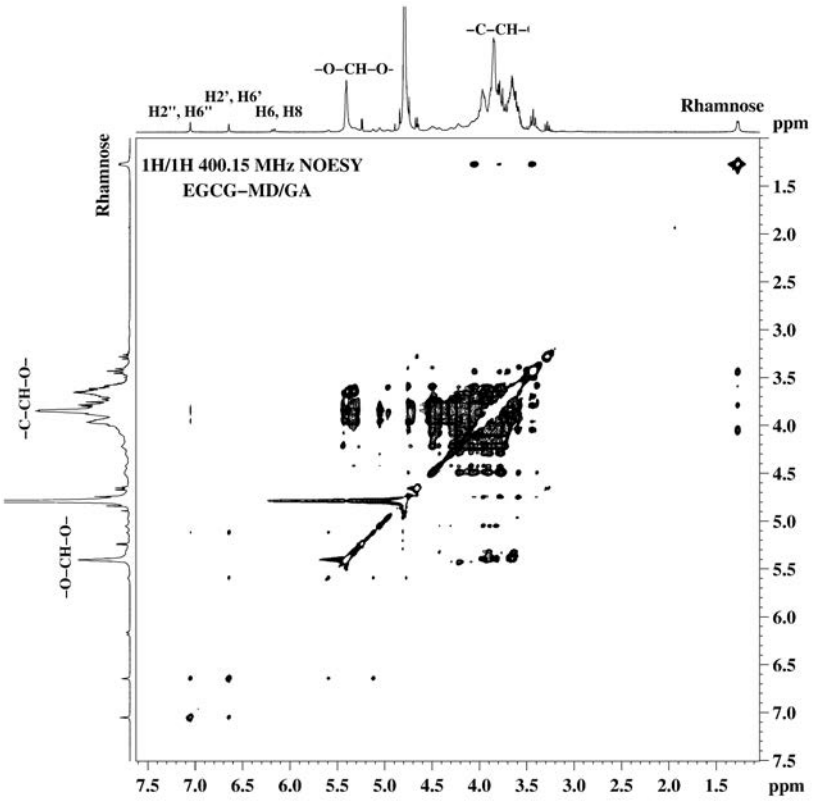

Figure 4.17: 400.15 MHz 2D $^{1}H/^{1}H$ NOESY spectra of EGCG-MD/GA in D_2O.

4.6.2 T_1 Relaxation investigation

The NMR relaxation measurements can provide structural and dynamic information about molecules and molecular aggregates [129], [133], [135]. For protons in solution there are three principal mechanisms of spin-lattice relaxation: dipole-dipole interaction, chemical shift anisotropy and spin-rotational interaction, however, the first one tends to be dominant. Spin-lattice relaxation times are related via correlation times to the mobility of the molecules and may be used to estimate the possibility for intermolecular aggregate formation [135], [136], [137]. Examples of spin-lattice relaxation times (T_1) determined for protons belonging to EGCG and carbohydrate polymer matrix for the samples studied are shown in Table 4.3.

Table 4.3: Selected spin-lattice relaxation times (T_1, in s) determined for selected ^1H chemical shifts (in ppm) belonging to EGCG, MD and GA in D_2O at 30 ℃.

Sample	EGCG (δ, ppm)			MD and GA (δ, ppm)					
	7.03	6.6	6.17	5.4	5.23	4.1-3.5	3.4	3.3	1.28
EGCG	1.691	1.242	1.833						
MD/GA				0.907	1.958	0.558	1.339	2.017	0.715
EGCG+MD/GA	1.384	1.149	1.379	0.885	1.908	0.576	1.323	2.002	0.693
EGCG+MD+GA	1.321	1.115	1.316	0.875	1.828	0.559	1.323	2.142	0.701
EGCG/P	1.26	1.021	1.275	0.889	1.818	0.56	1.304	1.941	0.666

The relaxation times of protons from the individual functional groups of EGCG and polysaccharides MD and GA vary according to their internal mobility but the overall trends observed were identical for all groups. Only insignificant T_1 s alterations were detected for MD and GA protons in the presence of EGCG probably due to more effective dipole-dipole interaction between the rigid polymer molecules and EGCG. The relaxation times of EGCG protons were significantly longer than when it was encapsulated or physically mixed with MD/GA or MD+GA. Considering the complex structures and the high molecular weight of the species presented into MD and GA, the decreased T_1 s of EGCG were attributed mainly to the increased viscosity of the medium. It is significant to note that the measured relaxation times of EGCG in both physical mixtures were closely similar but longer than those in EGCG/P, even though the samples have been prepared at the same concentration and no difference in the viscosity could be assumed. This indicates that the microenvironments of the protons of EGCG in the EGCG/P and both physical mixtures (EGCG+MD/GA and EGCG+MD+GA) are different. The results strongly suggest that in the case of EGCG/P the EGCG molecules are entrapped into the MD/GA matrix of the nanoparticles.

4.6.3 Diffusion NMR spectroscopy

Diffusion ordered NMR spectroscopy (DOSY) was used to analyze overall structure of EGCG/P, to clarify the origin of the EGCG-polysaccharide interactions and to locate the EGCG molecules into the MD/GA matrix. The pulsed field gradient spin echo NMR technique is a straightforward procedure for measuring the diffusion coefficients of individual species. Particularly, useful information can be obtained regarding the size, molecular weight and shape of the species in solution under given conditions. In order to get insight into the structural modifications of the species presented in the EGCG/P and to account for changes in the solvent viscosity and minor fluctuations of samples temperature, it was useful to use an internal diffusion reference [79], [82], [77]. Since modifications of the solution composition could induced changes in the viscosity and these changes affect equally all species in the solution, the use of reference allows one to take into account the variation in solvent properties and correct the measured diffusion values [82]. The reference compounds should have chemical inertness, well resolved signals, negligible diffusion coefficient dependence on the solutes concentration and ideally presented already in the solution as either reference for chemical shifts or quantitative determination. Therefore, we found it useful to use TSP not only as chemical shift reference but also as an internal diffusion reference and all diffusion coefficients presented in Table 4.4 are given as a ratio D/D_{TSP} according procedure published before [82]. As it was mentioned above, MD and GA are complex structures that mainly consist of saccharide units connected in chains of variable length. Typically, EGCG is at least one half of the average size of MD and much less portion of those of GA. Therefore, it was found reasonable to compare the diffusion coefficient of EGCG, MD and GA in EGCG/P with that of the pure EGCG, MD/GA and both physical mixtures (EGCG+MD/GA and EGCG+MD+GA). Special care was taken to perform all experiments under identical conditions of concentration and temperature. Self-diffusion coefficients (D) of EGCG molecules present in EGCG/P, EGCG+MD/GA and EGCG+MD+GA were determined from the resonance signals of H2" and H6" protons of gallate moiety (at 7.03 ppm). The corresponding values of D for MD and GA were determined from the resonance signals of the

anomeric protons at 5.40 (MD) and 5.23 (GA) ppm, saccharide hydroxymethine protons at 4.15-3.50 ppm, 3.40 and 3.30 ppm, and methyl protons of rhamnose moieties at 1.27 ppm. The relative diffusion coefficients to TSP and the calculated standard deviations are presented in Table 4.4.

Table 4.4: Relative diffusion coefficients (related to TSP), with calculated standard deviations (in italics) of EGCG and MD/GA in D_2O at 30 ℃ for the samples studied.

Sample	EGCG (δ, ppm)	MD and GA (δ, ppm)					
	7.03	5.42	5.25	4.1-3.5	3.43	3.30	1.28
EGCG	0.62						
	0.01						
MD/GA		0.40	0.55	0.28	0.37	0.52	0.04
		0.04	*0.01*	*0.03*	*0.02*	*0.02*	*0.03*
EGCG+ MD/GA	0.49	0.45	0.57	0.37	0.42	0.61	0.07
	0.03	*0.08*	*0.03*	*0.07*	*0.04*	*0.04*	*0.03*
EGCG+MD+GA	0.49	0.49	0.58	0.35	0.46	0.61	0.09
	0.02	*0.04*	*0.02*	*0.04*	*0.03*	*0.05*	*0.01*
EGCG/P	0.45	0.37	0.52	0.30	0.37	0.50	0.06
	0.03	*0.04*	*0.05*	*0.05*	*0.06*	*0.04*	*0.03*

The D/D_{TSP} for MD and GA in EGCG/P and MD/GA were only slightly lower than the corresponding values in the physical mixtures (EGCG +MD/GA and EGCG+MD+GA). The higher D/D_{TSP} values determined for the components of MD and GA in EGCG+MD/GA and EGCG+MD+GA can be a result of EGCG initiated distortion of the branched polysaccharide structures of MD/GA. The decreased diffusion of MD and GA in EGCG/P is an indication for intermolecular interactions between EGCG and these species in the loaded nanoparticles. The relative diffusion coefficient of the pure EGCG was significantly higher than the corresponding values in the EGCG/P, EGCG+MD/GA and EGCG+MD+GA formulations. This was attributed mainly to the increased viscosity of the solution in the presence of MD and GA. However, the corresponding D/D_{TSP} values of EGCG were lower in EGCG/P than the corresponding values in both physical mixtures that reproduce the composition of EGCG/P. This reduction is a strong indication of an interaction between EGCG and the polysaccharide matrix.

Typical DOSY spectrum of EGCG/P is shown in Figure 4.18.

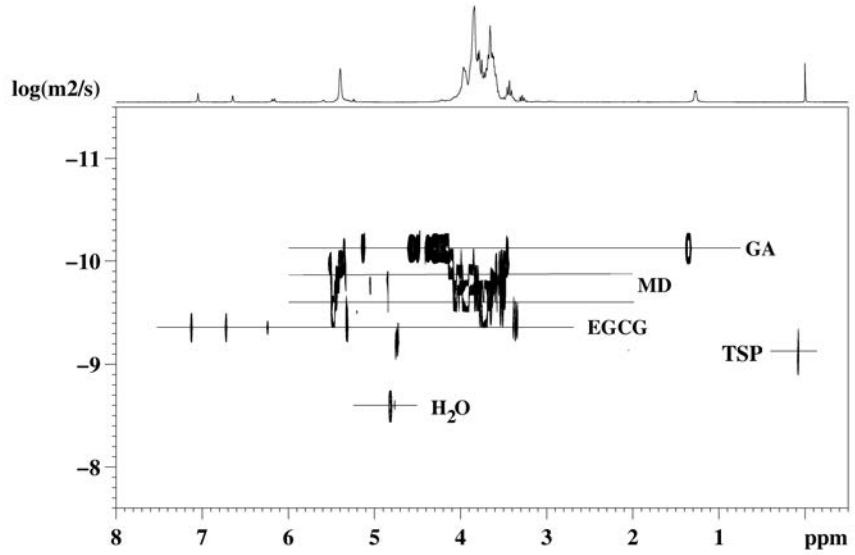

Figure 4.18: 400.15 MHz 2D DOSY spectra of EGCG-MD/GA in D_2O, at 30℃.

A bigger intensity ratio observed by DLS between big and small nanoparticles for EGCG/P (Figure 4.7), can explain the results of DOSY that show lower diffusion coefficients measured for the EGCG loaded nanoparticles when compared to unloaded ones.

4.7 Release studies

In vitro release studies were performed to study the diffusion of EGCG through the carbohydrate matrix in ultrapure water and buffer solutions at different pH values (pH 3, 5.5 and 10), using dialysis membranes of regenerated cellulose.

The results of EGCG dialysis in ultrapure water (pH 5.5) are depicted in Figure 4.19.

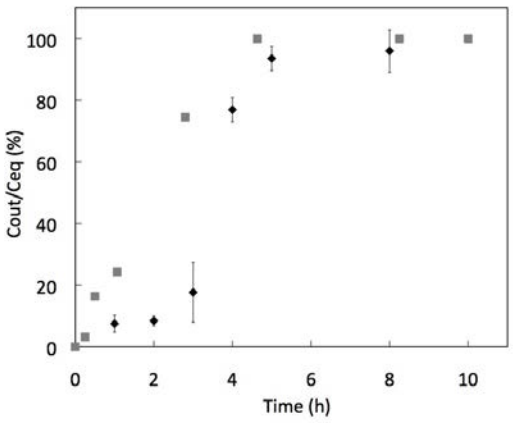

Figure 4.19: *In vitro* EGCG release profile of both dialyzed samples, free EGCG (in gray) and EGCG/P (in black), versus time in ultrapure water.

Figure 4.19 shows that EGCG diffusion through the membrane occurred approximately, in half of the time in comparison with EGCG/P, reaching the equilibrium concentration after 4 h and 8 h, respectively. These findings suggest that this process is slower for EGCG/P due to the entrapment of EGCG in the carbohydrate matrix, which decreases the diffusion rate of EGCG. EGCG stability after encapsulation was evaluated calculating the %DPPH* quenched of the released EGCG from the dialysis membrane, during time (Figure 4.20).

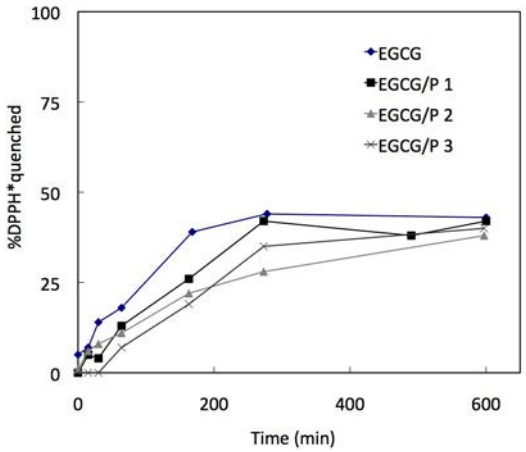

Figure 4.20: Concentration effects of antioxidant-DPPH radical reactions for EGCG and EGCG/P after dialysis (EGCG: 6.1 µM, EGCG/P 1: 5.5 µM, EGCG/P 2: 6.1 µM and EGCG/P 3: 6.1 µM).

From Figure 4.20, it is visible that the %DPPH* quenched increases with the increase of EGCG concentration in the membrane exterior. EGCG reaches the dialysis equilibrium concentration and consequently the maximum %DPPH* quenched, more rapidly than EGCG/P. These results confirm the successful incorporation of EGCG in the carbohydrate matrix and the maintenance of EGCG antioxidant properties. As seen from Hg porosimetry, EGCG/P are porous, which allows the release of EGCG from the particles.

The results of EGCG dialysis in buffer solution at pH 3 are depicted in Figure 4.21.

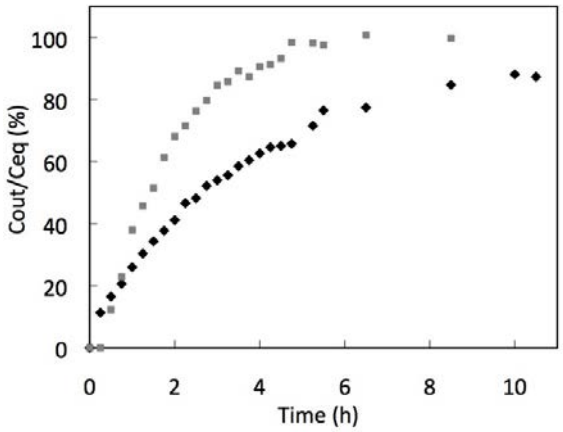

Figure 4.21: *In vitro* EGCG release profile of both dialyzed samples, EGCG (in gray) and EGCG/P (in black), versus time at pH 3.

Similarly, to the results obtained for dialysis in ultrapure water, free EGCG diffusion at pH 3, was faster than for EGCG/P. However, in this case, EGCG release from the carbohydrate matrix was incomplete, reaching a maximum of 90% of the equilibrium concentration, in the membrane exterior.

Figure 4.22 shows the release profile of EGCG from the EGCG loaded particles at pH 10, in comparison with free EGCG.

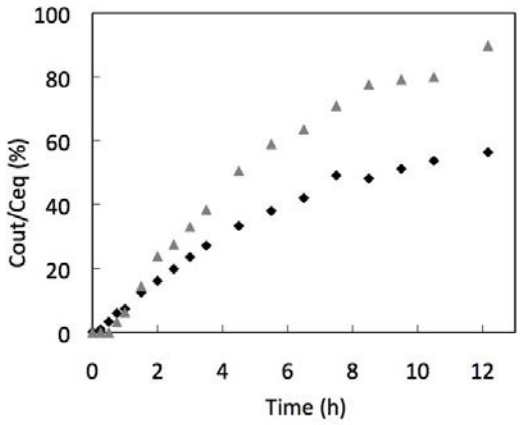

Figure 4.22: *In vitro* EGCG release profile of both dialyzed samples, free EGCG (in gray) and EGCG/P (in black), versus time at pH 10.

EGCG/P provided a continuous release of the entrapped EGCG for up to 26 h, with a maximum amount released of 70%. On the other hand, free EGCG was completely released from the dialysis membrane after 24 h. At basic pH (pH 10), EGCG release rate is slow for both dialyzed samples.

4.8 Cytotoxicity Studies

The cytotoxicity of encapsulated EGCG to Du145 cells was evaluated at a concentration of 100 µM by MTT reduction and caspase-3 activation assays, and compared with the activity of nonencapsulated antioxidant. This concentration and long incubation period (3 days) are normally the conditions used to study EGCG inhibitory effect because the uptake of free EGCG is concentration dependent [138]. As shown in Figure 4.23, Du145 cell line showed significantly lower metabolic activity in the presence of EGCG/P, compared with untreated control cells. After incubation for 64 h, encapsulated EGCG caused similar reduction of cell viability (38%) as free EGCG (34%). MD/GA did not induce significant toxicity on the cells.

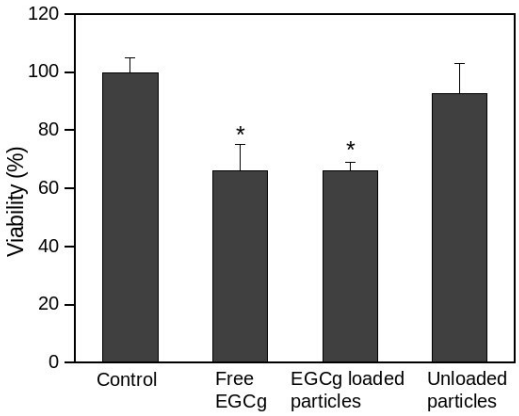

Figure 4.23: Viability of Du145 cells exposed for 64 h to free EGCG, EGCG/P and unloaded nanoparticles, as assessed by MTT reduction assay. *Significantly different from control ($p < 0.01$)

Encapsulated EGCG induced considerable caspase-3 activation similar to free EGCG, when compared with nontreated cells and cells treated with unloaded particles (Figure 4.24).

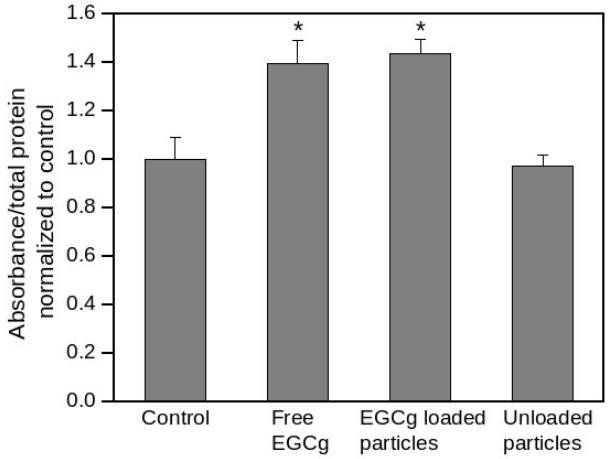

Figure 4.24: Activation of caspase-3 in Du145 cells exposed for 64 h to free EGCG, EGCG/P and unloaded nanoparticles. *Significantly different from control ($p < 0.01$).

Clonogenic assay, a standard analysis for screening cytotoxic activity of drugs, was used to study the effect of EGCG/P at different concentrations on prostate cancer cells. This assay is much more sensitive than that previously described due to very low cell-seeding density. Treatment of Du145 cells with increasing concentrations of encapsulated EGCG from 0 to 10 µM resulted in a concentration-dependent decline in cell survival, as evidenced by the reduction in surviving fraction (Figure 4.25a). The effectiveness of encapsulated EGCG was higher when compared with free EGCG at low concentration (1 and 2 µM). At concentrations of 25 µM or higher, all cells died. The surviving fraction of cells treated with MD/GA was similar or higher to the control sample (no treatment), confirming that the carbohydrate matrix is not toxic to Du145 cells (Figure 4.25b). Statistical analysis established that MD/GA at 1 mg/ml significantly increase the surviving fraction, compared with the control ($p < 0.05$).

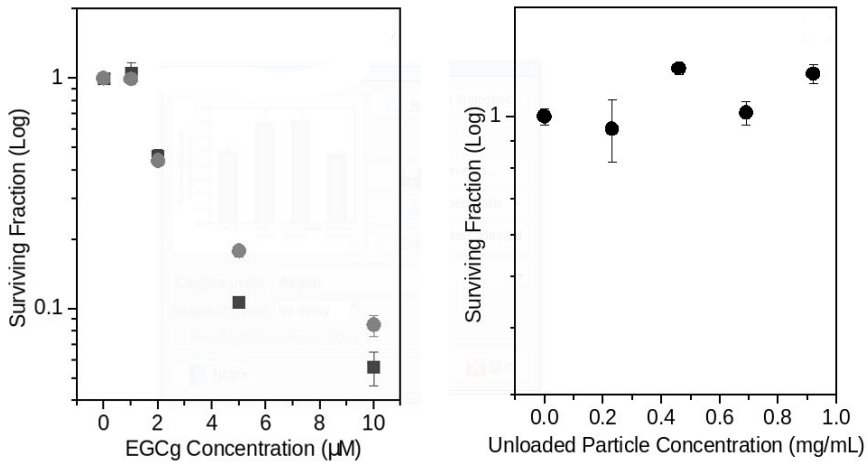

(a) (b)

Figure 4.25: Surviving fraction of DU145 assessed by clonogenic assay. (a) Cells incubated with free and encapsulated EGCG, normalized to initial EGCG concentration. (b) Cells incubated with unloaded particles.

Encapsulated EGCG, at a concentration of 100 µM, was able to reduce cell viability and induce caspase-3 activation in cultured prostate cancer

cells, comparable to the free EGCG [139], [140]. A similar conclusion was attained with encapsulated EGCG in polyelectrolyte coated gelatin NPs of 200 nm, which blocked HGF-induced intracellular signaling in the breast cancer cells as free EGCG [141]. A reduction in the number of the colonies by 10-20%, on applying low concentration (1-2 µM) of EGCG/P, is to be regarded as a demonstration of the ability to inhibit cell proliferation by NPs at lower concentration than that for free EGCG. These results are in agreement with the previous study using PLA-PEG NPs, in which it was shown that low concentrations of encapsulated EGCG (2.7 µM) is able to reduce the number of colonies more efficiently than free EGCG [142]. A possible reason for the efficacy increase at low EGCG concentrations is the efficient delivery by NPs. Moreover, it is expected that NPs increase EGCG stability. It was found that the EGCG is more stable in the presence of cells than in cell medium. Such behavior is attributed to stabilizing factors from cells such as proteins and antioxidants [138]. Gum arabic has antioxidant properties [143] and, thus, might augment protection of EGCG molecules, which is important for oral administration [144]. The molecular mechanisms of the biological effects of EGCG are still being studied, but it has been proposed that EGCG could exert its activity by binding to receptors (e.g., EGF-receptor) or intracellularly by inhibiting protein kinases [138]. It was demonstrated that there is a size-dependent cellular uptake of biodegradable particles [145], [146]. Particles of 50, 100 and 200 nm were internalized and distributed throughout the cells after 2 h, whereas 500 nm beads were localized largely at the periphery of the cells [145]. It is reasonable to assume that maltodextrin-gum arabic NPs are internalized by the cells. Gum arabic-coated iron oxide NPs with hydrodynamic diameters of approximately 120 nm were shown to have higher affinity to enter tumor cells than starch-coated NPs and were not cytotoxic [147]. At concentrations higher than 5 µM, the inhibitory effect of encapsulated EGCG was retained, but it was less pronounced when compared with free EGCG, which may be attributed to a saturated and limited capability of cellular uptake of NPs, as it has been observed for poly(d,l-lactide-co-glycolide) NPs [146], [148]. The decrease in NP uptake at higher concentration is possibly caused by aggregation or reveals competing binding sites. Aggregation, at some extension, might be favorable since it may prevent small particles from escaping a tumor

interstitium. The size of liposomes containing EGCG was shown to strongly influence the accumulation of the active molecule in basal cell carcinomas [8]. Large vesicles (> 300 nm) were more readily entrapped by the tumor.

4.9 Conclusions

EGCG was encapsulated by spray-drying using a combination of maltodextrin and gum arabic, as wall materials. The spray-drying technique and the process conditions selected were effective in encapsulating and stabilizing EGCG. Carbohydrate particles have proved to be adequate vehicles for the encapsulation of natural antioxidants because they maintain the antioxidant activity of EGCG. High loading efficiency was obtained, which is a promising result for scaling up the process and pharmaceutical applications. Cytotoxic studies suggest that these polysaccharide NPs can be used as nanochemopreventive tools as they can be used to deliver natural antioxidants capable of inhibiting steps of the tumorigenesis process.

Chapter 5

Collagen hydrolysate loaded particles

Contents

5.1 Introduction

Collagen is a multifunctional protein that plays an important role in the formation of tissues and organs, and is involved in various functional expressions of cells [6]. The major property of collagen is to provide tensile strength to tissues such as tendons, ligaments, skin, cartilage, blood vessels, and bones [149]. Collagen consists of three polypeptide α-chains

wound together in a rod-like helical structure. Each molecule is 300 nm in length and 1.5 nm in diameter with a molecular weight of 300 kDa. The sequence of amino acid residues in the chains is very specific: glycine is every third residue in repeating sequence; Gly-X-Y and proline and hydroxyproline amino acids are X and Y, respectively. Collagen triple helix structure is depicted in Figure 5.1.

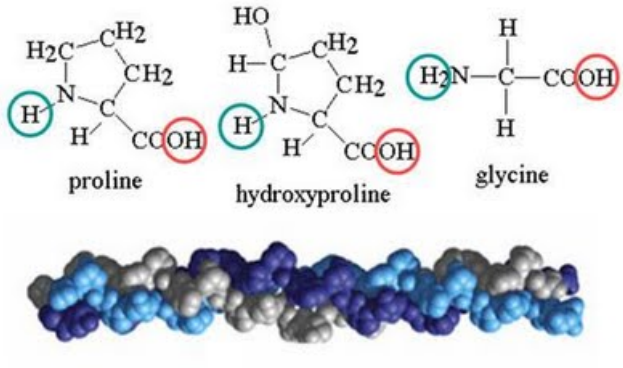

Figure 5.1: Collagen triple helix structure.

The molecular structure is stabilized by a net of intra and inter-chain hydrogen bonds between the –NH group of glycine and the carbonyl group C=O of residues from another polypeptide chain or by hydrogen bonds with water molecules [150]. From the twenty-seven types of collagens already identified, collagen type I is the most abundant and the most investigated for biomedical applications [42]. Type I collagen is the major structural protein distributed throughout the whole body accounting for 25% of total body protein and for 80% of total conjunctive tissue in humans [151]. It is an important component of bone, being the main extra cellular matrix protein for calcification, which also plays a role in osteoblast differentiation [152]. It is widely known that the digestion of collagen proteins or hydrolysates *in vivo* will generate peptides that may be useful for organic biosynthetic processes.

Collagen hydrolysate (CH) is obtained by enzymatic proteolysis of collagen and contains 20 amino acids, predominantly glycine, proline and hydroxyproline. Its average molecular weight ranging from 3 to 6 kDa is one of the

most important factors which determines its biological properties [153]. CH is considered to be an ideal ingredient in the field of functional foods due to its high nutritional value, high antihypertensive activity and low antigenicity. Due to its biochemical and nutritional properties, it has been proposed that collagen hydrolysate may be a therapeutic agent for the management of bone and joint disorders, as a bioavailable source of peptides [11]. These peptides have repeated unique Gly-Pro-Hyp sequences in their structure, and the observed antioxidative and antihypertensive properties have presumably been associated with this unique amino acid composition [154]. Moreover, collagen hydrolysate peptides have exhibited numerous other bioactivities, namely: antimicrobial activity, mineral binding capacity, the lipid-lowering effect, immunomodulatory activity and beneficial effects on skin, bone or joint health [153]. Some studies have been performed to confirm the *in vivo* biological activity of collagen hydrolysate, and some convincing data have been obtained for animal models [155], [156]. Oral administration of collagen hydrolysate increased bone mass content and density in rats and mice fed a calcium or protein deficient diet [155] and also increased the quantity of type I collagen and proteoglycans in the bone matrix of ovariectomized rats [156]. Saito *et al.* examined the effects of fish skin collagen hydrolysate administration in rats and their results suggest that ingestion of collagen hydrolysate peptides may have a beneficial effect on lipid absorption and metabolism [157]. Clinical investigations suggest that ingestion of CH reduces pain in patients suffering from osteoarthritis and collagen hydrolysate has been shown to be involved in cartilage matrix synthesis [158]. Because of these properties, collagen hydrolysate has long been used in pharmaceutical and dietary supplements [159], [160]. Recently, some peptides from marine sources were reported to act protectively against ultraviolet radiation-induced damage on mice skin [161].

In order to be active in the site of action, dietary compounds must be able to cross the intestinal barrier, reach the blood circulation and be available for metabolic process or storage in the body. However, collagen hydrolysate is exposed to a wide range of oxidants, such as, reactive oxygen species and that, unlike cells, the extent of antioxidant defenses, repair, and removal of this damage is limited. This damage results in altered structure and function of collagen hydrolysate [162].

Polymeric delivery systems have been developed to stabilize proteins and maintain their chemical integrity, assuring their convenient delivery. Polymers have also been widely investigated for use in protein-polymer conjugates. These systems have generally been utilized for prolonging the circulation half-lives of proteins or for delivering targeted payloads of protein pharmaceuticals to specific tissues.

In this study, CH loaded (in a proportion of 5 and 25 wt.%) particles were produced by spray-drying to provide CH a long-term stability, by its incorporation in a polysaccharide matrix, based on maltodextrin and gum arabic. This innovative protein-carbohydrate system protects CH from oxidation and allows its incorporation in functional food, particularly, beverages, since CH/P in solution doesn't exhibit color, odor or taste. CH/P were characterized in solid state and aqueous medium.

5.2 Physical characterization

5.2.1 CH/P morphological characterization and loading

Figures 5.2 and 5.3 show SEM micrographs of spray-dried unloaded particles and CH loaded particles. Results clearly demonstrated differences in shape and size, showing a wide size distribution ranging from 400 nm to 50 µm. CH/P morphology differs from spherical shape with extensive dented surface to a smooth surface with no visible dents. The variation of surface morphology may be attributed to a number of drying parameters such as drying rate and the particle composition, namely, the amount of CH loaded in the particle. Formation of dented surfaces of spray-dried particles was attributed to the shrinkage of the particles during the drying and cooling process [110]. Moreover, GA molecules interact strongly among themselves forming a multilayer framework, while their interaction with and among MD molecules is not so strong, producing "holes" in the structure [163]. Figure 5.2a shows that the main population observed in the unloaded particles is disk-like and corrugated with highly dented surfaces. The formation of spherical particles with smooth surface observed in Figures 5.2c and 5.2d is probably, attributed to a higher content in maltodextrin (low molecular weight sugar) in their composition. Low molecular weight sugars usually act as plasticizers preventing shrinkage of the surface during drying [164].

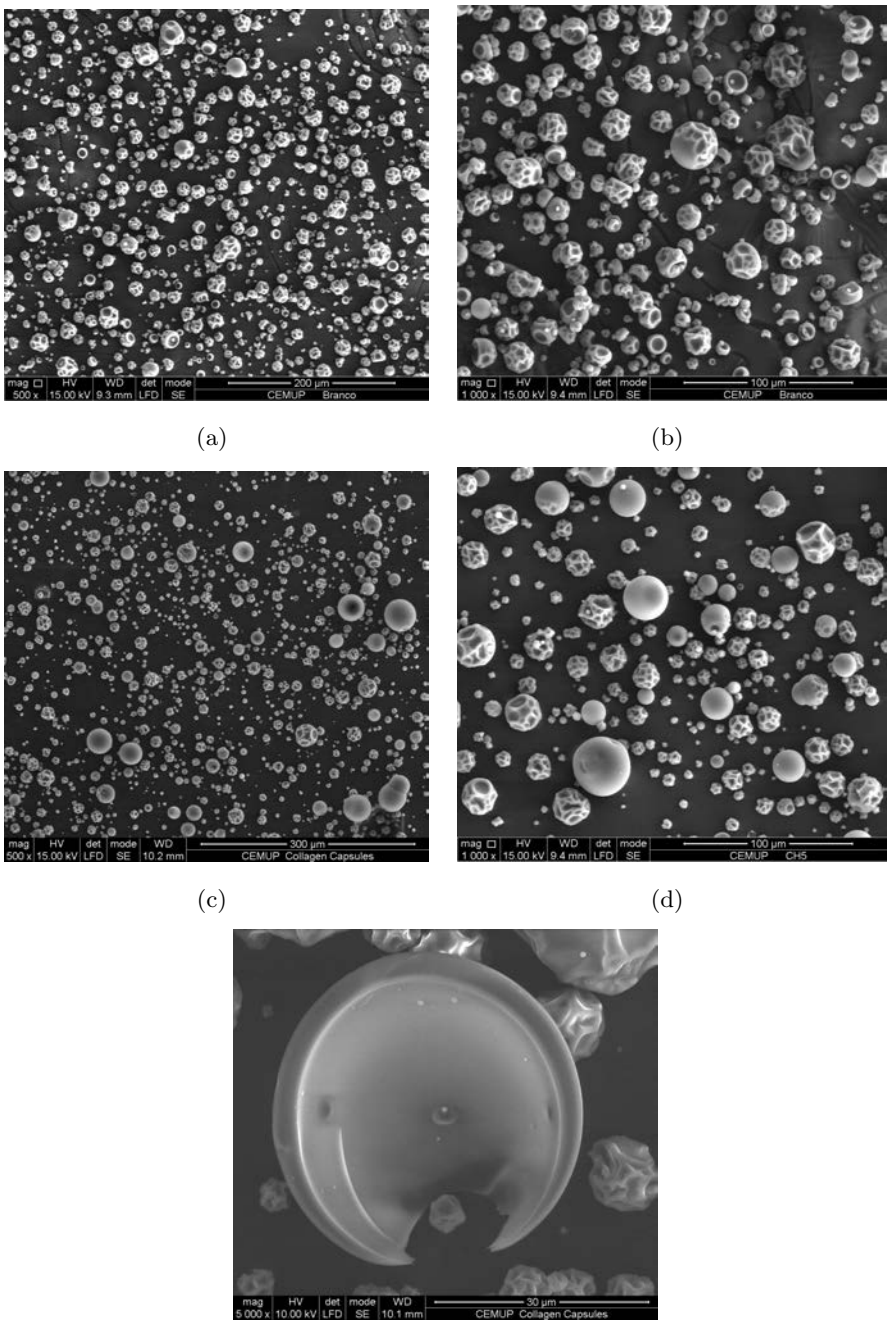

(a) (b)

(c) (d)

(e)

Figure 5.2: Visualization of MD/GA (a and b), and CH (5%) loaded particle size and surface morphology by scanning electron microscopy. Scale bars represent 300 µm (a), 100 µm (b), 300 µm (c), 100 µm (d) and 30 µm (e).

Additionally, SEM observations show that the spherical particles have a hollow core. The inner structure of the spray dried particles matches what Ré (1998) defines as a particle architecture, in which the active compound is evenly distributed throughout or embedded in the matrix of the wall material matrix [165]. On the other hand, collagen hydrolysate (25%) loaded particles have bigger diameters and it can be seen from Figure 5.3 that the majority of these large particles are of spherical shape. A possible reason for the observed phenomenon is the higher content of CH in the particles, since the use of CH leads to a smooth particle surface [166].

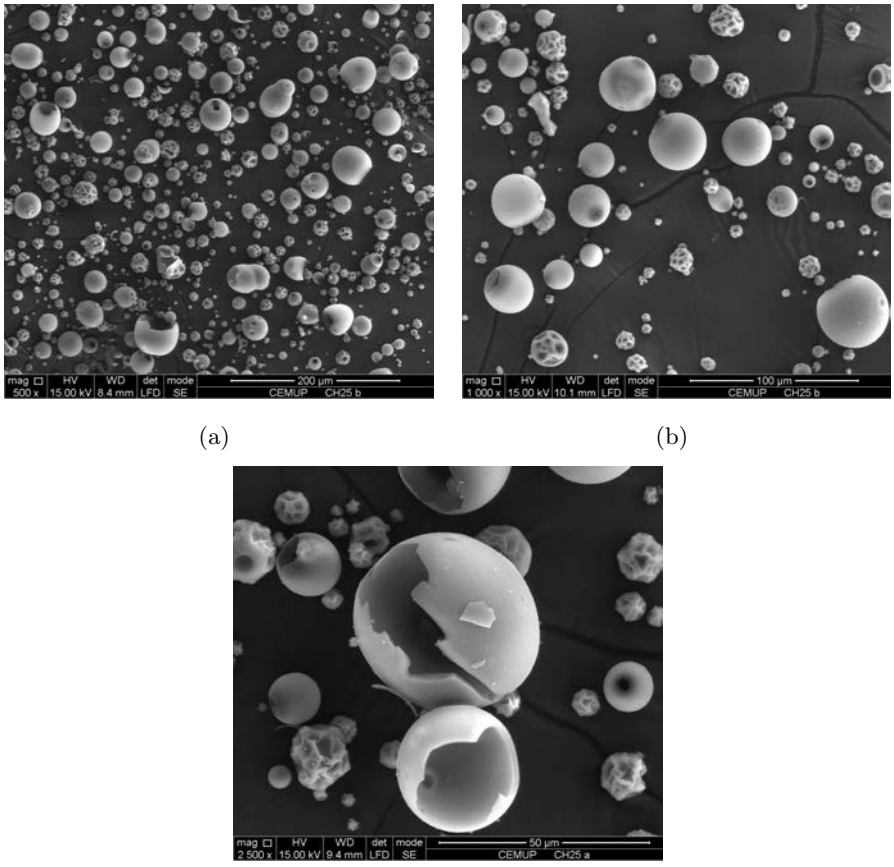

(a) (b)

(c)

Figure 5.3: Visualization of CH (25%) loaded particle size and surface morphology by scanning electron microscopy. Scale bars represent 200 µm (a), 100 µm (b) and 50 µm (c).

From Figure 5.3 it is visible that the collapse of some particles occurred. According to Walton and Mumford (1999) as the solid concentration of the feed increases, the concentration gradient within the drying droplet decreases, foreseeing the critical surface concentration required for selective diffusion is attained more rapidly, and volatile retention is increased. However, it may be that, an increase in feed concentration simply increases the barrier to mass transfer, therefore, increasing volatile retention. If this were the case, the particles would tend to expand, rupture and collapse, or form blowholes during drying [167]. It is clear from SEM micrographs that the wall thickness of the spherical particles decreases with the amount of CH loaded in the particles. This population of particles, particularly presented in the 25% CH samples, shows holes or are broken, as depicted in Figure 5.3.

Collagen hydrolysate was extracted from the carbohydrate particles by MAE, with a loading efficiency of 86±7% and 85±4%, for particles loaded with 5% and 25% of CH, respectively. A comparison has been made of the recoveries obtained, employing different extracting temperatures and the higher loading efficiency was achieved at 100 ℃. This high loading efficiency indicates that this encapsulation method is suitable for preparing the CH/P formulations, in agreement with the values obtained previously for the catechin loaded particles (96±3%) [168].

5.2.2 Particle size distribution and surface charge

The particle size distribution of the suspended CH/P was determined using dynamic light scattering. CH/P size distribution was bimodal, comprising two populations of particles with average hydrodynamic diameters of 30 nm and 300 nm (Figure 5.4). These average hydrodynamic diameters are in the same range as the obtained for EGCG/P and MD/GA [168].

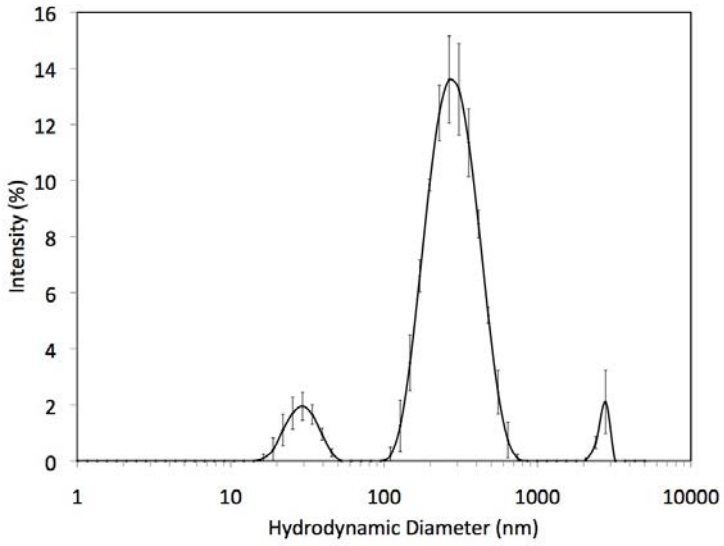

Figure 5.4: Average hydrodynamic diameter distribution of CH/P as determined by DLS. Average value ± standard deviation, number of experiments = 3

The surface charge of particles has a significant influence on the suspension stability, on the particle interactions with charged substances and on the adherence of drug delivery systems onto biological surfaces. The measured zeta potential of the CH/P surface was approximately -32±5 mV and -38±5 mV, for CH 5% and 25% loaded particles, respectively, indicating a strong negative charge at the particle's surface. In general, a zeta potential of ±30 mV is required as a minimum for a physical stable suspension solely stabilized by electrostatic repulsion [169]. Similarly to EGCG/P, the high negative zeta potential obtained for CH/P indicates the colloid stability and that there is no tendency to the formation of particle aggregates.

5.3 CH/P inner structure

The true density of the spray-dried CH/P as determined by helium pycnometry, ρ_{true}, was 1.01 g/cm^3 and 1.37 g/cm^3, for collagen hydrolysate 5% and 25% loaded particles, respectively. True density considers only the volume of the particles that is not permeable to the displacing gas (He).

These results are consistent with the morphology of the CH (25%) loaded particles that, as seen by SEM images (Figure 5.3), are broken and/ or with holes, allowing the He penetration. In contrast, the hollow particles (CH/P 5%) do not allow the He penetration, due to wall resistance and the low percentage of broken particles, as observed in Figure 5.2.

The apparent density of collagen hydrolysate (5%) loaded particles was further analyzed with mercury porosimetry, which measures both interparticle (intrapore spaces, between particles) and intraparticle porosity (interpore voids, within the particles). CH (5%) loaded particles revealed an inter- and intraparticle porosity of 0.2 and an apparent density of 0.51 g/cm^3. The value of total surface area measured by low and high-pressure mercury porosimetry was 1.76 m^2/g. The pore size distribution obtained for CH (5%) loaded particles is bimodal, with average pore diameters of 340 nm and 4 µm, as shown in Figure 5.5.

Apparently, the large size mode corresponds to external pores between particles, the low size mode to the internal pores, within the particles.

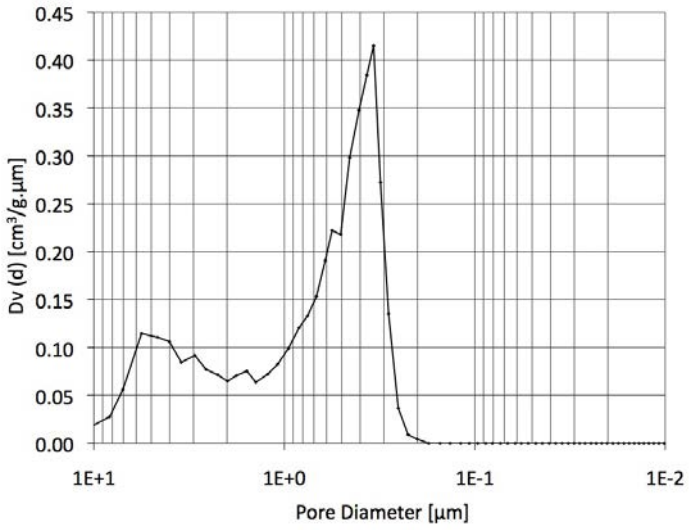

Figure 5.5: Pore size distribution determined by mercury porosimetry for CH (5%) loaded particles.

5.4 CH intermolecular interactions with MD/GA particles

5.4.1 ATR analysis

The ATR spectra of the CH loaded particles are shown in Figure 5.6, in comparison to the corresponding spectra of free collagen hydrolysate and unloaded particles. Collagen hydrolysate shows a characteristic ATR spectrum, with adsorption bands of amide I at approximately 1650 cm^{-1} [170]. The amide I band results from the stretching vibration of the peptide carbonyl group (C=O). The intensity of the characteristic collagen hydrolysate absorption bands increases from the CH (5%) loaded particles to the CH (25%) loaded particles, due to the higher amount of the collagen hydrolysate loaded in the particles. The presence of these bands in the CH/P is not visible in the unloaded particle's spectrum. In addition, GA is a mixture of branched polysaccharides and glycoprotein containing numerous functional groups, which may be responsible for hydrogen bonds, between MD/GA/CH.

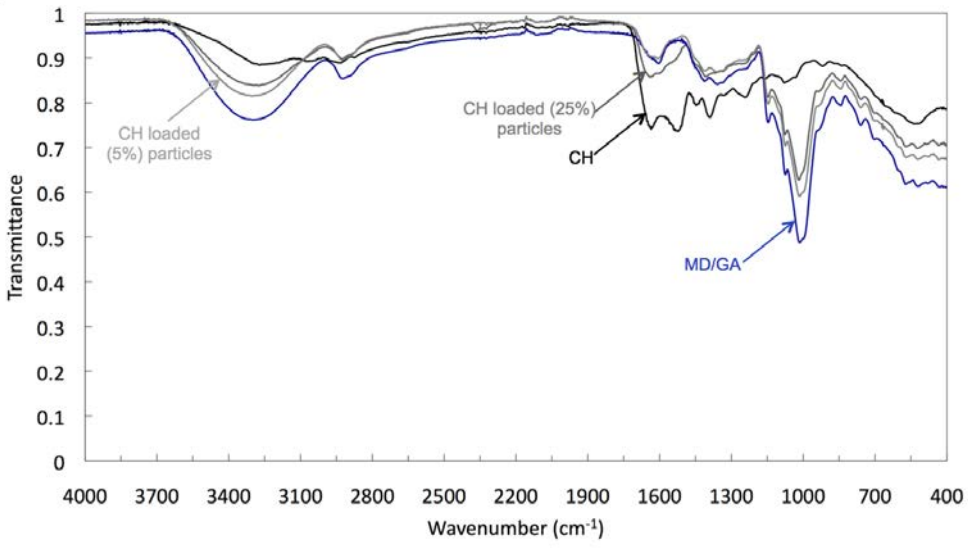

Figure 5.6: ATR spectra of free collagen hydrolysate, collagen hydrolysate loaded and unloaded particles.

5.4.2 NMR spectroscopy

Typical 400.15 MHz ^{1}H NMR spectra of collagen hydrolysate, unloaded and collagen hydrolysate loaded particles (with 5 and 25% of CH) are presented in Figure 5.7. The ^{1}H NMR spectra of unloaded and both CH/P are dominated by the intense, broad and overlapped resonance signals characteristic for the polysaccharide structures of maltodextrin (MD) and gum arabic (GA).

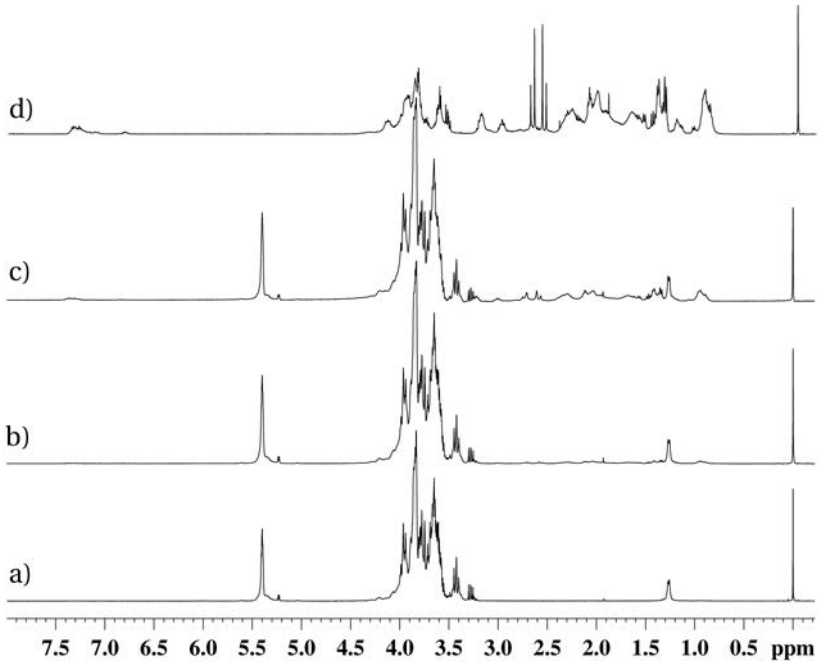

Figure 5.7: 400.15 MHz ^{1}H NMR spectra of unloaded (a), collagen hydrolysate (5%) loaded particles (b), collagen hydrolysate (25%) loaded particles (c), collagen hydrolysate (d).

Resonance signals of the anomeric and hydroxymethine protons of saccharide residues of the polysaccharide structures of MD and GA in the ^{1}H NMR spectra of unloaded and CH/P were observed at 5.40-5.20 and 4.5-3.2 ppm. The broad signal at 5.40 ppm was attributed to the anomeric protons of glucose units of MD. The corresponding resonance signals of the glucose methine protons appeared in the spectral area 4.15-3.5 ppm. The resonance

signal at 1.27 ppm was assigned to C6 methyl protons of rhamnose moieties from GA. The assignment of the resonance signals of MD and GA is in agreement to the data published recently [171]. Proton NMR spectra of collagen hydrolysate and collagen hydrolysate loaded samples are usually complex because of the large number of components in the samples, resulting in spectra with complex line shapes and significant overlap of the resonance signals. However, resonance signals appearing in ^{1}H NMR spectra (between 4.5 and 0.5 ppm and in the aromatic spectral area) containing collagen hydrolysate could be assigned to the most abundant amino acids (Gly, Ala, Pro, HyPro, and Glu) in the complex structure of collagen hydrolysate [149]. The observed broadening of the resonance lines suggests involvement of the saccharide and peptide residues into high molecular structures with low mobility and variation in the spin-spin relaxation time (T_2). In both, ^{1}H NMR spectra of CH/P (loaded with 5 and 25% of collagen hydrolysate) were observed resonance signals characteristic of collagen hydrolysate. This shows that collagen hydrolysate is incorporated into the polymeric matrix of polysaccharide particles. Diffusion ordered NMR spectroscopy (DOSY) was used to analyze overall structure of CH/P, to clarify the origin of the collagen hydrolysate-polysaccharide interactions and to determine the location of collagen hydrolysate into the carbohydrate matrix. The pulsed field gradient spin echo (PFGSE) NMR technique is a straight forward procedure for measuring the diffusion coefficients of individual species. Useful information can be obtained regarding the size, molecular weight and shape of the species in solution under given conditions. In order to get insight into the structural modifications of the species presented in the CH/P and to account for changes in the solvent viscosity and minor fluctuations of samples temperature, we found it useful to use an internal diffusion reference [82], [77]. Since modifications of the solution composition could induce changes in the viscosity and these changes affect equally all species in the solution, the use of reference allows one to take into account the variation in solvent properties and correct the measured diffusion values. We found it useful to use TSP not only as chemical shift reference but also as an internal diffusion reference and all diffusion coefficients presented in Table 5.1 are given as a ratio D/D_{TSP} according procedure published before [82]. Self-diffusion coefficients (D) of the collagen hydrolysate (D_{CH}) present in CH/P at con-

centration of 5 and 25% collagen hydrolysate were determined from the resonance signals at 1.02 ppm. The corresponding values of D for MD and GA (DMD and DGA) were determined from the resonance signals at 5.50 and 1.27 ppm, respectively. The results are presented in Table 5.1. The diffusion coefficients measured for MD and GA in CH/P are similar to the corresponding values in the unloaded particles. However, the diffusion coefficients of collagen hydrolysate in the both CH/P samples are lower than the corresponding values in the free collagen hydrolysate. The reduction of the diffusion coefficients of collagen hydrolysate in the collagen hydrolysate loaded particles samples studied is a strong indication of an association process between collagen hydrolysate and polysaccharides, due to hydrogen bonds between their polar (OH, COOH, NH_2, NH) functional groups.

Table 5.1: Relative diffusion coefficients (related to TSP), with calculated standard deviations (in italics), of collagen hydrolysate, MD and GA in D_2O at 30 ℃ for the samples studied.

Sample	D_{CH}	D_{MD}	D_{GA}
Collagen hydrolysate	0.55		
	0.0004		
Unloaded particles		0.36	0.04
		0.04	*0.03*
Collagen hydrolysate (5%) loaded particles	0.50	0.34	0.03
	0.02	*0.02*	*0.001*
Collagen hydrolysate (25%) loaded particles	0.46	0.33	0.04
	0.0001	*0.02*	*0.02*

5.5 *In vitro* release

Drug release from a polymeric matrix is controlled by several factors, such as the solubility of the drug within the surrounding medium, the size of the drug molecule and its mobility within the polymeric network, and the dissolution rate of the polymer and polymer-drug interactions [172]. The *in vitro* release profile of CH in ultrapure water, is illustrated in Figure 5.8.

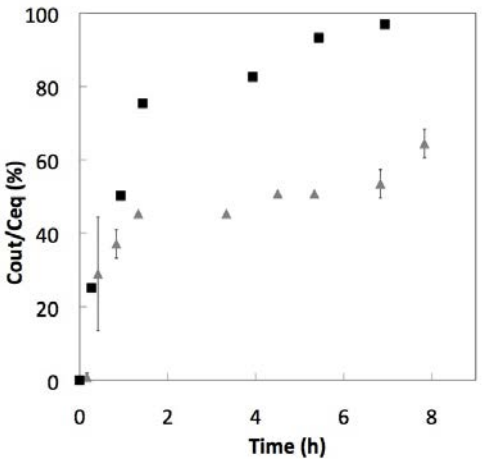

Figure 5.8: *In vitro* release profile of free CH (in black) and collagen hydrolysate from CH (25%) loaded particles (in gray) versus time in ultrapure water. Average ± standard deviation, number of experiments = 2.

The release rate of collagen hydrolysate from the CH (25%) loaded particles is compared to free CH (Figure 5.8). The free molecules of CH are completely released after 8 h. On the contrary, it is visible that the diffusion rate of CH from the polymeric matrix to the dialysis solution decreases in average 30% over the time, compared to free CH molecules. The maximum concentration of CH detected in the dialysis solution is equivalent to 65% of the loaded CH in the particles. These results show evidence of the entrapment of CH in the maltodextrin-gum arabic matrix, which are supported by the interactions between CH and the polysaccharides described in the ATR and NMR analysis.

5.6 Conclusions

CH loaded particles were produced by spray-drying technique, using a carbohydrate matrix of maltodextrin and gum arabic. Particles of different size, zeta potential and surface morphology were obtained by varying the amount of CH used in the formulation. CH was entrapped into the polymer matrix, with high loading efficiency, and without undergoing any chemical changes during particles preparation. ATR and NMR studies demonstrate that CH

chemical integrity was preserved after the spray-drying process and that it is incorporated in the matrix by hydrogen bonds between MD/GA/CH. The studied particles present good functionality and potential for foods, beverages and nutraceuticals purposes, since they were able to mask the CH undesirable taste and odor and also its yellow color. This method may be generally applied to carry and delivery active compounds in powder form with extended shelf life, optimized technological, functional and organoleptic characteristics.

Chapter 6

Concluding Remarks

In this thesis, the approach to the preservation of epigallocatechin gallate and collagen hydrolysate therapeutic properties is based on a carbohydrate particle formulation followed by spray-drying.

Spray-drying is a common process used for encapsulation in the pharmaceutical and food industries because it is a simple inexpensive method in which polysaccharides can be used to entrap and protect sensitive compounds. A combination of maltodextrin and gum arabic, two components already used in pharmaceutical and food industries (US FDA approved), was used to protect EGCG and CH from degradation, increasing their stability and bioavailability.

EGCG exhibits antioxidant, anti-bacterial, anti-inflammatory, chemopreventive and antitumor activities. However, EGCG as a polyphenol is susceptible to oxidation and consequently, its low bioavailability and short half-life limit its therapeutic application. To overcome this drawback EGCG was incorporated in a maltodextrin-gum arabic matrix, guarantying its physical and chemical protection and therefore improving its bioavailability.

The EGCG loading efficiency determined at the optimum extraction temperature was 96±3%, which is a promising result for scaling up the process and pharmaceutical applications. ATR results confirmed the presence of EGCG within the carbohydrate matrix by intermolecular dipole-dipole interactions, maintaining its integrity after the spray-drying process. NMR spectroscopy has been applied to study the structure and composition of EGCG loaded particles. Diffusion ordered NMR spectroscopy combined

with spin-lattice relaxation time determinations provided valuable information on the structure and intermolecular interactions of EGCG/P. The decreased translation diffusivity and spin-lattice relaxation times of the species presented in the EGCG/P suggest the entrapment of EGCG in the polysaccharide matrix and predict the potential of these vehicles for sustained delivery/release of EGCG. These results are supported by the significant changes observed for the dynamic parameters of EGCG. NMR study show how a synergistic combination of NMR spectroscopic techniques can be used to characterize the structural behaviour of complex nanoscaled intermolecular aggregates and better understand this EGCG polymer based vehicle. Antioxidant activity assay revealed that the functional activity of EGCG was preserved even after the spray-drying process. This result demonstrates that spray-drying is a viable and rapid approach to produce antioxidant particles that retain high potency. Maltodextrin and gum arabic, were studied as carriers for cancer prevention and therapy. This study confirmed the ability of nanoparticles to retain EGCG inhibitory effects of the proliferative activity of prostate cancer cells. Furthermore, the system was not cytotoxic to Du145 prostate cells, suggesting that the polysaccharide nanoparticles can be used as nanochemopreventive tools.

The synthetic approach to the formulation of particles with the capability to incorporate small to large-sized molecules in the carbohydrate matrix and simultaneously allowing the entrapment of other medium-sized molecules in the mesopores can be extended to other systems foreseeing chemical stabilization and protection from degradation in adverse conditions for pharmaceutical applications and, particularly, as drug delivery systems.

Based on these findings, collagen hydrolysate, a macromolecule, was incorporated with success into the carbohyrate matrix studied. Polysaccharide particles have proved to be adequate vehicles for the entrapment of collagen hydrolysate, with a loading efficiency of 86±7% and 85±4%, for CH/P with 5% and 25% of CH loaded, respectively. SEM observations clearly demonstrated differences in size and shape, comparing to EGCG/P. CH/P morphology differs from spherical shape with indentation to a main population of hollow particles with a smooth surface and large size, which is superior for CH/P (25%). The lower true density obtained for the CH (5%) loaded particles can be explained by their morphology and wall resistance,

as seen by SEM images.

Structural interactions between the carbohydrate matrix and the collagen hydrolysate were studied by ATR and NMR spectroscopy. These studies confirm the incorporation of CH within the matrix and suggest an association process between collagen hydrolysate and polysaccharides, through hydrogen bonds among their polar functional groups. In vitro release profiles reveal that the diffusion rate of CH from the polymeric matrix to the dialysis solution decreases in average 30% over the time, compared to free CH molecules. These findings are supported by the NMR-DOSY results of the diffusion coefficients.

The encapsulation process studied allows obtaining stable and handling spray-dried loaded powders with extended shelf life and improved dissolution/release rate, which could find application in the food and pharmaceutical fields. Thus, the information gained from this research contributes to enhancing the activity and stability of bioactive compounds, such as EGCG and CH.

Appendix A

Abbreviations and Symbols

A.1 Abbreviations

A	Absorbance
AFM	Atomic force microscopy
ATR-IR	Attenuated total reflection - infrared spectroscopy
AUC	Value of the area under the curve
BPPLED	Bipolar pulsed field gradient longitudinal eddy delay
CH	Collagen hydrolysate
CH/P	Collagen hydrolysate loaded particles
CLSM	Confocal laser scanning microscopy
COSY	Two-dimensional $^{1}H/^{1}H$ correlation spectrosocopy
Cryo-SEM	Cryogenic scanning electron microscopy
DE	Dextrose equivalency
DLS	Dynamic light scattering
DOSY	Diffusion ordered NMR spectroscopy
DPPH*	2, 2,diphenyl-1-picrylhydrazyl radical
EGCG	Epigallocatechin gallate
EGCG/P	Epigallocatechin gallate loaded particles
FTIR	Fourier transform infrared spectroscopy
GA	Gum arabic
He	Helium
Hg	Mercury
HSQC	Heteronuclear single quantum coherence spectroscopy

MAE	Microwave-assisted extraction
MD	Maltodextrin
MD/GA	Maltodextrin-gum arabic particles (unloaded particles)
MWCO	Molecular weight cut-off
NMR	Nuclear magnetic resonance
NOESY	Nuclear Overhauser effect spectroscopy
NPs	Nanoparticles
NTA	Nanoparticle tracking analysis
OLE	Olive leaf extract
OS	Oxidative stress
PE	Plating efficiency
PFGSE	Pulsed field gradient spin echo
RDSC	Relative DPPH* scavenging capacity
ROS	Reactive oxygen species
SEM	Scanning electron microscopy
TE	Trolox equivalents
TEM	Transmission electron microscopy
TSP	Sodium trimethylsilyl-[2,2,3,3-d4]-propionate
UV-Vis	Ultraviolet-visible spectroscopy

A.2 Symbols

b	Path length of the cuvette or sample holder
c	Concentration
d_p	Particle hydrodynamic diameter
d_{mean}	Mean pore diameter
D	Diffusion coefficient
D_{pore}	Pore diameter
$D_v(d)v$	Volume pore size distribution
e	Dielectric constant
f	Friction coefficient
$f\,(ka)$	Henry's function
g	Pulse gradient
$G(\tau)$	Autocorrelation function as a function of time

k_B	Boltzmann constant
K	Scattering vector
n	Refraction index of the medium
P	Pressure
r^2	Correlation coefficient
R_H	Hydrodynamic average intensity radius of the particles
S	Total surface area
T	Temperature
T_1	Nuclear spin-lattice relaxation time
T_2	Nuclear spin-lattice relaxation time
U_E	Electrophoretic mobility
V	Volume
V_{tot}	Total intruded volume of mercury
z	Zeta potential
γ	Surface tension
δ	Magnetic field pulse gradients
Δ	Diffusion times
ε	Molar absorptivity
ε_p	Total porosity
η	Viscosity
θ	Contact angle
θ	Detection angle
λ	Wavelength
ρ_{bulk}	Bulk density
ρ_{true}	True density

Bibliography

[1] P. M. M. Schrooyen, R. Meer, and C. G. Kruif, "Microencapsulation: its application in nutrition," *Proceedings of the Nutrition Society*, vol. 60, pp. 475–479, 2001.

[2] D. L. McKay and J. B. Blumberg, "The role of tea in human health: An update," *Journal of the American College of Nutrition*, vol. 21, no. 1, pp. 1–13, 2002.

[3] Q.-X. A. Sang, Y. Jin, R. G. Newcomer, S. C. Monroe, X. Fang, D. R. Hurst, S. Lee, Q. Cao, and M. A. Schwartz, "Matrix metalloproteinase inhibitors as prospective agents for the prevention and treatment of cardiovascular and neoplastic diseases," *Current Topics in Medicinal Chemistry*, vol. 6, pp. 289–316, 2006.

[4] S. Rocha, R. Generalov, M. d. C. Pereira, I. Peres, P. Juzenas, and M. A. Coelho, "Epigallocatechin gallate-loaded polysaccharide nanoparticles for prostate cancer chemoprevention," *Nanomedicine*, vol. 6, no. 1, pp. 79–87, 2011.

[5] M. Makimura, M. Hirasawa, K. Kobayashi, J. Indo, S. Sakanaka, T. Taguchi, and S. Otake, "Inhibitory effect of tea catechins on collagenase activity," *J Periodontol.*, vol. 64, no. 7, pp. 630–636, 1993.

[6] C. H. Lee, A. Singla, and Y. Lee, "Biomedical applications of collagen," *International Journal of Pharmaceutics*, vol. 221, pp. 1–22, 2001.

[7] A. Dube, K. Ng, J. A. Nicolazzo, and I. Larson, "Effective use of reducing agents and nanoparticle encapsulation in stabilizing catechins in alkaline solution," *Food Chemistry*, vol. 122, pp. 662–667, 2010.

[8] J.-Y. Fang, W.-R. Lee, S.-C. Shen, and Y.-L. Huanga, "Effect of liposome encapsulation of tea catechins on their accumulation in basal cell carcinomas," *Journal of Dermatological Science*, vol. 42, no. 101-109, p. 101, 2006.

[9] W. Friess, "Collagen - biomaterial for drug delivery," *European Journal of Pharmaceutics and Biopharmaceutics*, vol. 45, pp. 113–136, 1998.

[10] V. Zague, "A new view concerning the effects of collagen hydrolysate intake on skin properties," *Arch Dermatol Res*, vol. 300, pp. 479–483, 2008.

[11] F. Cúneo, L. C. Paiva, A. M. P. Neto, S. S. Morais, and J. A. Farfan, "Effect of dietary supplementation with collagen hydrolysates on bone metabolism of postmenopausal women with low mineral density," *Maturitas*, vol. 65, pp. 253–257, 2010.

[12] J.-P. Bonjour, "Dietary protein: An essential nutrient for bone health," *Journal of the American College of Nutrition*, vol. 24, no. 6, pp. 526–536, 2005.

[13] W. R. Gombotz and D. K. Pettit, "Biodegradable polymers for protein and peptide drug delivery," *Bioconjugate Chem.*, vol. 6, pp. 332–351, 1995.

[14] K. G. H. Desai and H. J. Park, "Recent developments in microencapsulation of food ingredients," *Drying Technology*, vol. 23, pp. 1361–1394, 2005.

[15] P. R. Lockman, R. J. Mumper, M. A. Khan, and D. D. Allen, "Nanoparticle technology for drug delivery across the blood-brain barrier." *Drug Development and Industrial Pharmacy*, vol. 28, no. 1, pp. 1–13, 2002.

[16] G. V. Barbosa-Cánovas, E. Ortega-Rivas, P. Juliano, and H. Yan, *Food powders - phisical properties, processing, and functionality*, ser. Food engineering series. New York: Kluwer Academic/Plenum Publishers, 2005.

[17] F. Ronsse, J. Pieters, and K. Dewettinck, "Modelling heat and mass transfer in batch, top-spray fluidised bed coating processes," *Powder Technology*, vol. 190, pp. 170–175, 2009.

[18] S. Gouin, "Microencapsulation: industrial appraisal of existing technologies and trends," *Trends in Food Science & Technology*, vol. 15, pp. 330–347, 2004.

[19] P. Laine, P. Kylli, M. Heinonen, and K. Jouppila, "Storage stability of microencapsulated cloudberry (*Rubus chamaemorus*) phenolics," *J. Agric. Food Chem.*, vol. 56, pp. 11 251–11 261, 2008.

[20] S. A. Desobry, F. M. Netto, and T. P. Labuza, "Comparison of spray-drying, drum-drying and freeze-drying for β-carotene encapsulation and preservation," *Journal of Food Science*, vol. 62, no. 6, pp. 1158–1162, 1997.

[21] Z. Fang and B. Bhandari, "Encapsulation of polyphenols - a review," *Trends in Food Science & Technology*, vol. 21, pp. 510–523, 2010.

[22] Z. Liu, J. Zhou, Y. Zeng, and X. Ouyang, "The enhancement and encapsulation of agaricus bisporus flavor," *Journal of Food Engineering*, vol. 65, pp. 391–396, 2004.

[23] A. Gharsallaoui, G. Roudaut, O. Chambin, A. Voilley, and R. Saurel, "Applications of spray-drying in microencapsulation of food ingredients: An overview," *Food Research International*, vol. 40, pp. 1107–1121, 2007.

[24] L. Deladino, P. S. Anbinder, A. S. Navarro, and M. N. Martino, "Encapsulation of natural antioxidants extracted from ilex paraguariensis," *Carbohydrate Polymers*, vol. 71, no. 1, pp. 126 – 134, 2008.

[25] B. F. Gibbs, S. Kermasha, I. Alli, and C. N. Mulligan, "Encapsulation in the food industry: a review." *International journal of food sciences and nutrition*, vol. 50, no. 3, pp. 213–224, 1999.

[26] K. Dewettinck, L. Deroo, W. Messens, and A. Huyghebaert, "Agglomeration tendency during top-spray fluidized bed coating with gums,"

Lebensmittel-Wissenschaft und-Technologie, vol. 31, no. 6, pp. 576–584, 1998.

[27] A. Madene, M. Jacquot, J. Scher, and S. Desobry, "Flavour encapsulation and controlled release - a review," *International Journal of Food Science and Technology*, vol. 41, pp. 1–21, 2006.

[28] M. Rosenberg, I. J. Kopelman, and Y. Talmon, "Factors affecting retention in spray-drying microencapsulation of volatile materials," *J. Agric. Food Chem.*, vol. 38, pp. 1288–1294, 1990.

[29] I. Goubet, J.-L. L. Quere, and A. J. Voilley, "Retention of aroma compounds by carbohydrates: Influence of their physicochemical characteristics and of their physical state. a review," *J. Agric. Food Chem.*, vol. 46, pp. 1981–1990, 1998.

[30] G. A. Reineccius, "The spray drying of food flavors," *Drying Technology*, vol. 22, no. 6, pp. 1289–1324, 2004.

[31] F. Shahidi and X. Han, "Encapsulation of food ingredients," *Crit Rev Food Sci Nutr.*, vol. 33, no. 6, pp. 501–547, 1993.

[32] S.-W. Lee, M.-H. Kim, and C.-K. Kim, "Encapsulation of ethanol by spray drying technique: effects of sodium lauryl sulfate," *International Journal of Pharmaceutics*, vol. 187, pp. 193–198, 1999.

[33] C. I. Beristain, H. S. García, and E. J. Vernon-Carter, "Spray-dried encapsulation of cardamom (*Elettaria cardamomum*) essential oil with mesquite (*Prosopis julifora*) gum," *Lebensm.-Wiss. u.-Technol.*, vol. 34, pp. 398–401, 2001.

[34] J. Osés, M. Fabregat-Vázquez, R. Pedroza-Islas, S. A. Tomás, A. Cruz-Orea, and J. I. Maté, "Development and characterization of composite edible films based on whey protein isolate and mesquite gum," *Journal of Food Engineering*, vol. 92, pp. 56–62, 2009.

[35] C. Beristain and E. Vernon-Carter, "Studies on the interaction of arabic (*Acacia Senegal*) and mesquite (*Prosopis juliora*) gum as emulsion stabilizing agents for spray dried encapsulated orange peel oil." *Drying Technology*, vol. 29, pp. 645–667, 1995.

[36] M. Rosenberg and T.-Y. Sheu, "Microencapsulation of volatiles by spray-drying in whey protein-based wall systems," *Ini. Dairy Journal*, vol. 6, pp. 273–284, 1996.

[37] S. Young, X. Sarda, and M. Rosenberg, "Microencapsulating properties of whey proteins. 1. microencapsulation of anhydrous milk fat," *Journal of Dairy Science*, vol. 76, no. 10, pp. 2868–2877, 1993.

[38] A. Millqvist-Fureby, U. Elofsson, and B. Bergenstahl, "Surface composition of spray-dried milk protein-stabilised emulsions in relation to pre-heat treatment of proteins," *Colloids and Surfaces B: Biointerfaces*, vol. 21, pp. 47–58, 2001.

[39] J. Imagi, T. Yamanouchi, K. Okada, M. Tanimoto, and R. Matsuno, "Properties of agents that effectively entrap liquid lipids," *Biosci Biotechnol Biochem.*, vol. 56, no. 3, pp. 477–480, 1992.

[40] H. Yoshii, A. Soottitantawat, X.-D. Liu, T. Atarashi, T. Furuta, S. Aishima, M. Ohgawara, and P. Linko, "Flavor release from spray-dried maltodextrin gum arabic or soy matrices as a function of storage relative humidity," *Innovative Food Science & Emerging Technologies*, vol. 2, pp. 55–61, 2001.

[41] A. Pierucci, L. Andrade, E. Baptista, N. Volpato, and M. Rocha-Leo, "New microencapsulation system for ascorbic acid using pea protein concentrate as coat protector." *J Microencapsul.*, vol. 23, no. 6, pp. 654–662, 2006.

[42] P. B. Malafaya, G. A. Silva, and R. L. Reis, "Natural-origin polymers as carriers and scaffolds for biomolecules and cell delivery in tissue engineering applications," *Advanced Drug Delivery Reviews*, vol. 59, pp. 207–233, 2007.

[43] S. L. Kosaraju, L. Dath, and A. Lawrence, "Preparation and characterisation of chitosan microspheres for antioxidant delivery," *Carbohydrate Polymers*, vol. 64, pp. 163–167, 2006.

[44] B. Hu, C. Pan, Y. Sun, Z. Hou, H. Ye, B. Hu, and X. Zeng, "Optimization of fabrication parameters to produce chitosan-tripolyphosphate

nanoparticles for delivery of tea catechins," *J. Agric. Food Chem.*, vol. 56, pp. 7451–7458, 2008.

[45] V. Sinha, A. Singla, S. Wadhawan, R. Kaushik, R. Kumria, K. Bansal, and S. Dhawan, "Chitosan microspheres as a potential carrier for drugs," *International Journal of Pharmaceutics*, vol. 274, pp. 1–33, 2004.

[46] G. A. Reineccius and S. Anandaraman, "Stability of encapsulated orange peel oil," *Food Technology*, vol. 40, no. 11, pp. 88–93, 1986.

[47] L. A. Wagner and J. J. Warthesen, "Stability of spray-dried encapsulated carrot carotenes," *Journal of Food Science*, vol. 60, no. 5, pp. 1048–1053, 1995.

[48] A. M. Righetto and F. M. Netto, "Effect of encapsulating materials on water sorption, glass transition and stability of juice from immature acerola," *International Journal of Food Properties*, vol. 8, pp. 337–346, 2005.

[49] S. Ersus and U. Yurdagel, "Microencapsulation of anthocyanin pigments of black carrot (*Daucuscarota L.*) by spray drier," *Journal of Food Engineering*, vol. 80, pp. 805–812, 2007.

[50] L. Zhang, D. Mou, and Y. Du, "Procyanidins: Extraction and microencapsulation," *Journal of the Science of Food and Agriculture*, vol. 87, pp. 2192–2197, 2007.

[51] J. Loksuwan, "Characteristics of microencapsulated β-carotene formed by spray drying with modified tapioca starch, native tapioca starch and maltodextrin," *Food Hydrocolloids*, vol. 21, pp. 928–935, 2007.

[52] Y.-H. Kuan, R. Bhat, C. Senan, P. A. Williams, and A. A. Karim, "Effects of ultraviolet irradiation on the physicochemical and functional properties of gum arabic," *J. Agric. Food Chem.*, vol. 57, pp. 9154–9159, 2009.

[53] D. Kanakdande, R. Bhosale, and R. S. Singhal, "Stability of cumin oleoresin microencapsulated in different combination of gum arabic,

maltodextrin and modiffied starch," *Carbohydrate Polymers*, vol. 67, pp. 536–541, 2007.

[54] J. Goldstein, D. Newbury, D. Joy, C. Lyman, P. Echlin, E. Lifshin, L. Sawyer, and J. Michael, *Scanning electron microscopy and x-ray microanalysis, Volume 1*, third edition ed., ser. Scanning electron microscopy and x-ray microanalysis. New York: Kluver Academic/ Plenim Publishers, 2003, vol. 1.

[55] L. Champion-Lapalu, A. Wilson, G. Fuchs, D. Martin, and J.-P. Planche, "Cryo-scanning electron microscopy: A new tool for interpretation of fracture studies in bitumen/polymer blends," *Energy & Fuels*, vol. 16, pp. 143–147, 2002.

[56] J. L. Alonso and W. H. Goldmann, "Feeling the forces: atomic force microscopy in cell biology." *Life Sciences*, vol. 72, no. 23, pp. 2553–2560, 2003.

[57] M. J. Wozniak, N. Kawazoe, T. Tateishi, and G. Chen, "Monitoring of mechanical properties of serially passaged bovine articular chondrocytes by atomic force microscopy." *Micron Oxford England 1993*, vol. 40, no. 8, pp. 870–875, 2009.

[58] M. Schneider and T. F. McKenna, "Comparative study of methods for the measurement of particle size and size distribution of polymeric emulsions," *Part. Part. Syst. Charact.*, vol. 19, pp. 28–37, 2002.

[59] H. Mirhosseini, C. Tan, N. Hamid, and S. Yusof, "Effect of arabic gum, xanthan gum and orange oil on flavor release from diluted orange beverage emulsion," *Food Chemistry*, vol. 107, pp. 1161–1172, 2007.

[60] A. Malloy and B. Carr, "Nanoparticle tracking analysis - thehalosystem," *Part. Part. Syst. Charact.*, vol. 23, pp. 197–204, 2006.

[61] P. Saravanapavan and L. L. Hench, "Mesoporous calcium silicate glasses. II. textural characterisation," *Journal of Non-Crystalline Solids*, vol. 318, no. 1-2, pp. 14–26, 2003.

[62] D. Brabazon and A. Raffer, "Advanced characterization techniques for nanostructures," in *Emerging Nanotechnologies for Manufacturing*, W. Ahmed and M. J. Jackson, Eds. Boston: William Andrew Publishing, 2010, pp. 59–91.

[63] C. A. L. y León, "New perspectives in mercury porosimetry," *Advances in Colloid and Interface Science*, vol. 76-77, pp. 341–372, 1998.

[64] S. Westermarck, A. M. Juppob, L. Kervinen, and J. Yliruusib, "Pore structure and surface area of mannitol powder, granules and tablets determined with mercury porosimetry and nitrogen adsorption," *European Journal of Pharmaceutics and Biopharmaceutics*, vol. 46, pp. 61–68, 1998.

[65] W. Duvernay, J. Assad, C. Sabliov, M. Lima, and Z. Xu, "Microwave extraction of antioxidant components from rice bran," *Pharmaceutical Engineering*, vol. 25, no. 4, pp. 1–5, 2005.

[66] G. Raman and V. G. Gaikar, "Microwave-assisted extraction of piperine from *Piper nigrum*," *Ind. Eng. Chem. Res.*, vol. 41, pp. 2521–2528, 2002.

[67] S. Shah, R. C. Richter, and H. S. Kingston, "Microwave-assisted organic extraction and evaporation: An integrated approach," *LCGC North America*, vol. 20, no. 3, pp. 280–286, 2002.

[68] X. Pan, G. Niu, and H. Liu, "Microwave-assisted extraction of tea polyphenols and tea caffeine from green tea leaves," *Chemical Engineering and Processing*, vol. 42, pp. 129–133, 2003.

[69] O. J. Williams, G. V. Raghavan, V. Orsat, and J. Dai, "Microwave assisted extraction of capsaicinoids from capsicum fruit," *Journal of Food Biochemistry*, vol. 28, pp. 113–122, 2004.

[70] N. Hong, V. Yaylayan, G. Raghavan, J. Par, and J. Blanger, "Microwave-assisted extraction of phenolic compounds from grape seed," *Nat Prod Lett.*, vol. 15, no. 3, pp. 197–204, 2001.

[71] Z. Guo, Q. Jin, G. Fan, Y. Duan, C. Qin, and M. Wen, "Microwave-assisted extraction of effective constituents from a chinese herbal

medicine radix puerariae," *Analytica Chimica Acta*, vol. 436, pp. 41–47, 2001.

[72] G. A. C. Kiss, E. Forgcs, T. Cserhti, T. Mota, H. Morais, and A. Ramos, "Optimisation of the microwave-assisted extraction of pigments from paprika (*Capsicum annuum L.*) powders," *Journal of Chromatography A*, vol. 889, pp. 41–49, 2000.

[73] J. Greener, B. Abbasi, and E. Kumacheva, "Attenuated total reflection fourier transform infrared spectroscopy for on-chip monitoring of solute concentrations," *Lab Chip,*, vol. 10, pp. 1561–1566, 2010.

[74] D. E. Bugay, "Characterization of the solid-state: spectroscopic techniques," *Advanced Drug Delivery Reviews*, vol. 48, pp. 43–65, 2001.

[75] J. N. S. Evans, "Biomolecular NMR spectroscopy." Oxford University Press, 1995.

[76] H. Gunther, *NMR Spectroscopy. Basic principles, concepts and application in chemistry*, second edition ed., ser. Scanning electron microscopy and x-ray microanalysis. New York: John Wiley & Sons, 1994.

[77] Y. Cohen, L. Avram, and L. Frish, "Diffusion NMR spectroscopy in supramolecular and combinatorial chemistry : An old parameter-new insights," *Angewandte Chemie International Edition*, vol. 44, no. 4, pp. 520–544, 2005.

[78] D. Y. D. Atilla Ambrus, "Diffusion-ordered nuclear magnetic resonance spectroscopy for analysis of DNA secondary structural elements," *Analytical Biochemistry*, vol. 367, pp. 56–67, 2007.

[79] T. Brand, E. J. Cabrita, and S. Berger, "Intermolecular interaction as investigated by NOE and diffusion studies," *Progress in Nuclear Magnetic Resonance Spectroscopy*, vol. 46, pp. 159–196, 2005.

[80] C. J. Johnson, "Diffusion ordered nuclear magnetic resonance spectroscopy: principles and applications," *Progress in Nuclear Magnetic Resonance Spectroscopy*, vol. 34, pp. 203–256, 1999.

[81] D. Wu, A. Chen, and C. S. Johnson, "An improved diffusion ordered spectroscopy experiment incorporating bipolar-gradient pulses," *Journal of Magnetic Resonance*, vol. Series A, no. 115, pp. 260–264, 1995.

[82] E. J. Cabrita and S. Berger, "DOSY studies of hydrogen bond association: Tetramethylsilane as a reference compound for diffusion studies," *Magn. Reson. Chem.*, vol. 39, no. S1, pp. S142–S148, 2001.

[83] Z. Cheng, J. Moore, and L. L. Yu, "High-throughput relative DPPH radical scavenging capacity assay," *J. Agric. Food Chem.*, vol. 54, pp. 7429–7436, 2006.

[84] I. Henriksen, S. A. Sande, G. Smistad, T. Agren, and J. Karlsen, "In vitro evaluation of drug release kinetics from liposomes by fractional dialysis," *International Journal of Pharmaceutics*, vol. 119, pp. 231–238, 1995.

[85] A. Gèeze, M. Venier-Julienne, D. Mathieu, R. Filmon, R. Phan-Tan-Luu, and J. Benoit, "Development of 5-iodo-2'-deoxyuridine milling process to reduce initial burst release from PLGA microparticles," *International Journal of Pharmaceutics*, vol. 178, pp. 257–268, 1999.

[86] Y. Luo, D. Chen, L. Ren, X. Zhao, and J. Qin, "Solid lipid nanoparticles for enhancing vinpocetine's oral bioavailability," *Journal of Controlled Release*, vol. 114, pp. 53–59, 2006.

[87] W. R. Duan, D. S. Garner, S. D. Williams, C. L. Funckes-Shippy, I. S. Spath, and E. A. G. Blomme, "Comparison of immunohistochemistry for activated caspase-3 and cleaved cytokeratin 18 with the TUNEL method for quantification of apoptosis in histological sections of pc-3 subcutaneous xenografts," *Journal of Pathology*, vol. 199, no. 2, pp. 221–228, 2003.

[88] B. A. Warden, L. S. Smith, G. R. Beecher, D. A. Balentine, and B. A. Clevidence, "Catechins are bioavailable in men and women drinking black tea throughout the day," *The Journal of Nutrition*, vol. 131, no. 6, pp. 1731–1737, 2001.

[89] Y. Gilgun-Sherki, E. Melamed, and D. Offen, "Oxidative stress induced-neurodegenerative diseases: the need for antioxidants that penetrate the blood brain barrier," *Neuropharmacology*, vol. 40, pp. 959–975, 2001.

[90] D. V. Ratnam, D. Ankola, V. Bhardwaj, D. Sahana, and M. R. Kumar, "Role of antioxidants in prophylaxis and therapy: A pharmaceutical perspective," *Journal of Controlled Release*, vol. 113, pp. 189–207, 2006.

[91] H. Sies, "Oxidative stress: oxidants and antioxidants," *Experimental Physiology*, vol. 82, pp. 291–295, 1997.

[92] J. Fuchs and J. Thiele, "The role of oxygen in cutaneous photodynamic therapy," *Free Radic Biol Med.*, vol. 24, no. 5, pp. 835–847, 1998.

[93] P. Juzenas, W. Chen, Y.-P. Sun, M. A. N. Coelho, R. Generalov, N. Generalova, and I. L. Christensen, "Quantum dots and nanoparticles for photodynamic and radiation therapies of cancer," *Advanced Drug Delivery Reviews*, vol. 60, pp. 1600–1614, 2008.

[94] J. D. Carter, N. N. Cheng, Y. Qu, G. D. Suarez, and T. Guo, "Nanoscale energy deposition by X-ray absorbing nanostructures," *J. Phys. Chem. B*, vol. 111, no. 40, pp. 11 622–11 625, 2007.

[95] A. A. Krasnovsky, N. N. Drozdova, A. V. Ivanov, and R. V. Ambartsumian, "Activation of molecular oxygen by infrared laser radiation in pigment-free aerobic systems," *Biochemistry (Moscow)*, vol. 68, no. 9, pp. 963–966, 2003.

[96] S. Jockusch, N. J. Turro, E. K. Thompson, M. Gouterman, J. B. Callisb, and G. E. Khalil, "Singlet molecular oxygen by direct excitation," *Photochemical & Photobiological Sciences*, vol. 7, pp. 235–239, 2008.

[97] L.-O. Klotz, K.-D. Kröncke, and H. Sies, "Singlet oxygen-induced signaling effects in mammalian cells," *Photochem. Photobiol. Sci.*, vol. 2, pp. 88–94, 2003.

[98] H. Sies, "Strategies of antioxidant defense," *European Journal of Biochemistry*, vol. 215, no. 2, pp. 213–219, 1993.

[99] T. Finkel and N. J. Holbrook, "Oxidants, oxidative stress and the biology of ageing," *Nature*, vol. 408, pp. 239–247, 2000.

[100] B. Halliwell, "Free radicals, antioxidants, and human disease: curiosity, cause, or consequence," *The Lancet*, vol. 344, no. 8924, pp. 721–724, 1994.

[101] C. Kandaswami and E. J. Middleton, "Free radical scavenging and antioxidant activity of plant flavonoids," *Adv Exp Med Biol.*, vol. 366, pp. 351–376, 1994.

[102] E. J. Middleton, C. Kandaswami, and T. C. Theoharides, "The effects of plant flavonoids on mammalian cells: Implications for inflammation, heart disease, and cancer," *Pharmacol Rev*, vol. 52, no. 4, pp. 673–751, 2000.

[103] W. Stahl, H. v. d. Berg, J. Arthur, A. Bast, J. Dainty, R. M. Faulks, C. Gaartner, G. Haenen, P. Hollman, B. Holst, F. J. Kelly, M. C. Polidori, C. Rice-Evans, S. Southon, T. v. Vliet, and Jos, "Bioavailability and metabolism," *Molecular Aspects of Medicine*, vol. 23, pp. 39–100, 2002.

[104] K. Dvorakova, R. T. Dorr, S. Valcic, B. Timmermann, and D. S. Alberts, "Pharmacokinetics of the green tea derivatives, EGCG, by the topical route of administration in mouse and human skin," *Cancer Chemother Pharmacol*, vol. 43, no. 4, pp. 331–335, 1999.

[105] F. Catterall, L. J. King, M. N. Clifford, and C. Ioannides, "Bioavailability of dietary doses of 3H-labelled tea antioxidants (+)-catechin and (-)-epicatechin in rat," *Xenobiotica*, vol. 33, no. 7, p. 743, 2003.

[106] Y. Cai, N. D. Anavy, and H.-H. S. Chow, "Contribution of presystemic hepatic extraction to the low oral bioavailability of green tea catechins in rats," *Drug Metabolism and Disposition*, vol. 30, no. 11, pp. 1246–1249, 2002.

[107] M. N. Kumar, R. A. Muzzarelli, C. Muzzarelli, H. Sashiwa, and A. J. Domb, "Chitosan chemistry and pharmaceutical perspectives," *Chem. Rev.*, vol. 104, pp. 6017–6084, 2004.

[108] T. Y. Sheu and M. Rosenberg, "Microstructure of microcapsules consisting of whey proteins and carbohydrates," *Journal of Food Science*, vol. 63, no. 3, pp. 491–494, 1998.

[109] R. Vehring, "Pharmaceutical particle engineering via spray drying," *Pharmaceutical Research*, vol. 25, no. 5, pp. 999–1022, 2008.

[110] M. Rosenberg, I. J. Kopelman, and Y. Talmon, "A scanning electron microscopy study of microencapsulation," *Journal of Food Science*, vol. 50, no. 1, pp. 139–144, 1985.

[111] B. Baras, M. A. Benoit, and J. Gillard, "Parameters influencing the antigen release from spray-dried poly(dl-lactide) microparticles," *International Journal of Pharmaceutics*, vol. 200, no. 1, pp. 133–145, 2000.

[112] Y. J. Fu, F. L. Mi, T. B. Wong, and S. S. Shyu, "Characteristic and controlled release of anticancer drug loaded poly (D,L-lactide) microparticles prepared by spray drying technique," *Journal of Microencapsulation*, vol. 18, no. 6, pp. 733–747, 2001.

[113] H. Y. Li and J. Birchall, "Chitosan-modified dry powder formulations for pulmonary gene delivery," *Pharmaceutical Research*, vol. 23, no. 5, pp. 941–950, 2006.

[114] L. Mu and S. S. Feng, "Fabrication, characterization and in vitro release of paclitaxel (taxol (r)) loaded poly (lactic-co-glycolic acid) microspheres prepared by spray drying technique with lipid/cholesterol emulsifiers," *Journal of Controlled Release*, vol. 76, no. 3, pp. 239–254, 2001.

[115] T. Y. Ting, I. Gonda, and E. M. Gipps, "Microparticles of polyvinylalcohol for nasal delivery .1. generation by spray-drying and spray-desolvation," *Pharmaceutical Research*, vol. 9, no. 10, pp. 1330–1335, 1992.

[116] F.-J. Wang and C.-H. Wang, "Sustained release of etanidazole from spray dried microspheres prepared by non-halogenated solvents," *Journal of Controlled Release*, vol. 81, no. 3, pp. 263–280, 2002.

[117] M. Rosenberg, Y. Talmon, and I. J. Kopelman, "The microstructure of spray-dried microcapsules," *Food Microstructure*, vol. 7, no. 1, pp. 15–23, 1988.

[118] J. F. P. S. Gomes, S. Rocha, M. C. Pereira, I. Peres, S. Moreno, J. Toca-Herrera, and M. A. N. Coelho, "Lipid/particle assemblies based on maltodextrin-gum arabic core as bio-carriers," *Colloids and Surfaces B-Biointerfaces*, vol. 76, no. 2, pp. 449–455, 2010.

[119] D. Alvarez and A. G. Borrego, "Apparent versus true density for the volume-to-weight transformation in coal blends," *Journal of Microscopy-Oxford*, vol. 220, pp. 221–228, 2005.

[120] J. Elversson, K. Andersson, and A. Millqvist-Fureby, "An atomic force microscopy approach for assessment of particle density applied to single spray-dried carbohydrate particles," *Journal of Pharmaceutical Sciences*, vol. 96, no. 4, pp. 905–912, 2007.

[121] J. Elversson and A. Millqvist-Fureby, "Particle size and density in spray drying - effects of carbohydrate properties," *Journal of Pharmaceutical Sciences*, vol. 94, no. 9, pp. 2049–2060, 2005.

[122] BS2955, *Glossary of terms relating to powders*, ser. Glossary of terms relating to powders. London: British Standards Institution, 1958.

[123] J. Swarbrick, *Encyclopedia of Pharmaceutical Technology*, 3rd ed. Taylor & Francis Group, 2006, vol. 6.

[124] C. S. Eskilsson and E. Bjorklund, "Analytical-scale microwave-assisted extraction," *Journal of Chromatography A*, vol. 902, no. 1, pp. 227–250, 2000.

[125] Z. Piñeiro, M. Palma, and C. G. Barroso, "Determination of catechins by means of extraction with pressurized liquids," *Journal of Chromatography A*, vol. 1026, no. 1-2, pp. 19–23, 2004.

[126] A. Perva-Uzunalic, M. Skerget, Z. Knez, B. Weinreich, F. Otto, and S. Gruner, "Extraction of active ingredients from green tea (*Camellia sinensis*): Extraction efficiency of major catechins and caffeine," *Food Chemistry*, vol. 96, no. 4, pp. 597–605, 2006.

[127] L. Y. Zhang and S. L. Kosaraju, "Biopolymeric delivery system for controlled release of polyphenolic antioxidants," *European Polymer Journal*, vol. 43, no. 7, pp. 2956–2966, 2007.

[128] A. Barras, A. Mezzetti, A. Richard, S. Lazzaroni, S. Roux, P. Melnyk, D. Betbeder, and N. Monfilliette-Dupont, "Formulation and characterization of polyphenol-loaded lipid nanocapsules," *International Journal of Pharmaceutics*, vol. 379, no. 2, pp. 270–277, 2009.

[129] W. Pigman, D. Horton, and A. Herp, "The carbohydrates: chemistry and biochemistry," D. H. . A. H. W. Pigman, Ed., 2009, vol. 1.

[130] J. Xu, T. Tan, J.-C. Janson, L. Kenne, and C. Sandstrm, "NMR studies on the interaction between (-)-epigallocatechin gallate and cyclodextrins, free and bonded to silica gels," *Carbohydrate Research*, vol. 342, no. 6, pp. 843–850, 2007.

[131] Y. Dror, Y. Cohen, and R. Yerushalmi-Rozen, "Structure of gum arabic in aqueous solution," *Journal of Polymer Science: Part B: Polymer Physics*, vol. 44, no. 22, pp. 3265–3271, 2006.

[132] L. Ninni, A. Meirelles, and G. Maurer, "Thermodynamic properties of aqueous solutions of maltodextrins from laser-light scattering, calorimetry and isopiestic investigations," *Carbohydrate Polymers*, vol. 59, no. 3, pp. 289–303, 2005.

[133] D. D. Mclntyre, H. Ceri, and H. J. Vogel, "Nuclear magnetic resonance studies of the heteropolysaccharides alginate, gum arabic and gum xanthan," *Starch - Stärke*, vol. 48, no. 7-8, pp. 285–291, 1996.

[134] M. L. German, A. L. Blumenfeld, V. P. Yuryev, and V. B. Tolstoguzov, "An NMR study of structure formation in maltodextrin systems," *Carbohydrate Polymers*, vol. 11, no. 2, pp. 139–146, 1989.

[135] V. I. Bakhmutov, *Practical NMR Relaxation for Chemists.* Chichester: John Wiley & Sons, 2004.

[136] S. W. R. Freeman and R. R. Ernst, "High-resolution NMR study of relaxation mechanisms in a two-spin system," *J. Chem. Phys.*, vol. 52, no. 3, pp. 1529–1544, 1970.

[137] B. L. T. Ray Freeman, H. D. W. Hill and L. D. Hall, "Dipolar contribution to NMR spin-lattice relaxation of protons," *J. Chem. Phys.*, vol. 61, no. 11, pp. 4466–4473, 1974.

[138] J. Hong, H. Lu, X. Meng, J. Ryu, Y. Hara, and Y. C.S., "Stability, cellular uptake, biotransformation, and efflux of tea polyphenol (-)-pigallocatechin-3-gallate in ht-29 human colon adenocarcinoma cells," *Cancer Res.*, vol. 62, no. 24, pp. 7241–7246, 2002.

[139] L. Chung, T. Cheung, S. Kong, K. Fung, Y. Choy, Z. Chan, and T. Kwok, "Induction of apoptosis by green tea catechins in human prostate cancer du145 cells," *Life Sci.*, vol. 68, no. 10, pp. 1207–1214, 2001.

[140] A. Paschka, R. Butler, and C. Young, "Induction of apoptosis in prostate cancer cell lines by the green tea component, (-)-epigallocatechin-3-gallate," *Cancer Lett.*, vol. 130, no. 1-2, pp. 1–7, 1998.

[141] T. G. Shutava, S. S. Balkundi, P. Vangala, J. J. Steffan, R. L. Bigelow, J. A. Cardelli, D. P. ONeal, and Y. M. Lvov, "Layer-by-layer-coated gelatin nanoparticles as a vehicle for delivery of natural polyphenols," *ACS Nano*, vol. 3, no. 7, p. 18771885, 2009.

[142] I. A. Siddiqui, V. M. Adhami, D. J. Bharali, B. B. Hafeez, M. Asim, S. I. Khwaja, N. Ahmad, H. Cui, S. A. Mousa, and H. Mukhtar, "Introducing nanochemoprevention as a novel approach for cancer control: Proof of principle with green tea polyphenol epigallocatechin-3-gallate," *Cancer Res.*, vol. 69, no. 5, pp. 1712–1716, 2009.

[143] A. R. A. Abd-Allah, A. A. Al-Majed, A. M. Mostafa, O. A. Al-Shabanah, A. G. E. L. Din, and M. N. Nagi, "Protective effect of arabic gum against cardiotoxicity induced by doxorubicin in mice: A possible mechanism of protection," *J Biochem Molecular Toxicology*, vol. 16, no. 5, pp. 254–259, 2002.

[144] M. P. Desai, V. Labhasetwar, E. Walter, R. J. Levy, and G. L. Amidon, "The mechanism of uptake of biodegradable microparticles in caco-2

cells is size dependent," *Pharmaceutical Research*, vol. 14, no. 11, pp. 1568–1573, 1997.

[145] J. Rejman, V. Oberle, I. S. Zuhorn, and D. Hoekstra, "Size-dependent internalization of particles via the pathways of clathrinand caveolae-mediated endocytosis," *Biochem. J.*, vol. 377, pp. 159–169, 2004.

[146] F. Yan, C. Zhang, Y. Zheng, L. Mei, L. Tang, C. Song, H. Sun, and L. Huang, "The effect of poloxamer 188 on nanoparticle morphology, size, cancer cell uptake, and cytotoxicity," *Nanomedicine*, vol. 6, no. 1, pp. 170–178, 2010.

[147] L. Zhang, F. Yu, A. Cole, B. Chertok, A. David, J. Wang, and V. Yang, "Gum arabic-coated magnetic nanoparticles for potential application in simultaneous magnetic targeting and tumor imaging," *AAPS J.*, vol. 11, no. 4, pp. 693–699, 2009.

[148] M. G. Qaddoumi, H. Ueda, J. Yang, J. Davda, V. Labhasetwar, and V. H. L. Lee, "The characteristics and mechanisms of uptake of PLGA nanoparticles in rabbit conjunctival epithelial cell layers," *Pharmaceutical Research*, vol. 21, no. 4, pp. 641–648, 2004.

[149] G. Zernia and D. Huster, *Investigation of Collagen Dynamics by Solid-State NMR Spectroscopy*, ser. Modern Magnetic Resonance. Springer Netherlands, 2006.

[150] N. O. Metreveli, K. K. Jariashvili, L. O. Namicheishvili, D. V. Svintradze, E. N. Chikvaidze, A. Sionkowska, and J. Skopinska, "UV-vis and FT-IR spectra of ultraviolet irradiated collagen in the presence of antioxidant ascorbic acid," *Ecotoxicology and Environmental Safety*, vol. 73, pp. 448–455, 2010.

[151] F. Guillerminet, H. Beaupied, V. Fabien-Soule, D. Tome, C.-L. Benhamou, C. Roux, and A. Blais, "Hydrolyzed collagen improves bone metabolism and biomechanical parameters in ovariectomized mice: An *in vitro* and *in vivo* study," *Bone*, vol. 46, pp. 827–834, 2010.

[152] Y. Takeuchi, K. Nakayama, and T. Matsumoto, "Differentiation and cell surface expression of transforming growth factor-beta receptors are

regulated by interaction with matrix collagen in murine osteoblastic cells," *The Journal of Biological Chemistry*, vol. 271, no. 7, pp. 3938–3944, 1996.

[153] M. C. Gómez-Guillén, B. Giménez, M. E. López-Caballero, and M. M. P, "Functional and bioactive properties of collagen and gelatin from alternative sources: A review," *Food Hydrocolloids*, pp. 1–15, 2011.

[154] S. E. Kim and E. Mendis, "Bioactive compounds from marine processing byproducts - a review," *Food Research International*, vol. 39, pp. 383–393, 2006.

[155] J. Wu, M. Fujioka, K. Sugimoto, G. Mu, and Y. Ishimi, "Assessment of effectiveness of oral administration of collagen peptide on bone metabolism in growing and mature rats," *Journal of Bone and Mineral Metabolism*, vol. 22, pp. 547–553, 2004.

[156] Y. Nomura, K. Oohashi, M. Watanabe, and S. Kasugai, "Increase in bone mineral density through oral administration of shark gelatin to ovariectomized rats," *Nutrition*, vol. 21, no. 11, pp. 1120–1126, 2005.

[157] M. Saito, C. Kiyose, T. Higuch, N. Uchida, and H. Susuki, "Effect of collagen hydrolysates from salmon and trout skins on the lipid profile in rats," *J. Agric. Food Chem.*, vol. 57, pp. 10 477–10 482, 2009.

[158] M. Nemati, M. Oveisi, H. Abdollahi, and S. O., "Differentiation of bovine and porcine gelatins using principal component analysis," *Journal of Pharmaceutical and Biomedical Analysis*, vol. 34, pp. 485–492, 2004.

[159] P. Benito-Ruiz, M. M. Camacho-Zambrano, J. N. Carrillo-Arcentales, M. A. Mestanza-Peralta, C. A. Vallejo-Flores, S. V. Vargas-López, R. A. Villacís-Tamayo, and L. A. Zurita-Gavilanes, "A randomized controlled trial on the efficacy and safety of a food ingredient, collagen hydrolysate, for improving joint comfort," *International Journal of Food Sciences and Nutrition*, vol. 60, no. S2, pp. 99–113, 2009.

[160] L. Zuckley, K. M. Angelopoulou, M. R. Carpenter, S. McCarthy, B. A. Meredith, G. Kline, M. Rowinski, D. Smith, T. J. Angelopoulos, and

J. M. Rippe, "Collagen hydrolysate improves joint function in adults with mild symptoms of osteoarthritis of the knee," *Medicine & Science in Sports & Exercise*, vol. 36, no. 5, pp. S153–S154, 2004.

[161] H. Hou, B. Li, X. Zhao, Y. Zhuang, G. Ren, M. Yan, Y. Cai, X. Zhang, and L. Chen, "The effect of pacific cod (*Gadus macrocephalus*) skin gelatin polypeptides on uv radiation-induced skin photoaging in ICR mice," *Food Chemistry*, vol. 115, no. 3, pp. 945–950, 2009.

[162] M. D. Rees, E. C. Kennett, J. M. Whitelock, and M. J. Davies, "Oxidative damage to extracellular matrix and its role in human pathologies," *Free Radical Biology & Medicine*, vol. 44, pp. 1973–2001, 2001.

[163] R. Pedroza-Islas, E. Vernon-Carter, C. Durán-Domínguez, and S. Trejo-Martínez, "Using biopolymer blends for shrimp feedstuff microencapsulation - I. microcapsule particle size, morphology and microstructure," *Food Research International*, vol. 32, pp. 367–374, 1999.

[164] Z. Y. Zhang, Q. N. Ping, and B. Xiao, "Microencapsulation and characterization of tramadol-resin complexes," *Journal of Controlled Release*, vol. 66, pp. 107–113, 2000.

[165] M. I. Ré, "Microencapsulation by spray drying," *Drying Technology*, vol. 16, pp. 1195–1236, 1998.

[166] H. Yushu and S. Venkatraman, "The effect of process variables on the morphology and release characteristics of protein-loaded PLGA particles," *Journal of Applied Polymer Science*, vol. 101, no. 5, pp. 3053–3061, 2006.

[167] D. Walton and C. Mumford, "The morphology of spray-dried particlesthe effect of process variables upon the morphology of spray-dried particles," *Chemical Engineering Research and Design*, vol. 77, no. 5, pp. 442–460, 1999.

[168] I. Peres, S. Rocha, J. Gomes, S. Morais, M. C. Pereira, and M. Coelho, "Preservation of catechin antioxidant properties loaded in carbohydrate nanoparticles," *Carbohydrate Polymers*, vol. 86, no. 1, pp. 147 – 153, 2011.

[169] R. H. Muller, C. Jacobs, and O. Kayser, "Nanosuspensions as particulate drug formulations in therapy rationale for development and what we can expect for the future," *Advanced Drug Delivery Reviews*, vol. 47, no. 1, pp. 3–19, 2001.

[170] B. C. Vidal and M. L. S. Mello, "Collagen type I amide I band infrared spectroscopy," *Micron*, vol. 42, pp. 283–289, 2011.

[171] I. Peres, S. Rocha, M. C. Pereira, M. Coelho, M. Rangel, and G. Ivanova, "NMR structural analysis of epigallocatechin gallate loaded polysaccharide nanoparticles," *Carbohydrate Polymers*, vol. 82, pp. 861–866, 2010.

[172] E. Balmayor, K. Tuzlakoglu, H. Azevedo, and R. Reis, "Preparation and characterization of starch-poly-ε-caprolactone microparticles incorporating bioactive agents for drug delivery and tissue engineering applications," *Acta Biomaterialia*, vol. 5, pp. 1035–1045, 2009.